Forecasting Research

Met O 11 Scientific Note No. 15

Dynamical aspects of the October storm 1987: A study of a successful fine-mesh simulation

by

G.J. Shutts

September 1989

Meteorological Office (Met O 11)
London Road, Bracknell, Berkshire RG12 2SZ, England

MET O 11 Scientific Note No. 15

DYNAMICAL ASPECTS OF THE OCTOBER STORM 1987 : A STUDY OF A SUCCESSFUL FINE-MESH SIMULATION

by

G.J. Shutts

September 1989

LONDON, METEOROLOGICAL OFFICE
Met.O.15. Scientific Note No.15

Dynamical aspects of the October storm 1987: a study of a successful fine-mesh simulation.

08971089 551.515.11 FH2A
551.509.313

Met O 11 (Forecasting Research)
Meteorological Office
London Road
Bracknell
Berkshire RG12 2SZ
ENGLAND

Abstract

A diagnostic study of a successful numerical simulation of the October Storm, 1987 is described. This good, non-operational forecast was obtained using the Meteorological Office's Fine-Mesh model run from a revised analysis at 00Z on October 15 1987. The Met. Office's Mesoscale model was also run from initial conditions at 12Z October 15 obtained by interpolating the above Fine-mesh forecast fields to examine the benefits of very high horizontal resolution (15 km gridlength).

Diagnostic maps and cross-sections derived are used to address two scientific issues:

(i) the role of weak moist slantwise stability (or, alternatively, positive slantwise convective potential energy)

(ii) the dynamical significance of the 'cloud head' in the satellite imagery

It is appears that the baroclinic zone, in which the storm develops, is highly receptive to forcing by an upper trough and the warm boundary layer air just ahead of the main surface front is characterised by substantial slantwise convective available energy. The cloud head is identified with a region of intense slantwise ascent in the warm air just above the main frontal zone. Its great meridional extent is associated with the upper tropospheric outflow and horizontal spreading of air which has recently undergone rapid slantwise ascent. The low-level temperature field exhibits, throughout the development period, a remarkable shape-preserving thermal ridge of considerable intensity. A

pronounced warm core with local potential temperature maximum is evident as the depression centre crosses Central England.

The sensitivity of the forecast to the removal of surface energy fluxes and latent heat of condensation are investigated separately. It is found that on the time scale of the simulation, surface energy fluxes have negligible impact on the explosive development. On the other hand, the contribution of latent heat release to the development appears to dominate the dry baroclinic instability process.

1. Introduction

In the period immediately following the Great Storm of October 16 1987, a substantial inquiry into forecast model performance and forecasting practices was launched in the wake of media criticism of the Meteorological Office. Considerable research interest was triggered both within and outside the Office into the causes and consequences of the winds which in six hours wreaked havoc over Southern England (see March 1988 issue of *Weather and Met. Mag.* April 1988). The work to be described here is part of a programme of research initiated following the Storm to study the dynamical structure of depressions which deepen explosively (central pressure falling by more than 24 mb. in 24 hours) with particular emphasis on the sub-synoptic scale processes. The study of the Storm presented here has formed the major part of the project : comparison with other explosive developments studied will be referred to, but the details will be published in a companion paper.

It is clear from subjective analyses, operational and re-run forecasts that the Storm's development period lay between 00Z October 15 and 00Z on the 16th so that the latest relevant start time is 00Z on the 15th. The 24 hour forecast from the operational Fine-Mesh model initiated at this time was in marked conflict with the subjective analysis (Lorenc et al, 1988). The global model on the other hand positioned the low reasonably well but was not deep enough.

However, a revised Fine-Mesh analysis giving extra weight to the observations, and which included late AIREP data missing the ± 90 minute time-window centred on the analysis time, resulted in an excellent forecast. In some respects, this 'best' Fine-Mesh forecast was better than the operational three-hourly Fine-Mesh *analyses* in the 24 hour period from 00Z on the 15th. For instance the central pressure of the forecast depression at 00Z on the 16th was 2 mb. lower than the operational analysis and in better agreement with the

surface observations. A Fine-Mesh model forecast from the interpolated global model analysis at 00Z Oct. 15 also gave an excellent forecast confirming the operational forecast failed primarily because of analysis deficiencies.

The purpose of this paper is to study this best Fine-Mesh model simulation as if it were a perfect forecast. No attempt will be made to verify it against routine synoptic observations though it will be used to support the interpretation of satellite imagery. A simple visual comparison between hand-analysed sea-level pressure charts (eg. Woodroffe, 1988) and the model fields assures one that this is indeed an excellent simulation of the actual event. Furthermore, the higher level of dynamical consistency in the model fields at different times compared to analysed fields gives one more confidence in the interpretation of the system's evolution.

There has in the last ten years been considerable interest in the simulation of explosive cyclogenesis in limited area numerical models with gridlengths smaller than 100 km. Most of these modelling studies have been carried out in the USA and have centred on notorious storms, eg. the Presidents' Day storm of 18-19 February 1979 (Bosart and Lin,1984; Uccellini et al, 1984) and the QE II storm of 9-10 September 1978, (Gyakum, 1983 ; Anthes et al, 1983). Kuo and Reed (1988) carried out numerical simulations of the explosive cyclogenesis event featured in a study by Reed and Albright (1986). It will be seen later that many aspects of this eastern Pacific development and its simulation resemble the October Storm.

Controversy has surrounded which, if any, key physical processes require accurate parametric representation since neither of the above cases was simulated successfully by the operational NMC limited area model of that time. Possible model deficiencies considered were lack of resolution, inadequate planetary boundary layer and/or convective parametrization or simply poor

initial conditions. Anthes et al (1983) showed, using a mesoscale model that no single cause for failing to predict explosive deepening could be identified though high vertical and horizontal resolution were essential. Sanders (1987) has demonstrated that since 1985 the operational NMC limited area model has improved markedly in its ability to forecast explosive deepeners.

The Meteorological Office Fine-Mesh model (which came into operational service in 1982 and covers an area bounded by the meridians 80 W and 40 E, and latitude circles 80 and 30 N with a horizontal gridlength of $\simeq$ 75 km) has had a good record for predicting explosive deepening events. In the absence of a high resolution mesoscale observational network, model simulations provide comprehensive, dynamically-consistent datasets for understanding the structure of real storms. Furthermore, the model may be re-run with certain physical processes removed in order to obtain some measure of their relative importance (Mullen and Baumhefner, 1988).

The diagnostic study presented in this paper will concentrate on two important scientific issues. Firstly, it has been recognised for a long time that the effect of latent heat release in frontal clouds will tend to reduce the effective static stability and increase the growth rate of unstable baroclinic systems. In particular, Emanuel et al (1987) have demonstrated that as the stability to ascent along absolute momentum surfaces tends to zero, so the growth rate of baroclinic waves tends to twice its dry value. More importantly, the structure of the baroclinic system becomes highly asymmetrical with respect to the regions of ascending and descending motion. In this zero moist potential vorticity limit, the ascending motion is predicted to occur in a sloping sheet of infinitesimal width suggestive of the form of rearward ascent observed at cold fronts in real depressions. Equally interesting, though less amenable to mathematical analysis, is the case in which there is potential *instability* along

absolute momentum surfaces. It is important therefore to attempt to make some assessment of the existence of potential slantwise convective available potential energy (SCAPE) in the early stages of development of the October Storm.

The second question to be addressed here concerns the origin and significance of the 'cloud head' observed in satellite imagery (Bottger et al, 1975). This takes the form of an unusually extensive sheet of predominantly stratiform cloud which grows in the early development phase of explosive cyclogenesis. Bottger et al (1975) argue that the appearance of such a cloud form is virtually always accompanied by the development of an intense depression containing hurricane force winds and is a valuable precursor in the absence of adequate data coverage over the oceans. The October Storm was, indeed, accompanied by a classic cloud head : model upper tropospheric relative humidity fields are presented which show the equivalent feature in the best Fine-Mesh simulation and how it fits in with the dynamical structure of the Storm. It is also speculated that the cloud head may be a manifestation of the synoptic forcing by an upper trough of a frontal environment possessing substantial SCAPE.

The above issues provide a context within which to discuss the model diagnostics. It would be inappropriate to draw general conclusions based on this single case study though many of our findings are supported by other case studies not described here.

In addition to describing the Fine-Mesh model simulation of the Storm, some sensitivity experiments have been carried out to examine the influence of surface energy fluxes, latent heat release and convective parametrization.

2 Synoptic evolution of the model Storm

Four types of chart, out of a wide range of diagnostics studied, have been found to be particularly useful in representing the Storm's evolution; these are mean sea-level pressure, isotachs and wind vectors at 250 mb., wet-bulb potential temperature (θ_w) at 850 mb. and potential vorticity (PV) on the 330 K isentropic surface with 900 mb. potential temperature (θ) superimposed. Figs. 1-3 show these charts at 00Z Oct. 15, 12Z Oct. 15 and 00Z Oct. 16 respectively (ie. T+0, T+12 and T+24). At midnight on the 15th there are two separate centres of low pressure, 982 and 989 mb, located at 18 and 27 W respectively (Fig.1a) - the latter being the system which develops into the Storm. A very strong west-southwesterly airstream extends eastwards towards Northern Spain with another depression centred over Southern England. At 250 mb. a jetstreak with speed ≈ 175 knots lies upstream of the surface depressions at 40 W and the main upper trough axis near 30 W (Fig. 1b). The surface depressions are associated with two waves in the θ_w field with local enhancements of the very intense gradients. θ_w values of greater than 20°C appear to the south of the baroclinic zone (Fig. 1c). High potential vorticity values (> 6 PV units as defined by Hoskins et al, 1985) occur in separate maxima at 31 W and 38 W on the 330 K isentropic surface (Fig. 1d). Inspection of subsequent PV charts at 03 and 06Z reveal that for some (as yet unidentified) reason the PV maximum at 38 W increases by ≈ 3 PV units during this period but thereafter maintains its intensity. As a quasi-conservative variable one would hope that PV maxima retain their values though diagnostic interpolation and model truncation errors inevitably detract from this property.

At 12Z the low has deepened by 19mb. to 970 mb. and is centred near 14W (Fig. 2a). The 250 mb. jetstreak at this time is now almost directly over the low with a reduced speed of about 155 knots. (Fig. 2b) with an intense and

rather small-scale PV maximum in the cyclonic shear zone further west (Fig.2d). The θ_w field now shows a single wave coinciding with the position of the surface low and embedded in a long and intense frontal zone (Fig. 2c). The most intense θ_w gradient at 850 mb. in the crest of the thermal ridge lies just north-west of the low centre. The thermal ridge in the 900 mb. θ field is located just downstream of the upper-level PV maximum and is suggestive of the mutual coupling discussed by Hoskins et al (1985).

At 00Z on October 16 the model low centre arrived at the south coast of England with a central pressure of 957 mb. and an intense core of tight pressure gradient and strong winds whose radius was no more than $\simeq$ 400 km (Fig. 3a). A pressure gradient of comparable intensity covers much of France and Belgium. The depression goes on deepening to 956 mb. at 03Z and 955 mb. at 06Z on the 16th. Fig. 3a should be compared to the subjective analysis in Fig. 4 deduced by Woodroffe (1988) which shows the low centre about 100 km further back than the model and deeper by about 5 mb. It is interesting to note that the operational subjective analysis for the same time depicted a low in a similar position but with central pressure of 960 mb. - illustrating the degree of uncertainty in the true value. The 250 mb. jetstreak has now become elongated with two wind speed maxima of $\simeq$ 140 knots - one just south of Brittany and the other over Northern Portugal (Fig. 3b). A remarkably intense frontal zone lying across the UK is revealed in the θ_w field at 00Z (Fig. 3c) with a 10° C jump maintained across one or two model gridlengths. The frontal zone weakens considerably over Brittany near the low centre but is intense further south over Spain and Portugal. Another interesting feature is the suggestion of a local θ_w maximum near the centre of the low (also in the 900 mb. θ field of Fig. 3d). It is this combination of low-level warmth below an

upper-level PV maximum which, from balance considerations, is required for a surface depression of exceptional intensity (Thorpe, 1986).

3. Frontal structure and stability in the Storm environment

(a) Q-vectors, vertical motion and frontal evolution

The exceptional nature of the Storm is strikingly apparent from the time sequence of vertical velocity maps at 700 mb. shown in Figs. 5 a-e. At 00Z (Fig. 5 a) there are two regions of strong upward motion in the Atlantic, near 15W and 25W and both between 40N and 45N. The wavy pattern of vertical motion stretching from Portugal across Northern Spain to the Swiss Alps in Figs.5 a-d is orographically-forced gravity wave activity. By 06Z (Fig. 5b) the intensity of upward motion has almost doubled in the western centre with a peak ascent rate of over -100 mb./hour near 22W; the eastern centre has diminished in intensity and exhibited little movement. Compensating descent associated with the developing Storm is far weaker and difficult to identify. By 12Z (Fig. 5c)) an extremely compact ascent region, with vertical velocity maximum of -90 mb./hour, can be found near 44N 12W, followed by a broad wake of comparatively weak descent ($\simeq$ +10 mb/hour). The small scale of the updraught core is quite remarkable being defined by about four model gridpoints across its diameter. Comparing Fig. 5c with Fig. 2c it can be seen that the updraught core lies in the warm air and on the boundary of the zone of intense θ_w gradient, consistent with the ascent of high θ_w air from the boundary layer near or at the surface front. The scale of the upward motion core expanded in the along front direction by 18Z (Fig. 5d) but even by 00Z on the 16th (Fig. 5e) the intensity is maintained with vertical velocities of up to -90 mb./hour. Studies of other explosive cyclogenesis events carried out in the Meteorological Office have revealed that the longevity of this intense vertical motion phase is not typical.

In order to assess the geostrophic forcing of vertical motion and frontogenesis, maps of Q-vectors (Hoskins et al, 1978) with 700 mb. temperature superimposed have been obtained for six hourly intervals throughout the forecast period - three of which are reproduced here (Figs. 6 a-c for 00Z, 06Z and 12Z Oct. 15). At the analysis time, a rather complex pattern of Q- is associated with waves on the main baroclinic region between 10 W and 40 W (Fig. 6a). The convergence of Q near 41 N 25 W is consistent with the forcing of ascent in the low pressure system which goes on to develop into the Storm. At 06Z a single pattern of Q dominates with very strong convergence near the low centre (Fig. 6b). The upgradient sense of the vector in the strong baroclinic region just to the northwest of the Storm centre is consistent with powerful frontogenesis. Further upstream however, Q is down the temperature gradient indicating frontolysis (following a fluid parcel). This pattern amplifies and persists throughout the development of the Storm : Fig. 6c (for 12Z) is typical of later times. The thermal wave associated with the Storm is unusually shape-preserving and the Q pattern is consistent with its propagation.

(b) Vertical cross-sections and SCAPE

As discussed in the Introduction, the stability of the atmosphere to upright and quasi-two dimensional slantwise displacements is likely to be important in determining the intensity of cyclogenesis. To assess this and to get a better picture of the three-dimensional structure of the Storm, vertical cross-sections have been taken across the baroclinic zone at six hourly intervals throughout the forecast period. It is appropriate though, to concentrate on the vertical structure at 06Z allowing six hours for 'spin-up'. At this time the model Storm is growing most rapidly and the 700 mb. vertical velocity maximum has its peak value (100-110 mb./hr).

Fig. 7 shows the 850 mb. θ_w field with wind vectors at 06Z; the line of cross-section, taken normal to the region of most intense θ_w gradient and through the depression, is marked between the points A and B.

The unusual depth and intensity of the baroclinity is revealed in the θ cross-section (Fig. 8a) with a transition from 23°C to 12°C across the front at the surface. There is a local maximum of θ in a vertical column just ahead of the surface front position. The component of the wind normal to the front (Fig. 8b) shows the jet-core (69 ms^{-1}) to be located near 250 mb. and slightly to the warm air side of the surface frontal zone which coincides with a pronounced region of cyclonic shear in v. The v contours extend downwards leading to winds of $\simeq$ 40 ms^{-1} in the warm air at 850 mb. There is also an extension of high v values down the tropopause towards the cold air. The frontal zone is evident as an undulating layer of large vertical shear sloping up to 300 mb. at the northern end of the cross-section. Wind vectors in the plane of the cross-section show considerable ascent from near the surface front towards the jet and rearward relative to the cold air. The vertical velocity field (Fig. 8c) shows a dominant maximum of 92 mb./hr. Much of the tropospheric air on the warm side of the front is close to saturation although there is some dry air just above the boundary layer at the southern end of the cross-section and in a tongue extending down through the jet (Fig. 8d). The potential vorticity cross-section (Fig. 8e; regions of PV > 1 unit shaded) shows a tropopause descending from about 13 km above the warm air to 7 km over the cold air. The lower tropospheric frontal zone is characterised by PV values > 3 units - consistent with the high values found by Hoskins and Berrisford (1988) using ECMWF analyses. This combination of high surface potential temperature and lower tropospheric PV is consistent with the strong surface flow and 'hurricane-like' character of the developing vortex.

The potential for slantwise convection may be gauged from the plot (Fig. 8f) of absolute momentum (taken here to be given by $\int f dx + v$) and wet-bulb potential temperature (θ_w). In the warm air just ahead of the surface front, θ_w shows a maximum of over 21 °C : θ_w decreases with height along M surfaces throughout the troposphere indicating a high level of symmetric instability here. To quantify the level of instability, an M-surface ascent profile was plotted on a tephigram (Fig. 9; see Emanuel, 1983). For an air parcel lifted from 950 mb. along the surface M=110 ms^{-1} a considerable level of SCAPE is evident (shaded area). The layer from the surface to 550 mb. is only weakly symmetrically unstable : air parcels displaced upwards from the 550 mb. level however would be unstable and could, according to parcel theory, ascend to 300 mb.

For comparison, Figs. 10 a-c show the line of cross-section on the 850 mb. map of θ_w; an M / θ_w cross-section and an M surface tephigram respectively for 00Z 15th October. Fig. 10b indicates a very high level of potential instability for slantwise convection, particularly for the warm air just ahead of the surface front. Along the M=110 ms^{-1} surface, θ_w decreases from over 21° C at the sea surface to 16° C just beneath the tropopause. The lower troposphere in the warm air is also potentially-unstable to upright convection - assuming that the pseudo-adiabatic moist reference process is the relevant one. The M=110 ms^{-1} tephigram (Fig. 10c) shows that a striking level of SCAPE is present in the initial state of this Fine-Mesh forecast. In contrast, the vertical thermodynamic profile (denoted by the dots in Fig. 10 c) above the point where the same M surface intersects the surface indicates some degree of stability to upright convection.

The corresponding pictures for 12Z (Figs. 11 a-c) show that within the frontal zone, a fair approximation to slantwise neutrality appears to have been

achieved with M and θ_w surfaces almost parallel. This is confirmed by the M=115 ms^{-1} tephigram, though air parcels near the sea surface could, in principle, slantwise convect throughout the depth of the troposphere.

Although SCAPE is a concept arising from the application of parcel theory in two-dimensional flows (where absolute momentum conservation is guaranteed) it can be *defined* for the three-dimensional case by assuming Lagrangian conservation of both components of the absolute momentum. Shutts and Cullen (1987) showed that in semi-geostrophic theory, slantwise stability is a measure of the resistance to displacements along lines of intersection of constant $(fx+v_g)$ and $(fy-u_g)$ surfaces.

Quantitative estimates of SCAPE and its horizontal variation were obtained here by adapting a program used operationally to calculate CAPE. By defining absolute momentum components $M=\int f dx + v$ and $N=\int f dy - u$ where x and y are the horizontal distances (from some fixed origin) along latitude and longitude lines respectively, values of temperature, pressure and relative humidity are found along the line of intersection of specific M and N surfaces. Effectively the SCAPE routine takes an air parcel at each model gridpoint in the lowest model level ($\simeq$ 25 m above the surface) and computes the positive area on the equivalent tephigram following an 'ascent' along this line of constant M and N passing through the boundary layer gridpoint. At each level above, the gridbox containing the intersection point is located by assuming the monotonicity of M in x and N in y : the values of temperature, pressure and humidity at the intersection point are then found using bilinear interpolation. Fig. 12 a shows the distribution of SCAPE at the analysis time : the numbers (in hundreds of Joules kg^{-1}) are printed in the gridbox from which the (M, N) ascent was made. In the vicinity of the developing low, the line of intersection of M and N surfaces slope northwards by about four gridboxes. This needs to be borne in

mind when interpreting where the release of SCAPE might take place. The SCAPE values obtained confirm the high degree of slantwise instability inferred from the M surface tephigram. Maps of SCAPE at 06Z and 12Z also show extensive regions of potential instability though with decreasing area as time goes on. For comparison, Fig. 12 b shows a map of CAPE at the analysis time. Although some instability to upright convection is evident near the low centre it is much less extensive than the SCAPE. Trajectories calculated for air parcels in the region of the boundary layer with high SCAPE were found to ascend in about six hours to the tropopause. If the conversion of SCAPE to kinetic energy is taking place, then this rapid ascent is clearly a prerequisite.

Without conducting some carefully designed modelling experiments, it is not possible to be sure that this high level of SCAPE is an important factor in the Storm's vigour and small horizontal scale. The plausibility of this assumed relation depends on whether free slantwise convection is triggered by the upper tropospheric trough. The reality is that the theoretical distinction between localised free slantwise convection and synoptically-forced ascent at near slantwise neutrality is rather blurred.

4. Inferences from Satellite Imagery

The forecaster is frequently alerted to the possiblility of rapid cyclogenesis by a characteristic signature in the satellite imagery which Bottger et al (1975) named the 'cloud head'. Comparison of high quality satellite pictures with selected model fields during the development phase of the Storm can give valuable insights into its dynamical structure.

Fig. 13a is a NOAA AVHRR infra-red image at 0453 GMT on October 15 with prominent features schematised in Fig. 13b. The cloud head comprises an outer(white) region of dense and non-homogeneous cirrus and a region of lower

cloud with some progression from light to darker tones towards the south-east. On close inspection this sloping cloud shield is found to be highly striated throughout its length in a NW-SE or N-S direction. The cloud band to the south of this appears to contain lumpy convective tops embedded in a background of uniform medium level cloud. The surface front lies beneath this cloud band and along the northern edge of the convective cloud.

Since the Fine-Mesh model has no prognostic equation for cloud water, we must relate the presence or absence of cloud to the relative humidity field. For the purposes of comparison with IR imagery, the 400 mb. relative humidity (RH) (Fig. 14) is a convenient level to take and it will be assumed that cloud exists if RH > 90%. A large area with RH > 90% extends from 45 N 25 W to Portugal, the Bay of Biscay and SW England : there is no suggestion of a dry zone splitting this cloud mass - either at this level or any other level in the high troposphere. The dashed line denotes the position of the surface frontal zone in the model inferred from the 900 mb. potential temperature and the cross marks the low centre. By relating this frontal position to the IR image (Fig. 13a) and the vertical cross-sections (particularly Fig. 8b) one can be fairly confident that the cloud head corresponds to stratiform cloud produced in slantwise ascent on the warm side of the frontal zone. The progression of grey tones between the white upper cloud at the convex northern limit of the head through to the black regions just evident at its southern limit support the view that this is the primary baroclinic frontal zone (see discussion of cloud top temperature later in this section). If this identification is correct then the cloud band to the south of the head lies close to the primary jet core. One would normally expect the jetstream axis to coincide with the northern limit of the cloud band at the confluence of ascending moist and very dry airstreams (Oliver et al, 1964: Durran and Weber, 1988). It seems, therefore, that provided

some allowance is made for the lack of dryness in the air on the polar side of the primary jetstream, the IR image can be broadly reconciled with the model fields. The success of the simulation suggests that the humidity error - in some sense - was not important. On the other hand one would not necessarily expect the mesoscale structure of the vertical velocity field in this region to be correct.

By 15Z on the 15th the Storm is well developed and one can locate features in the IR imagery with more confidence. Fig. 15 shows the NOAA-9 IR image at 1447 Z . The surface cold front position can now be identified beneath a clearing in the jet cirrus near 46 N 11 W . The warm side of the front is clear of cloud here with a view to the sea surface. A rope cloud is just discernable in the visible image (not shown) separating transverse striations in the frontal surface from the cloud-free warm air. The low centre probably lies close to this rope cloud and beneath the bulge in the jet-cirrus. The forecast 400 mb relative humidity at 15Z shows a good depiction of the northern limit of the cloud head and a dry slot cutting in to the rear of the system (Fig.16). The depression centre, marked by the cross, appears to be too far forward at this stage since the analysis of Monk and Bader (1987) puts the low centre at a similar position (near 45 N 10 W) *at 18Z*. This would also be consistent with the fact that the simulated storm appeared to be forward of its correct position by about 2 hours when it arrived at the South coast of England at midnight.

Given the limitations imposed by satellite imagery interpretation, there seem to be many features of the imagery that are either absent or misrepresented by the model - in spite of the excellence of the dynamical aspects of the forecast. This misrepresentation may be due to errors in the initial conditions, systematic humidity errors or the failure of the model to explicitly resolve

certain mesoscale dynamical processes. Monk and Bader (1988) discuss the evolution of the Storm inferred from visible, infrared (IR) and water vapour radiance images and succeed in identifying the position of the surface front and low centre after 12Z on October 15. They draw particular attention to an apparent marked drying of air in a zone through the overall baroclinic leaf cloud between 00Z and 06Z on the 15th as identified in the water vapour channel. The northern part of the leaf later develops into the cloud head. They suggest that this drying could result from intense subsidence and might be associated with the intrusion of stratospheric air of high potential vorticity which - in line with the ideas of Hoskins et al (1985) - could initiate cyclogenesis.

Fig. 17 shows the 400 mb. vertical velocity at 03Z Oct. 15 from the forecast. No intense subsidence is evident at this time in the vicinity of the cloud head, nor can it be found at other levels or at other times between 00Z and 06Z. Assuming that the darkening in the dry wedge they observe corresponds to a fall in height from 400 mb. to 700mb. of the (effective) optically black layer at that wavelength, a subsidence rate of the order of 50 mb/hr would be required.

Two possible explanations will be considered here. Firstly, it is possible that the model has been unable to resolve a mesoscale frontal circulation responsible for rapid descent and drying. The other possibility is that before 00Z, jetstream cirrus was obscuring a 'canyon' of very dry air and that between 00Z and 06Z this veil of cloud moved away so as to give the appearance of rapid warming in the imagery. As can be seen from Fig. 16, an extensive area of very dry (< 10% RH) *tropospheric air* lay to the west of the developing system : descent of air from the stratosphere would not be needed to produce the missing dry zone.

Maps of cloud top temperature available from the FRONTIERS imaging system

(Browning and Carpenter, 1984)) were used to quantify some of the foregoing statements concerning the cross-sectional structure of the baroclinic zone. The cloud head itself is predominately characterised by temperatures in the range -30 to -40° C with a narrower zone in which the temperatures rise to > -9°C marking the frontal surface. Near the depression centre, values > +8°C can be found and the NOAA-9 visible image at this time indicates that cloud free regions exist there. Cloud top temperatures in the jet stream cirrus are similar to those within the cloud head though because of the tropical character of the air mass, these tops are much higher. A cross-section of model temperature was used in conjunction with this cloud top temperature map to infer the vertical profile of the cloud top across the baroclinic zone and through the Storm at 1630 Z (Fig. 18).

Finally, we comment on the transverse striations observed in the frontal cloud. These were evident on most of the images - particularly the visible channel - and consist of cloud lines several hundred kilometres long and ≈ 10 km apart oriented perpendicular to the thermal wind and terminating at the line convection rope cloud. They are rather reminiscent of cloud streets but this is difficult to reconcile with their location - in the region of the frontal surface. One would expect any shear-organised convection in the cold air to be obscured by stratiform frontal cloud and, if the forecast is to be believed, there is little vertical wind shear oriented at right angles to the front in the cold air . Another possibility is that they are some form of transverse roll instability associated with the intense frontal vertical wind shear.

5. Some additional model forecasts

The results of some other forecasts with the Fine-Mesh model (and one from the Mesoscale model) will now be described. These provide some insight into the

sensitivity of the successful Fine-Mesh model forecast to variations in analysis, resolution and physical parametrization - though not in any systematic way. The following forecast experiments were undertaken:

(A) Fine-Mesh model forecast from 00Z Oct.15 using the interpolated global model analysis

(B) As (A) except run with twice the horizontal resolution

(C) Best Fine-Mesh forecast run with no surface energy fluxes

(D) Best Fine-Mesh forecast run with no latent heat release

(E) Best Fine-Mesh forecast run with no convective parametrization

(F) Best Fine-Mesh forecast with improved humidity analysis

(G) Mesoscale model forecast from 12Z Oct. 15 and driven by the best Fine-Mesh forecast.

In some cases it will be sufficient merely to state the outcome of the integration.

Experiment A, whose analysis benefitted from the inclusion of the crucial AIREPS, produced a forecast which in many respects is better than that we have chosen to call the best Fine-Mesh forecast. The global model sea-level pressure analysis at 00Z Oct.15 (Fig. 19 a) is significantly different from Fine-Mesh analysis (Fig. 1 a) with a somewhat deeper and more uniform low pressure trough between 10 and 30 W. The separate vortex near 18 W in the Fine-Mesh analysis is virtually absent from the global model analysis. Fig. 19 b shows the 24 hour forecast PMSL and should be compared with Fig. 3 a. The central pressure of the low at 00Z Oct. 16 is only 2 mb. higher than that in the subjective analysis of Woodroffe (1988) (Fig. 4). Although Experiment A is very similar to the best Fine-Mesh forecast in general terms it is interesting to note how different is the structure of the vertical velocity field. Fig. 20 shows the 700 mb. vertical velocity at 06Z and should be compared with Fig. 5 b. The 'bulls-eye' vertical

velocity maximum in the best Fine-Mesh run has been replaced with a broad maximum near 45 N and a separate chain of maxima extending from near 41 N 20 W to the north coast of Spain. This splitting of the vertical velocity maximum does not persist however and by 12Z is a single, but noticeably broader maximum than the best Fine-Mesh simulation. Both simulations of the vertical velocity and relative humidity fields are difficult to reconcile with the satellite imagery. The fact that the structure of the vertical velocity field can be so different in two excellent forecasts of the Storm suggests that the real mesoscale structure of the vertical motion field need not resemble either forecast. Indeed this would have to be the case to reconcile the excessively large volume of saturated air in the simulated Storm with the dry zone inferred from the IR imagery.

An enhanced version of the Fine-Mesh model with ≈ 40 km horizontal gridlength was run on the ETA-10 computer using the global model analysis (Experiment B). This produced a very similar forecast to Experiment A though with a low of central pressure 2 mb. deeper at 00Z Oct. 16 - in excellent agreement with the subjective analysis.

In Experiment C it was found that switching off the surface flux of sensible and latent heat had negligible impact on the forecast deepening of the Storm.

The crucial role of latent heat release was demonstated by Experiment D ; Fig. 21 shows the 24 hour forecast PMSL from this run. The depression which grows into the Storm and deepens by 32 mb in the control run now only deepens by about 10 mb. The speed and track of the depression is largely unaffected. This experiment supports the idea that the baroclinic environment is exceptionally responsive to synoptic forcing *only in the presence of the moist process*. Mullen and Baumhefner (1988) (and Kuo and Reed (1988)) find that

about one half of the deepening can be attributed to the dry baroclinic process compared to the one third found here. The existence of large amounts of potential SCAPE may be the key to why this development is so sensitive to the moist diabatic process.

The effect of switching of the model's mass flux based convective parametrization scheme (Experiment E) was to increase the vertical velocity maximum at the core of the Storm and produce a low which at 00Z Oct. 16 was centred about one gridlength to the north-west of its position in the control run and about 3 mb. deeper.

Attempts were made to modify the humidity analysis in accordance with inferences from the satellite imagery (Experiment F). A deep slot of very dry air was created in the model's analysed cloud mass from 200 to 700 mb.. Unfortunately, by T+6 hours the humidity field was very similar to the control run with the complete removal of the dry slot. The model is known to suffer from a tendency to over-moisten the upper troposphere and lower stratosphere : presumably it is related to the difficulty in maintaining intense humidity gradients.

Finally, some diagnostics from a Mesoscale model forecast initialized at 12Z with the T+12 Best Fine-Mesh forecast fields will be presented. The Meteorological Office's Mesoscale model solves the non-hydrostatic primitive equations of motion on a horizontal grid with 15 km resolution and 16 unequally spaced terrain-following vertical levels (Golding, 1987). Boundary updates to the integration area are supplied from the best Fine-Mesh forecast. Given the relatively small horizontal area of the model at this resolution (1000 km x 1000 km) it is essentially a slave to the Fine-Mesh forecast though is capable of filling in some of the mesoscale detail which cannot be resolved by Fine-Mesh model.

The sea-level pressure and 10 m wind vectors at T+12 (00Z Oct. 16) are shown in Fig. 22 a. Since the depression only gets into the model domain a few hours before this time, its intensity is little different from the Fine-Mesh forecast. On the other hand, the potential temperature field at 310 m (Fig. 22 b) shows that intense frontogenesis has forced the temperature contrast across the front (≃ 10 K) down to the grid scale. This is in accord with the observed rapid temperature rise over southern England as the warm front swept northwards (Burt and Mansfield, 1988). Time series plots of temperature at various model gridpoints (not shown) indicate a temperature rise of up to 8 K in 100 minutes compared with similar rises in less than one hour noted by Burt and Mansfield.

Vertical cross-sections at T+12 were taken along the line indicated in Fig. 22 b : four of the most interesting of these are shown in Figs. 23. The cross-section of potential temperature (Fig. 23 a) shows an intense front with steep (1 : 40) isentropic surfaces up to a height of 1.5 km and a weaker baroclinic region above with gently sloping isentropes (1 : 230). Such a frontal structure is reminiscent of the numerical simulations of Gall et al (1988) and the sloping frontal discontinuity model of Shutts (1988). Two regions of intense baroclinity can be identified; one being the aforementioned frontal zone and the other located in the upper troposphere on the cyclonic side of the jetstream (see Fig. 23 b). These two zones can be clearly identified in the wind component normal to the cross-section which, through thermal wind balance, appear as zones of intense vertical wind shear. This double structure to the baroclinic zone can be traced back to the early stages of development of the model Storm though the two zones are not so clearly separated then.

The potential vorticity cross-section (Fig. 23 c) shows these two shear zones to be characterised by high PV, particularly the lower tropospheric frontal

region. The upper tropospheric PV feature can be identified with the tropopause fold associated with the subtropical jetstream. The extension of high PV values throughout the depth of the Storm core was highlighted by Hoskins and Berrisford (1988) and nicknamed the ' PV tower '. The relative humidity cross-section shows that the dry slot, which ultimately drives through the system in the middle and upper troposphere, is associated with fairly high PV values.

6. Discussion and Conclusions

An attempt has been made to deduce information concerning the dynamical structure of the October Storm through the study of numerical forecasts and high quality satellite imagery. Although the operational Fine-Mesh model forecast failed miserably to capture the formation of the Storm, an excellent forecast was obtained after the inclusion in the analysis of some late AIREP data. Given the fidelity with which the forecast replicates the unusually small scale and intensity of the depression, the simulation has been treated here as a substitute for a dynamically-consistent mesoscale dataset. No quantitative verification of the forecast has been possible due to the paucity of observations but satellite imagery has revealed aspects of the model cloud and humidity structure which are grossly in error .

As far as can be ascertained from operational and subjective analyses in a data sparse region, the Storm deepened by about 35 mb. in 24 hours which is an explosive deepening rate by the accepted definition (ie. 24 mb. over a period of 24 hours; Sanders and Gyakum, 1980) but not by any means unusual. What does seem remarkable about the development of the model Storm is the prolonged period of concentrated and intense ascent occurring near its core. In a study of a number of other explosive developments in the Fine-Mesh model (Shutts, 1989), it is notable how much broader in scale is the ascent region in general ; also,

any periods of intense ascent (< -70 mb./hr.) are usually short-lived (≈ 6 hours).

The diagnostic study carried out here was motivated by a single scientific hypothesis; namely, that the cloud head known to precede explosive developments which produce 'hurricane-like' cores, is a manifestation of intense slantwise convective ascent triggered by the approach of an upper level trough. The unusual lateral extent which characterises the cloud head was consequently assumed to result from the expansion of the outflow region beneath the tropopause. Likewise, it was assumed that the small scale and intensity of such developments was a direct result of vortex spin-up due to slantwise convective mass transfer. Reed and Albright (1986) make a similar suggestion in their study of an extreme cyclogeneis event in the Eastern Pacific and Kuo and Reed (1988) support this idea by carrying out a diagnostic analysis of a numerical simulation of the same event.

The study presented here is not inconsistent with these views though is unable to demonstrate that slantwise convection does actually takes place in the model. In fact we are on rather dangerous ground since slantwise convection is a quasi-two-dimensional concept and the Storm updraught region has a horizontal aspect ratio of order unity. Nevertheless, if parcel theory has any relevance, there ought to be a sense in which an isolated fluid parcel (rather than an infinite tube) perceives the lack of stability to slantwise displacements. Without a clearly defined theoretical model of isolated, free (or forced) slantwise convection, it is not possible to formulate the appropriate diagnostic tests. Extensive regions of the warm sector boundary layer of the Storm were found to have SCAPE values in excess of 1000 J Kg^{-1} which in parcel theory could be associated with convective velocities of > 45 ms^{-1}. In practice, dissipation and gravity wave excitation is likely to heavily damp the release of

kinetic energy.

The satellite imagery shows a definite double structure to the overall cloud mass throughout the development period of the Storm (and before). This takes the form of a cloud head, which is identified with stratiform cloud at the primary frontal surface, and dense cirrus of frontal and convective origin, close to, and on the warm side of the subtropical jet. The Fine-Mesh model simulation shows a similar double structure in the baroclinity, particularly in the mature phase of the Storm's development. In contrast the humidity field shows no evidence of two separate cloud systems and it is not until the dry slot finally overtakes the surface low (after 18Z) that the cloud mass is split. The lack of two separate cloud systems - in spite of the split baroclinity - is probably linked to a known, though unexplained, systematic tendency for excessive moistening of the model flow. Baroclinic double structure has been identified as a common feature of explosive deepeners in Fine-Mesh model simulations and is sometimes associated with the correct split cloud structure (Shutts, 1989).

The sensitivity experiments described in Section 5 showed that latent heat release was crucial to the Storm's formation. As much as two thirds of the central pressure deepening could be ascribed to the latent heat release - a larger figure than found in most other published case studies (Mullen and Baumhefner, 1988; Kuo and Reed, 1988). The best Fine-Mesh simulation was found to be insensitive to removal of the surface energy fluxes, the convective parametrization scheme or an increase in horizontal resolution - in agreement with the conclusions of Kuo and Reed (1988). Fine-Mesh forecasts at 75 and 40 km horizontal gridlengths, initialized with the 00Z Oct. 15 global analysis, were similar with the high resolution achieving an extra 3 mb. deepening of the Storm at T+24.

The Mesoscale model was able to simulate the extreme intensity of the warm front which crossed southern England during the evening and night of Oct. 15/16 with a potential temperature contrast of up to 10 K concentrated across about 2 model gridlengths. It also showed quite clearly, the split structure to the baroclinic zone with an intense sloping frontal surface and a separate primary jetstream on the warm side of the location of the surface front.

From a forecasting viewpoint, one is reassured that high resolution numerical models are capable of simulating such potentially damaging and life-threatening storms. Even so, the forecaster cannot rely on numerical products alone and must make the best use of satellite imagery and model diagnostics to complement his experience and intuition. The cloud head phenomenon and double structure are undoubtedly important clues that explosive cyclogenesis is about to take place. It is noteworthy that the Fastnet Storm of August 14 1979 was preceded by a cloud pattern very similar to the October Storm (Marshall, 1982).

The study presented here suggests that maps of SCAPE may help to indicate the degree of susceptability of the atmosphere to forcing by upper tropospheric short wave troughs. It is speculated that the small scale and vigour of depressions such as the October Storm and the Pacific storm studied by Reed and Albright (1986) may be associated with the organised release of slantwise convective available potential energy. A systematic study of SCAPE in a large number of high resolution forecasts will be needed to ascertain whether there is any useful association between the degree of instability and the tendency to form intense mesoscale low pressure systems.

Legends

Fig. 1 (a) Sea-level pressure at the analysis time 00Z Oct. 15 1987. Contour interval: 2 mb.

(b) Wind vectors and isotachs (knots) at the 250 mb. level at 00Z Oct. 15 1987; shaded region > 150 kts. Contour interval: 10 kts.

(c) Wet-bulb potential temperature at 850 mb. (°C) at 00Z Oct. 15 1987. Contour interval: 1°C.

(d) Potential vorticity on the 330 K isentropic surface (light shading, 6 to 10 PVU; dark shading > 10 PVU) with 900 mb. potential temperature superimposed for 00Z Oct. 15 1987. Contour intervals: 1 PV unit and 2.5 K respectively.

Figs. 2 a-d as above except for 12Z Oct. 15 1987.

Figs. 3 a-d as for Figs. 1 except for 00Z Oct.16 1987.

Fig. 4 Subjective analysis of the sea-level pressure at 00Z Oct. 16 1987 due to Woodroffe (1988)

Figs. 5 a-e Vertical velocity at 700 mb. for (a) 00Z Oct. 15, (b) 06Z, (c) 12Z, (d) 18Z, (e) 00Z Oct. 16. Contour interval: mb./hr.

Figs. 6 a-c Q-vectors and temperature at 700 mb. for (a) 00Z Oct. 15, (b) 06Z, (c) 12Z. Contour interval: 2 K.

Fig.7 Wind vectors and wet-bulb potential temperature at 850 mb. for 06Z Oct. 15 1987 with the line of cross-section superimposed.

Figs. 8 Vertical cross-sections along the line indicated in Fig. 7 at 06Z Oct. 15 :

(a) Potential temperature. Cont. int. 1 K.

(b) Normal component of the wind (solid, cont. int. 5 ms^{-1}), potential temperature (dash-dot, cont. int. 5 K) and wind vectors in the plane of the cross-section.

(c) Vertical velocity (shaded area is for rising motion). Cont. int. 5 mb./hr.

(d) Relative humidity (shaded > 90%). Cont. int. 5%.

(e) Potential vorticity (shaded > 2 PV units). Cont. int. 1 PV unit. Note that the plot uses height as a vertical coordinate.

(f) Absolute momentum (solid) and wet-bulb potential temperature (dash-dot). Cont. int. 5 ms^{-1} and 1 K respectively.

Fig. 9 Tephigram along the M=110 ms^{-1} surface, environment curve (thick solid), dew point curve (dashed), dots are taken from a vertical ascent and the thin solid lines are wet adiabats.

Fig. 10 a as for Fig. 7 except at 00Z Oct. 15.

Fig. 10 b as for Fig. 8f except for 00Z Oct. 15.

Fig. 10 c as for Fig. 9 except taken along the M=110 ms^{-1} line corresponding to the line of cross-section indicated in Fig. 10 a. Dewpoint curve omitted.

Figs. 11 a-c as for Figs. 10 except for 12Z Oct. 15 1987.

Fig. 12 (a) SCAPE values plotted in hundreds of J Kg^{-1} at 00Z Oct. 15.

(b) CAPE ,, ,, ,, ,,

Fig. 13 a NOAA-9 infra-red image (Channel 4) at 0453 Z on Oct. 15 1987.

Fig. 13 b Schematic picture of Fig. 13 a identifying cloud form definitions.

Fig. 14 400 mb. relative humidity at 06Z Oct. 15 (shaded > 90%). Cont. int. 10%.

Fig. 15 NOAA-9 satellite imagery IR (Ch. 4) at 1447 Z Oct. 15.

Fig. 16 400 mb. relative humidity (shaded > 90%) at 15Z Oct. 15 1987. Cont. int. 10%.

Fig. 17 400 mb. vertical velocity at 03Z on Oct. 15 1987. Cont. int. 10 mb./hr.

Fig. 18 Outline of the cloud boundaries across the baroclinic zone, inferred from cloud top temperature and the model's thermal structure

Fig. 19 Sea-level pressure maps from the Fine-Mesh model forecast initialized with the (interpolated) global model analysis for (a) 00Z Oct. 15 (analysis time) and (b) 00Z Oct. 16 . Cont. int. 5 mb.

Fig. 20 Vertical velocity at 700 mb. for 06Z Oct. 15 in the Fine-Mesh forecast from the global model analysis. Cont. int. 10 mb./hr.

Fig. 21 Sea-level pressure at T+24 (00Z Oct. 16) in the run without latent heat release. Cont. int. 5 mb.

Figs. 22 Mesoscale model forecast fields initialized with (and driven by) the best Fine-Mesh forecast from 12Z Oct. 15 :

(a) Sea-level pressure (cont. int. 2 mb.) and wind barbs (kts) at 00Z Oct. 16.

(b) Potential temperature at a height of 310 m. for 00Z Oct. 16. Cont. int. 1 K. Line along which cross-section were taken is indicated.

Fig. 23 Vertical cross-sections along the line shown in Fig. 22 b for 00Z Oct. 16 :

(a) Potential temperature. Cont. int. 2 K.

(b) Normal component of the wind. Cont. int. 5 ms^{-1}.

(c) Potential vorticity. Cont. int. 1 PV unit.

7. References

Anthes, R.A., Y.-H. Kuo and J.R. Gyakum (1983) ' Numerical simulations of a case of explosive marine cyclogenesis', Mon. Wea. Rev., 111, 1174-1188.

Browning, K.A. and K.M. Carpenter (1984) ' FRONTIERS five years on', Met. Mag. 113, 282-288.

Bosart, L.F. and S.C. Lin (1984)' A diagnostic analysis of the Presidents' Day storm of February 1979 ', Mon. Wea. Rev., 112, 2148-2177.

Bottger,H., M. Eckardt and U. Katergiannakis (1975) ' Forecasting extratropical storms with hurricane intensity using satellite information', J. Appl. Met., 14, 1259-1265.

Burt, S.D. and D.A. Mansfield (1988)' The Great Storm of 15-16 October 1987', Weather, 43, 90-114.

Durran, D.R. and D.B. Weber (1988) ' An investigation of the poleward edges of cirrus clouds associated with midlatitude jet streams', Mon. Wea. Rev., 116, 702-714.

Gyakum, J.R. (1983) ' On the evolution of the QE II storm. I : Synoptic aspects', Mon. Wea. Rev., 111, 1137-1155.

Emanuel, K. (1983) ' On assessing local conditional symmetric instability from atmospheric soundings', Mon. Wea. Rev., 111, 2016-2033.

Emanuel, K.A., M. Fantini and A.J. Thorpe (1987) ' Baroclinic instability in an environment of small stability to moist slantwise convection. Part I : Two-dimensional models'.

Gall, R.L., R.T. Williams and T.L. Clark (1987) ' On the minimum scale of surface fronts' J. Atmos. Sci., 44, 2562-2574.

Golding, B.W. (1987) ' Short range forecasting over the United Kingdom using a mesoscale forecasting system', *Short and Medium-range Numerical Weather Prediction*, p563, Met. Soc. Japan.

Hoskins, B.J. and P. Berrisford (1988) ' A potential vorticity perspective of the Storm of 15-16 October 1987', Weather, 43, 122-129.

Hoskins, B.J., I. Draghici and H.C. Davies (1978) ' A new look at the ω-equation' Quart. J. Roy. Met. Soc., 104, 31-38.

Hoskins,B.J., M.E. McIntyre and A.W. Robertson (1985) ' On the use and significance of isentropic potential vorticity maps', Quart. J. Roy. Met. Soc., 111, 877-916.

Kuo, Y.-H. and R.J. Reed (1988) ' Numerical simulation of an explosively deepening cyclone in the Eastern Pacific', Mon. Wea. Rev., 116, 2081-2105.

Lorenc, A.C., R.S. Bell, T. Davies and G.J. Shutts (1988) 'Numerical forecast studies of the October 1987 storm over Southern England', Met. Mag. 117 , 118-130.

Marshall, T.A. (1982) ' Weather satellite picture interpretation', Vol. 2, Directorate of Naval Oceanography and Meteorology, M.O.D., London.

Monk, G.A. and M.J. Bader (1988) ' Satellite images showing the development of the Storm of 15-16 October 1987', Weather, 43,

130-134.

Mullen, S. and D.P. Baumhefner (1988) ' Sensitivity of numerical simulations of explosive oceanic cyclogenesis to changes in physical parameterizations', Mon. Wea. Rev., 116, 2289-2329.

Oliver, V.J., R.K. Anderson and E.W. Ferguson (1964) 'Some examples of the detection of jetstreams from TIROS photographs', Mon. Wea. Rev., 92, 441-448.

Reed, R.J. and M.D. Albright (1986) ' A case study of explosive cyclogenesis in the Eastern Pacific', Mon. Wea. Rev., 114, 2297-2319.

Sanders, F. (1987) ' Skill of NMC operational dynamical models in prediction of explosive cyclogenesis', Weather and Forecasting, 2, 322-336.

Sanders, F. and J.R. Gyakum (1980) ' Synoptic-dynamic climatology of the 'bomb' ', Mon. Wea. Rev., 108, 1589-1606.

Shutts, G.J. (1987) Balanced flow states resulting from penetrative slantwise convection', J. Atmos. Sci., 44, 3363-3376.

Shutts, G.J. (1989) ' Frontal structure and slantwise stability in some Fine-Mesh model forecasts of cyclogenesis' (in prep.)

Shutts, G.J. and M.J.P. Cullen (1987) ' Parcel stability and its relation to semi-geostrophic theory', J. Atmos. Sci., 44, 1318-1330.

Thorpe, A.J. (1986) ' Synoptic scale disturbances with circular symmetry', Mon. Wea. Rev., 114, 1384-1389.

Uccellini, L.W., P.J. Kocin (1984) ' The Presidents' Day Cyclone of 18-19 R.A. Petersen, C.H. Wash and February 1979 : Synoptic overview and analysis K.F. Brill of the subtropical jet streak influencing the pre-cyclogenetic period', Mon. Wea. Rev., 112, 31-55.

Woodroffe, A. (1988) ' Summary of weather pattern developments of the storm of 15/16 October 1987', Met. Mag. 117 , 99-103.

Fig. 1

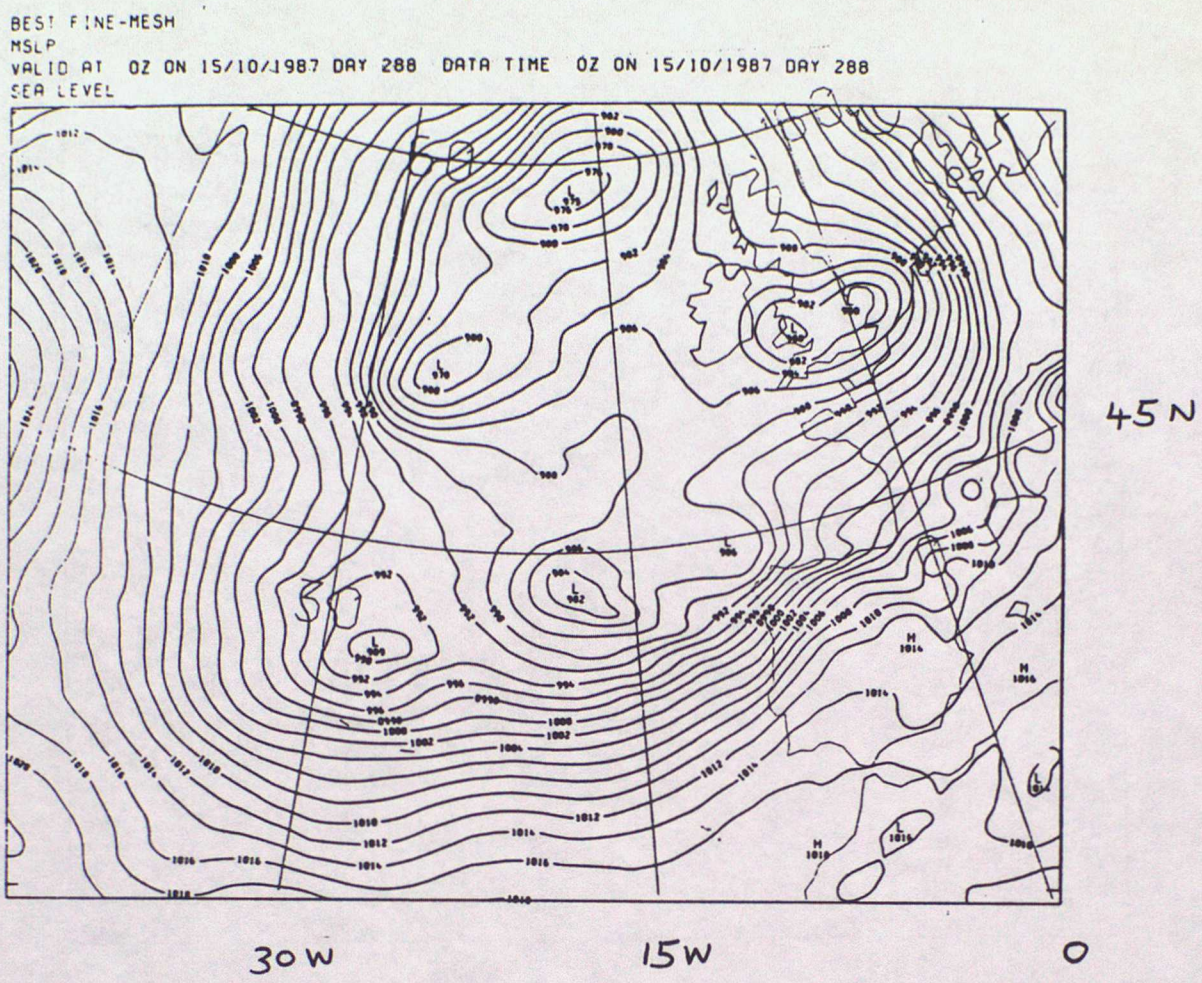

(a)

45 N

30 W 15 W 0

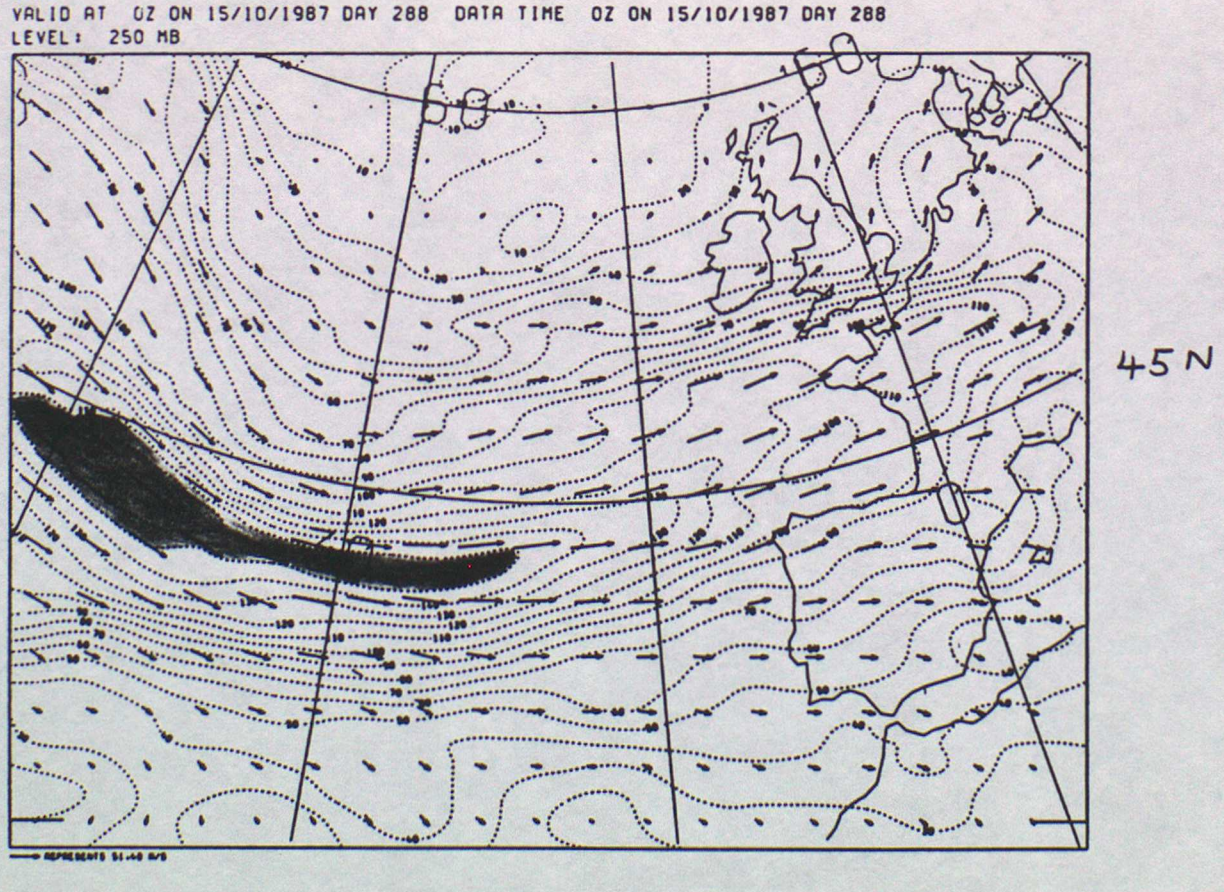

(b)

45 N

> 150 kts.

15 W 0

Fig 1

(c)

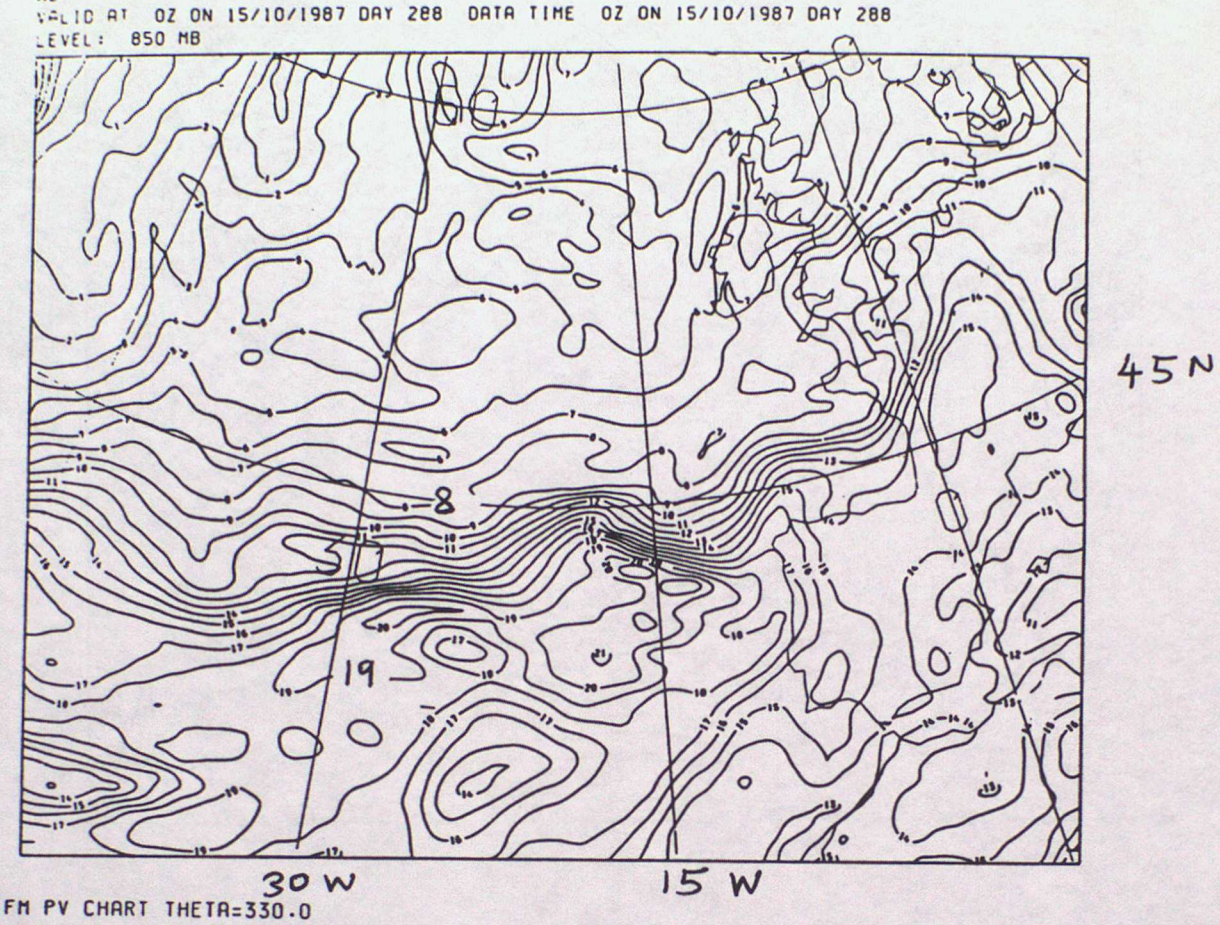
BEST FINE-MESH
VALID AT 0Z ON 15/10/1987 DAY 288 DATA TIME 0Z ON 15/10/1987 DAY 288
LEVEL: 850 MB
45N
30 W
15 W

(d)

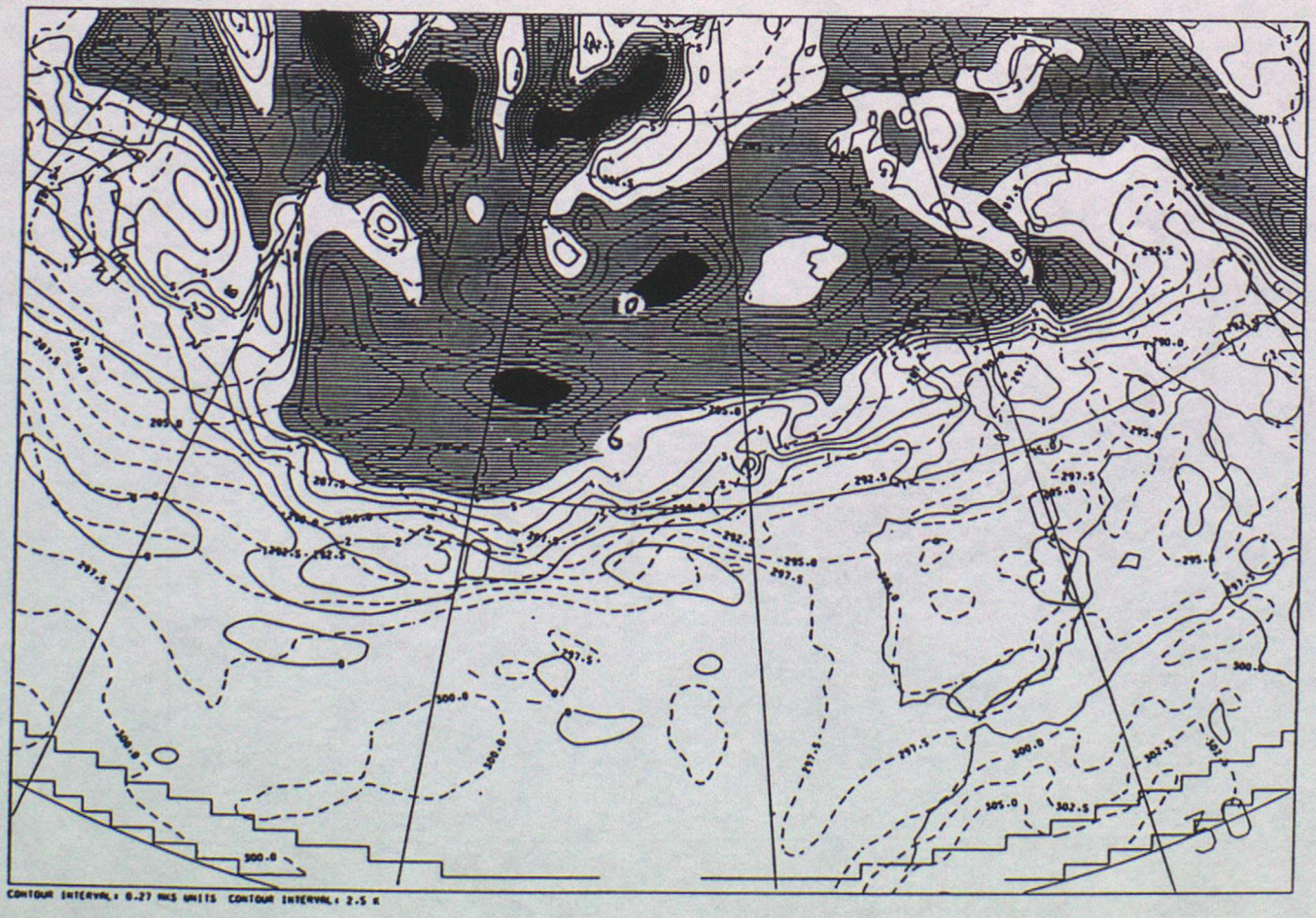
BEST FM PV CHART THETA=330.0
900MB POTENTIAL TEMPERATURE
VALID AT 0Z ON 15/10/1987 DAY 288 DATA TIME 0Z ON 15/10/1987 DAY 288
LEVEL: 50 MB
CONTOUR INTERVAL: 0.27 PVU'S CONTOUR INTERVAL: 2.5 K

Fig. 2

(a)

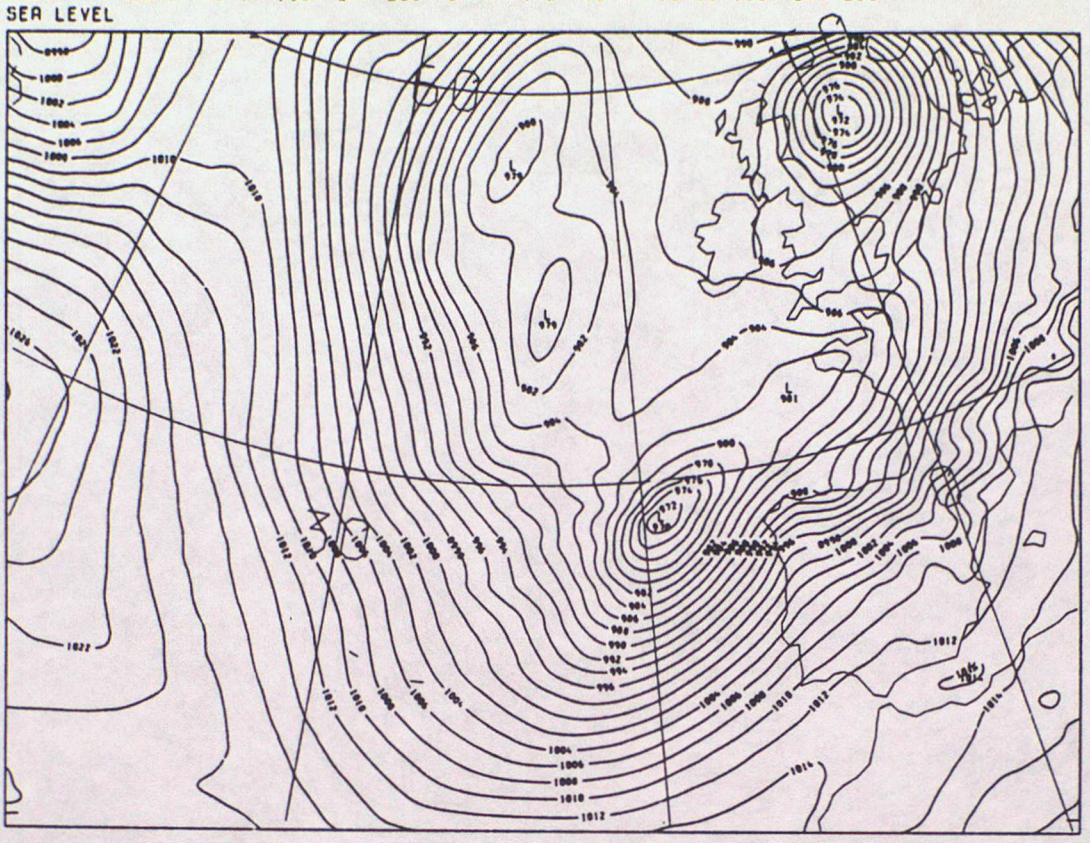

45N

30W 15W 0

(b)

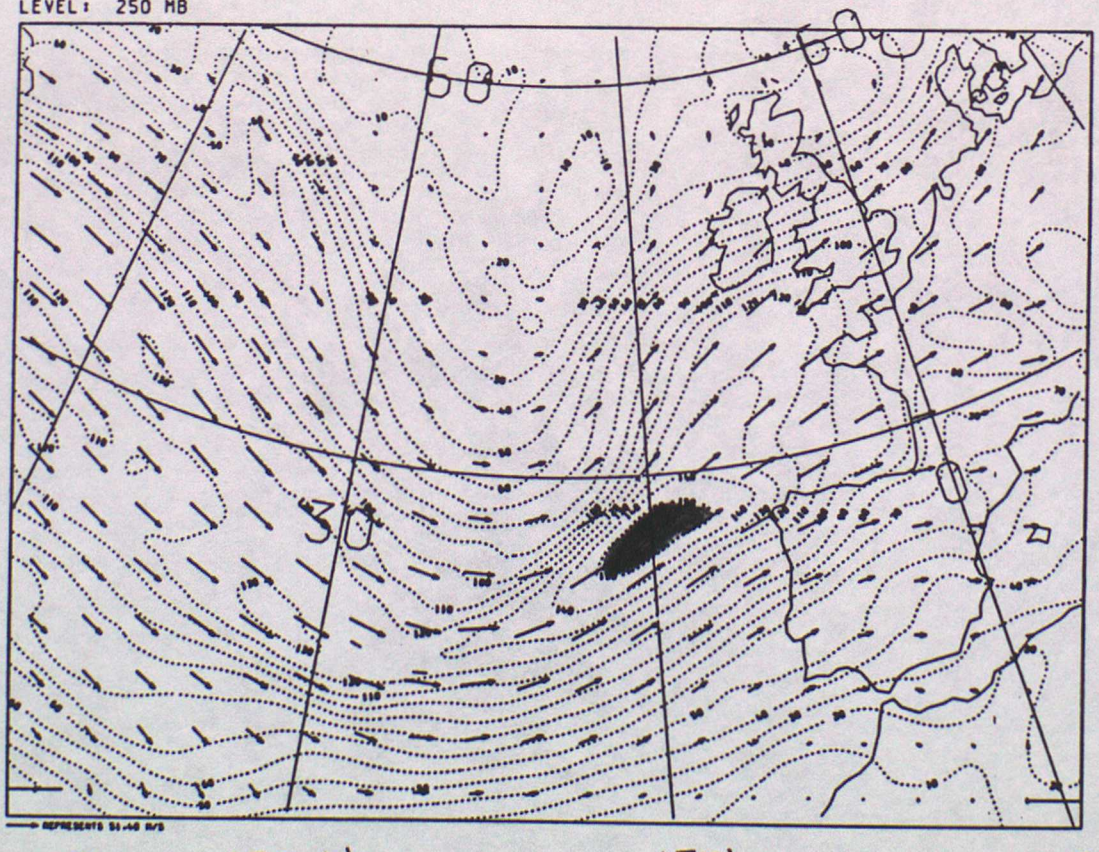

45 N

> 150 kts. 15W 0

Fig. 2

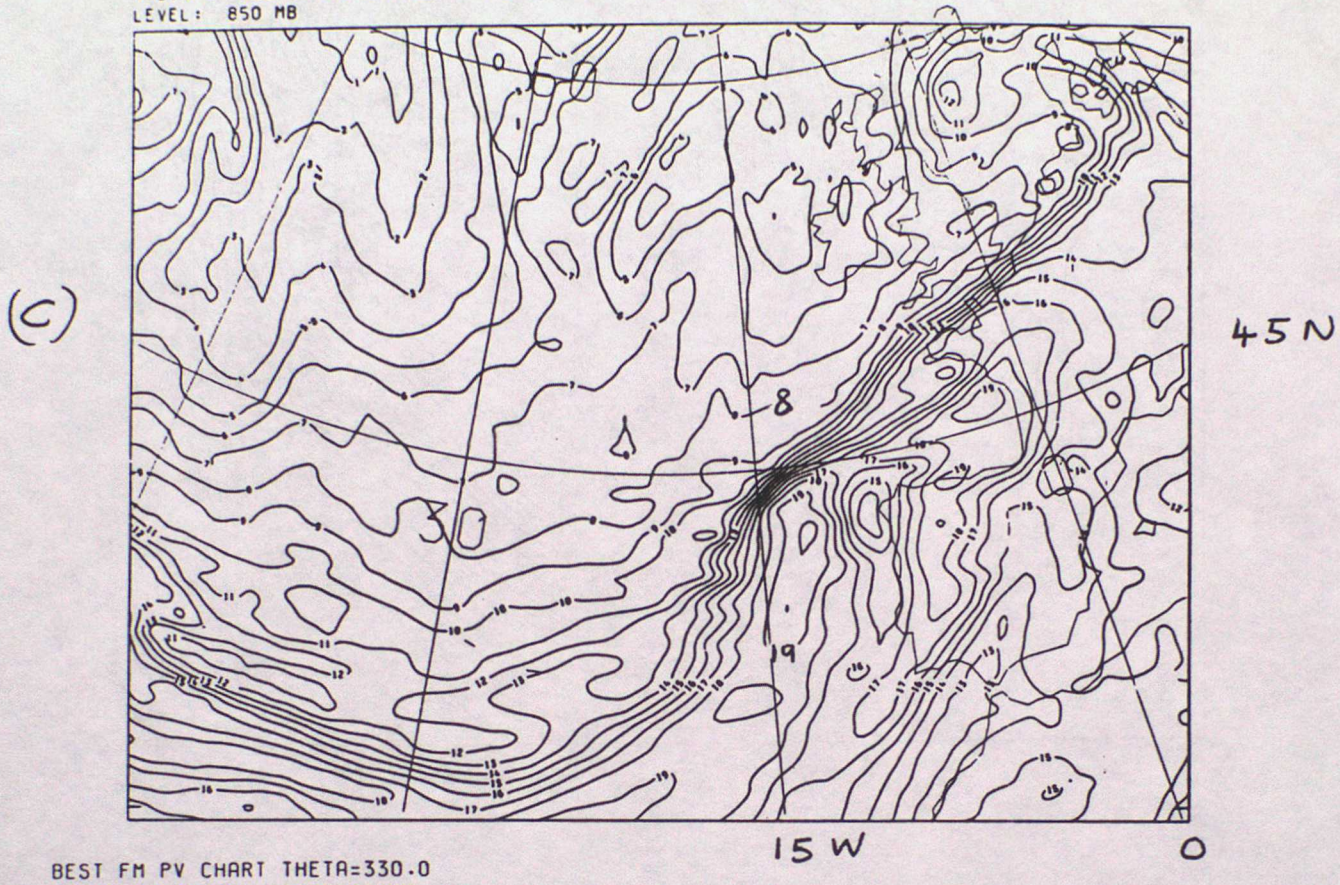
BEST FINE-MESH
HBPT
VALID AT 12Z ON 15/10/1987 DAY 288 DATA TIME 0Z ON 15/10/1987 DAY 288
LEVEL: 850 MB
(c)
45N
15 W
0

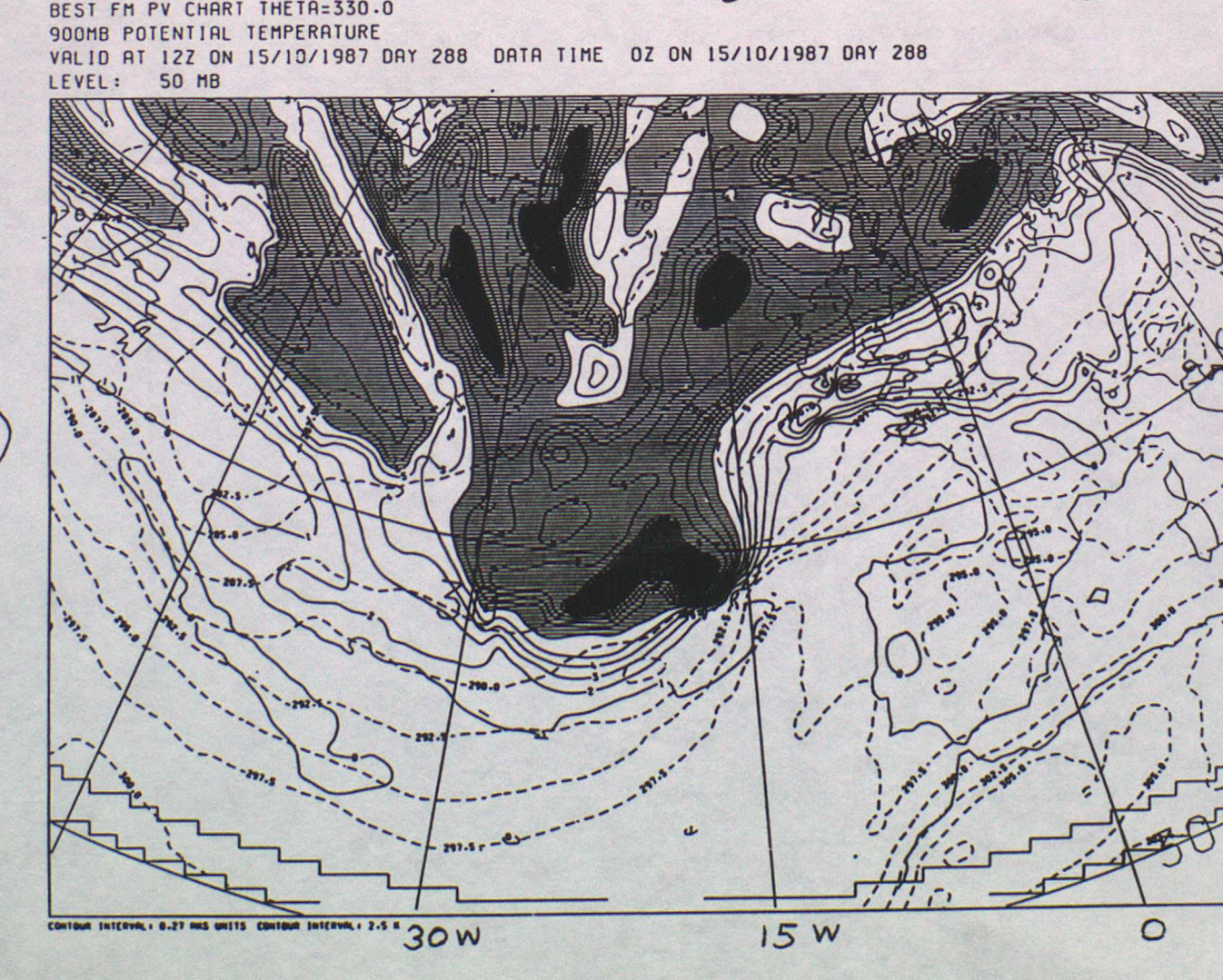
BEST FM PV CHART THETA=330.0
900MB POTENTIAL TEMPERATURE
VALID AT 12Z ON 15/10/1987 DAY 288 DATA TIME 0Z ON 15/10/1987 DAY 288
LEVEL: 50 MB
(d)
30W
15 W
0

Fig. 3

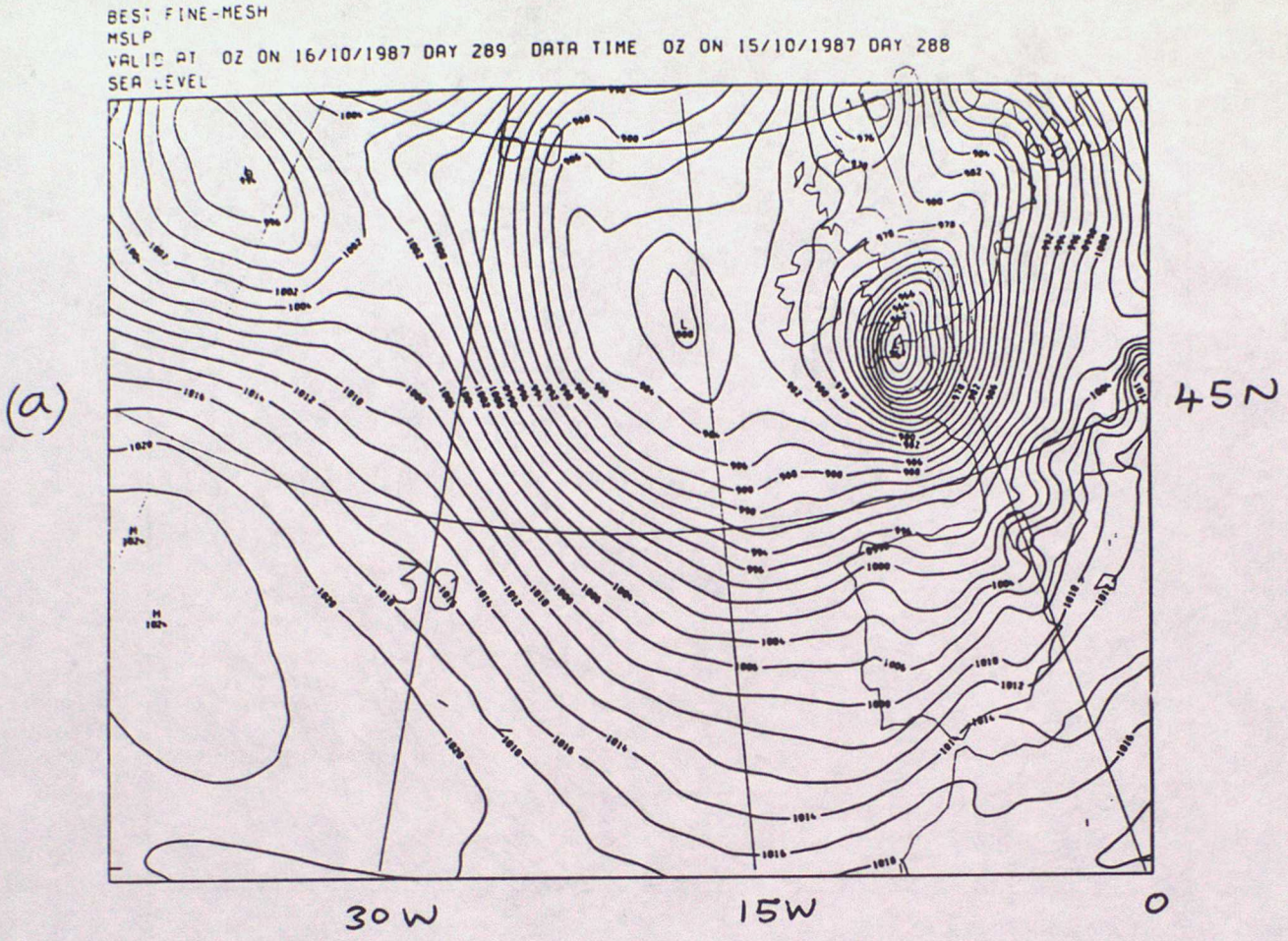
BEST FINE-MESH
MSLP
VALID AT 0Z ON 16/10/1987 DAY 289 DATA TIME 0Z ON 15/10/1987 DAY 288
SEA LEVEL
(a)
45N
30W
15W
0

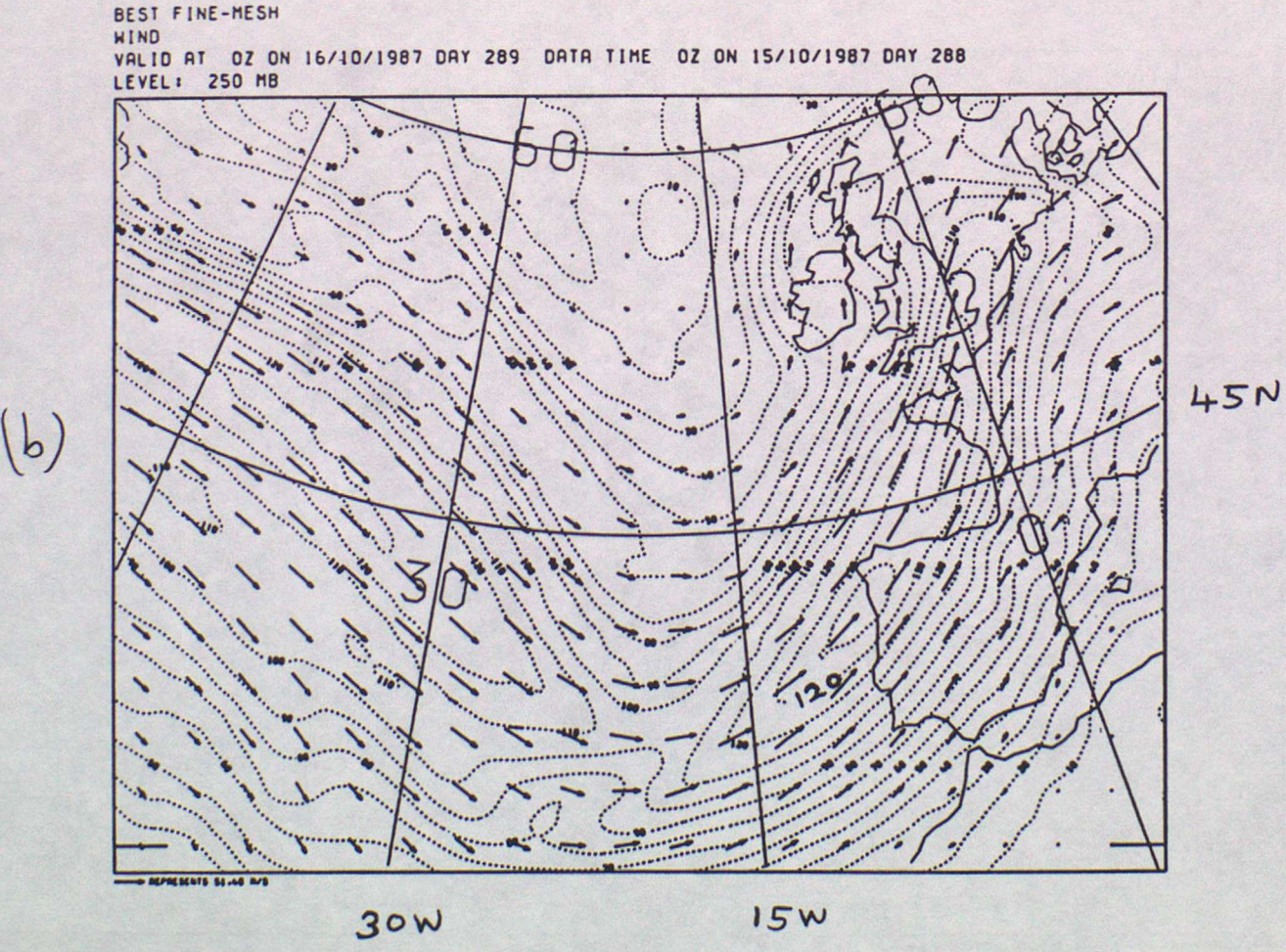
BEST FINE-MESH
WIND
VALID AT 0Z ON 16/10/1987 DAY 289 DATA TIME 0Z ON 15/10/1987 DAY 288
LEVEL: 250 MB
(b)
45N
30W
15W

Fig. 3

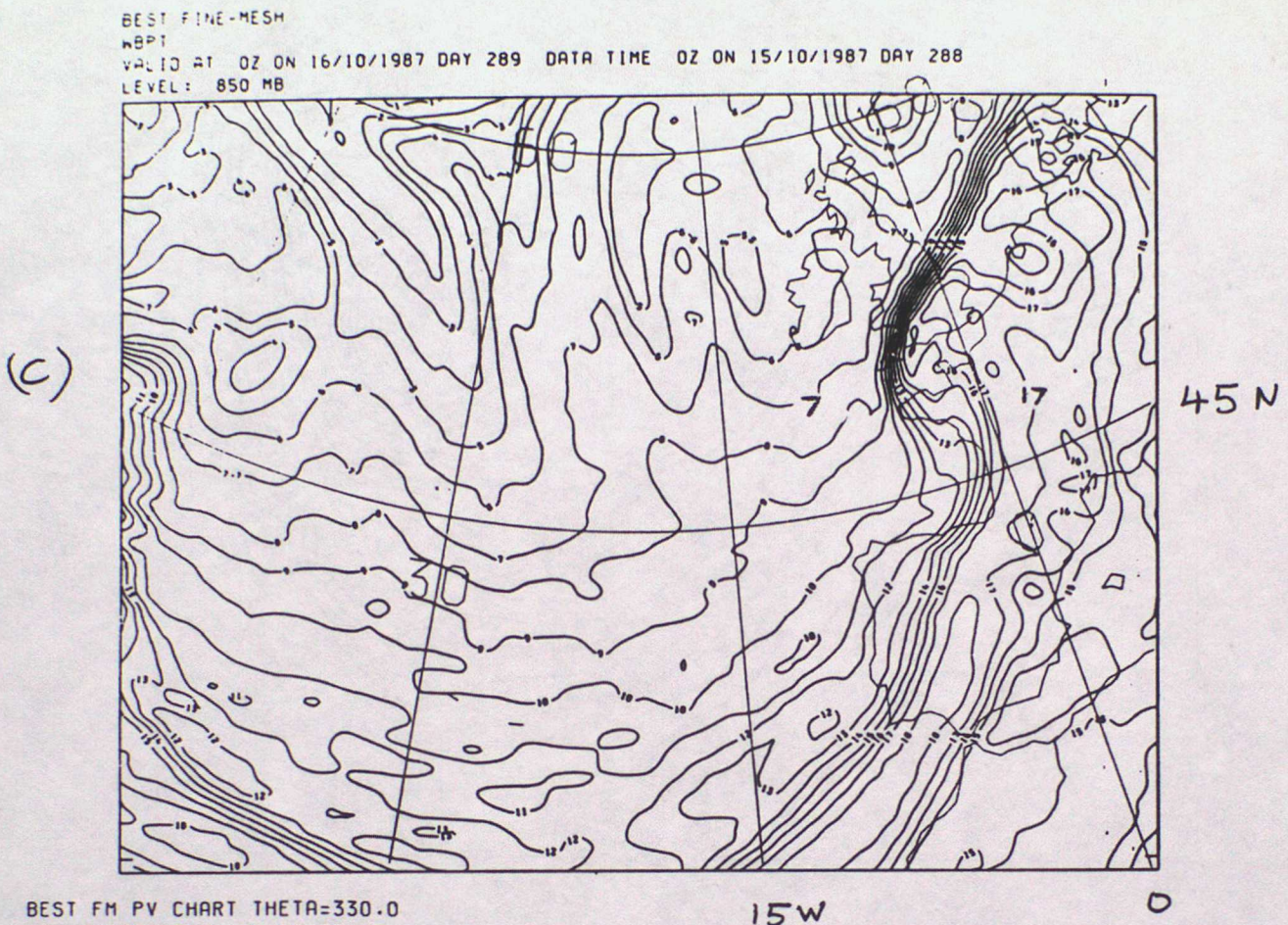
BEST FINE-MESH
MBPT
VALID AT 0Z ON 16/10/1987 DAY 289 DATA TIME 0Z ON 15/10/1987 DAY 288
LEVEL: 850 MB
(c)
45 N
15W
0

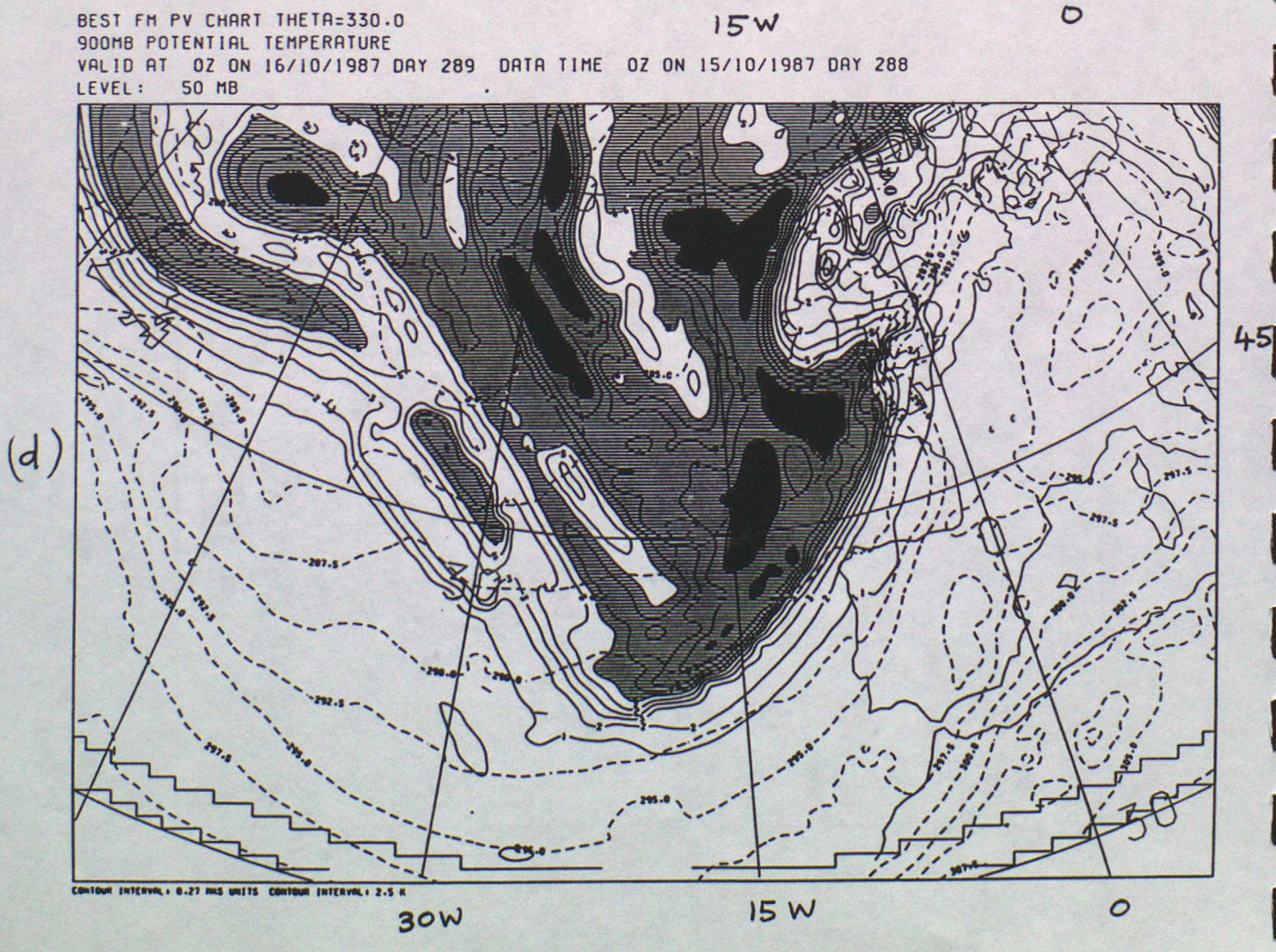
BEST FM PV CHART THETA=330.0
900MB POTENTIAL TEMPERATURE
VALID AT 0Z ON 16/10/1987 DAY 289 DATA TIME 0Z ON 15/10/1987 DAY 288
LEVEL: 50 MB
(d)
45
CONTOUR INTERVAL: 0.27 PVS UNITS CONTOUR INTERVAL: 2.5 K
30W
15 W
0

Fig. 4

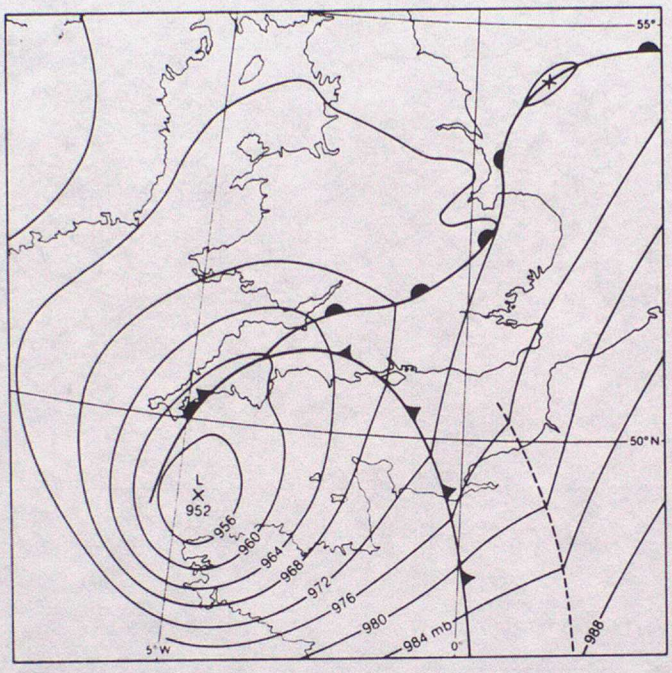

Fig. 5

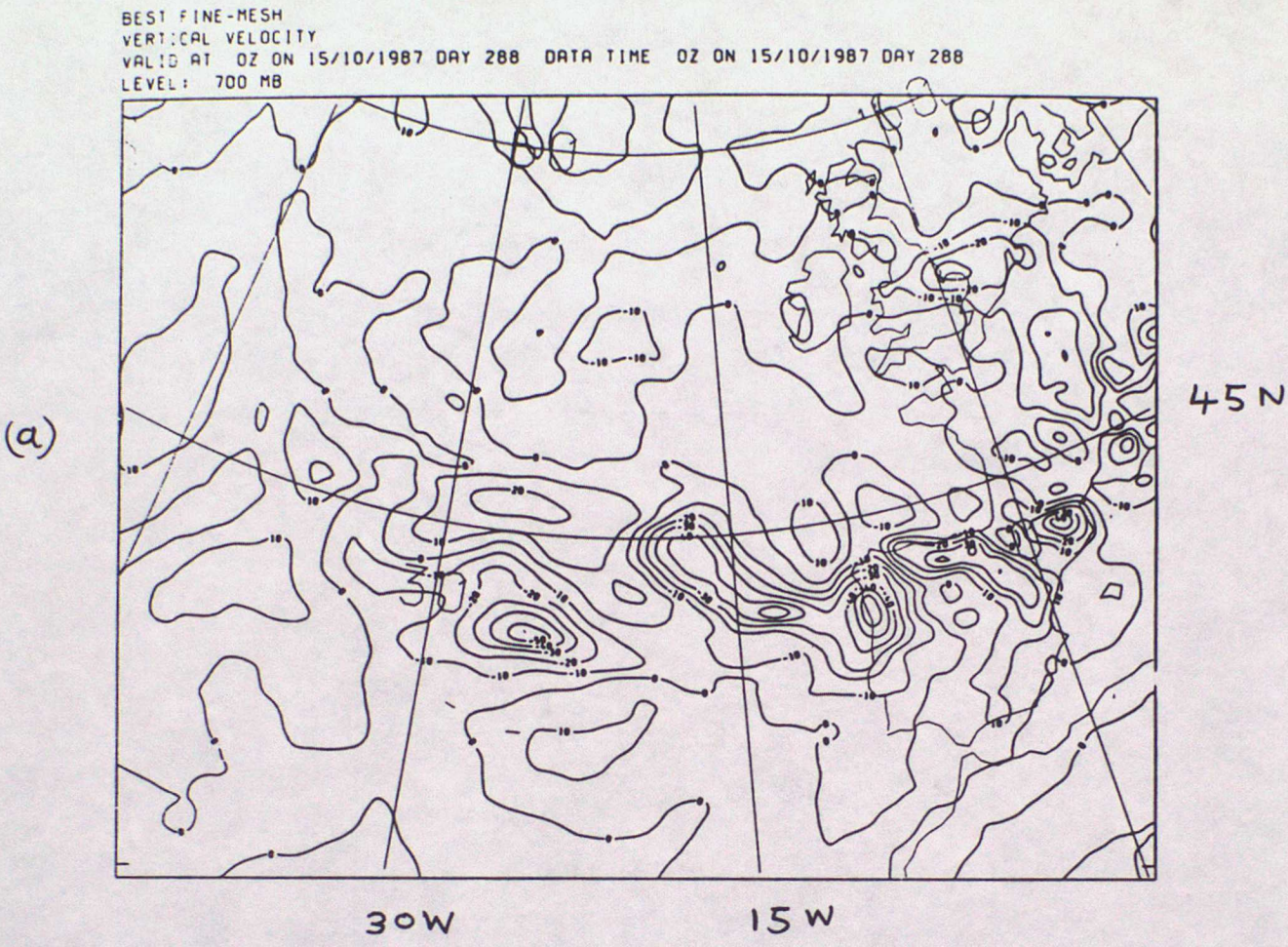
BEST FINE-MESH
VERTICAL VELOCITY
VALID AT 0Z ON 15/10/1987 DAY 288 DATA TIME 0Z ON 15/10/1987 DAY 288
LEVEL: 700 MB
(a)
45 N
30W
15 W

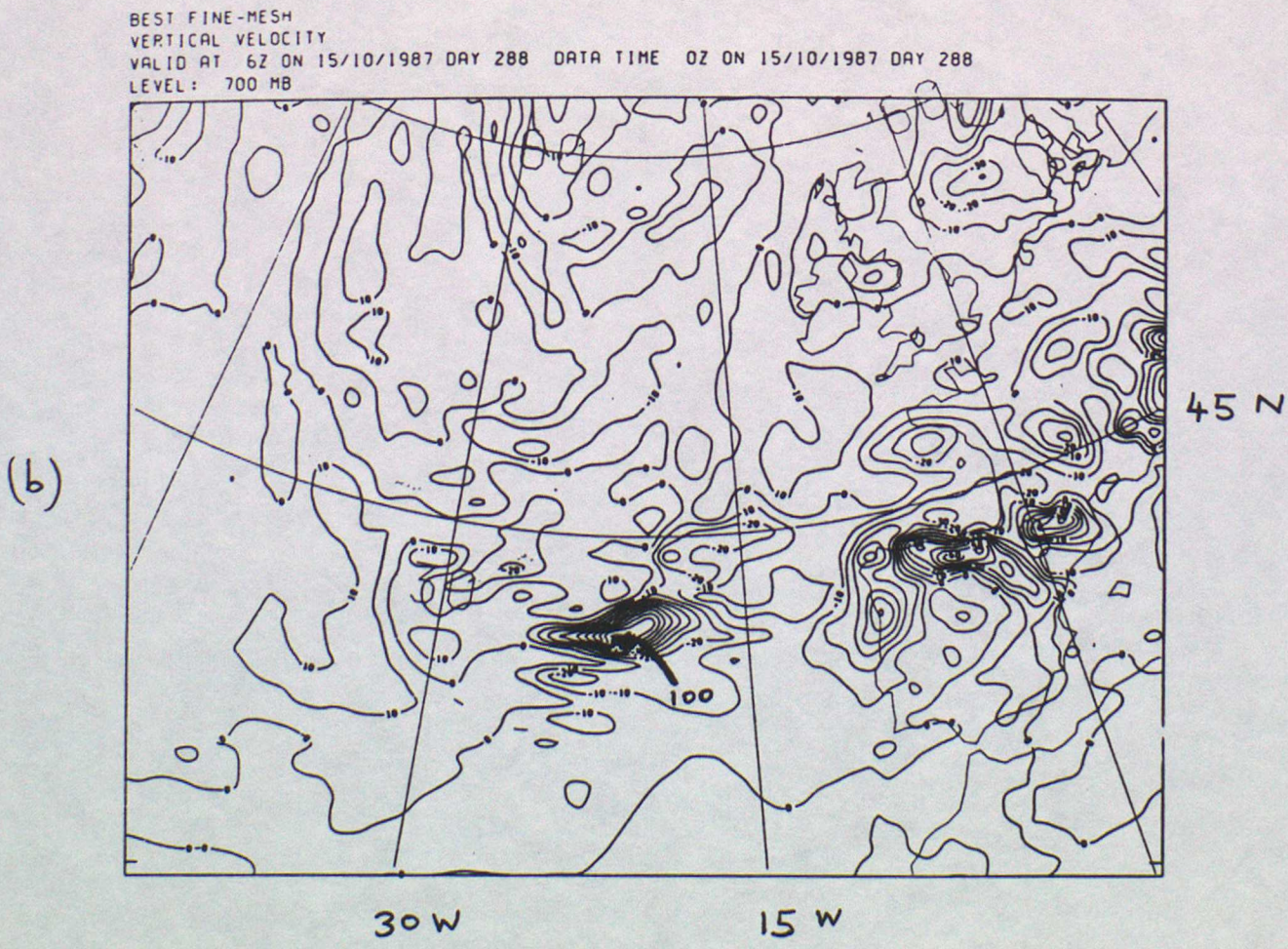
BEST FINE-MESH
VERTICAL VELOCITY
VALID AT 6Z ON 15/10/1987 DAY 288 DATA TIME 0Z ON 15/10/1987 DAY 288
LEVEL: 700 MB
(b)
45 N
100
30 W
15 W

Fig. 5

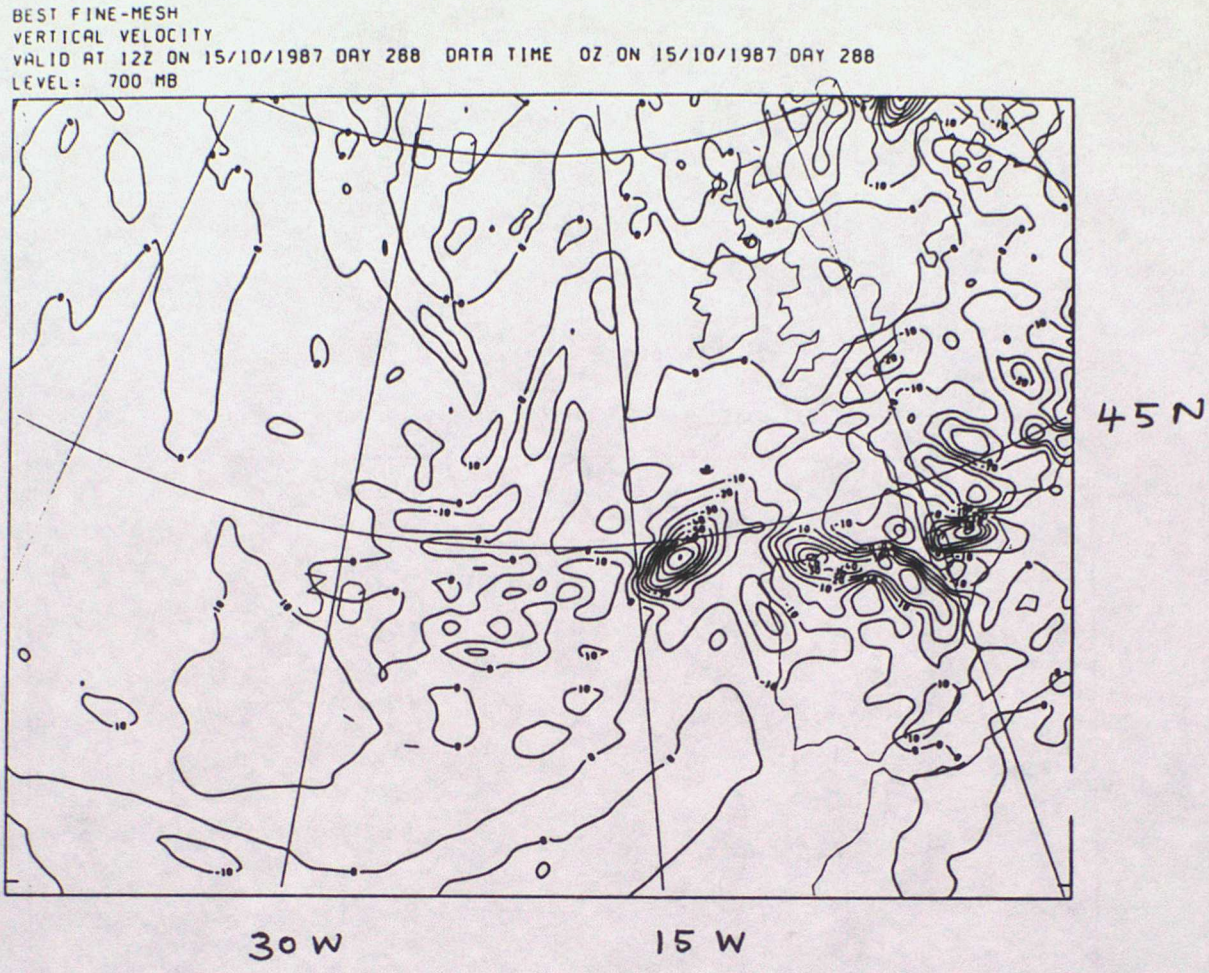
BEST FINE-MESH
VERTICAL VELOCITY
VALID AT 12Z ON 15/10/1987 DAY 288 DATA TIME 0Z ON 15/10/1987 DAY 288
LEVEL: 700 MB
(c)
45N
30W
15W

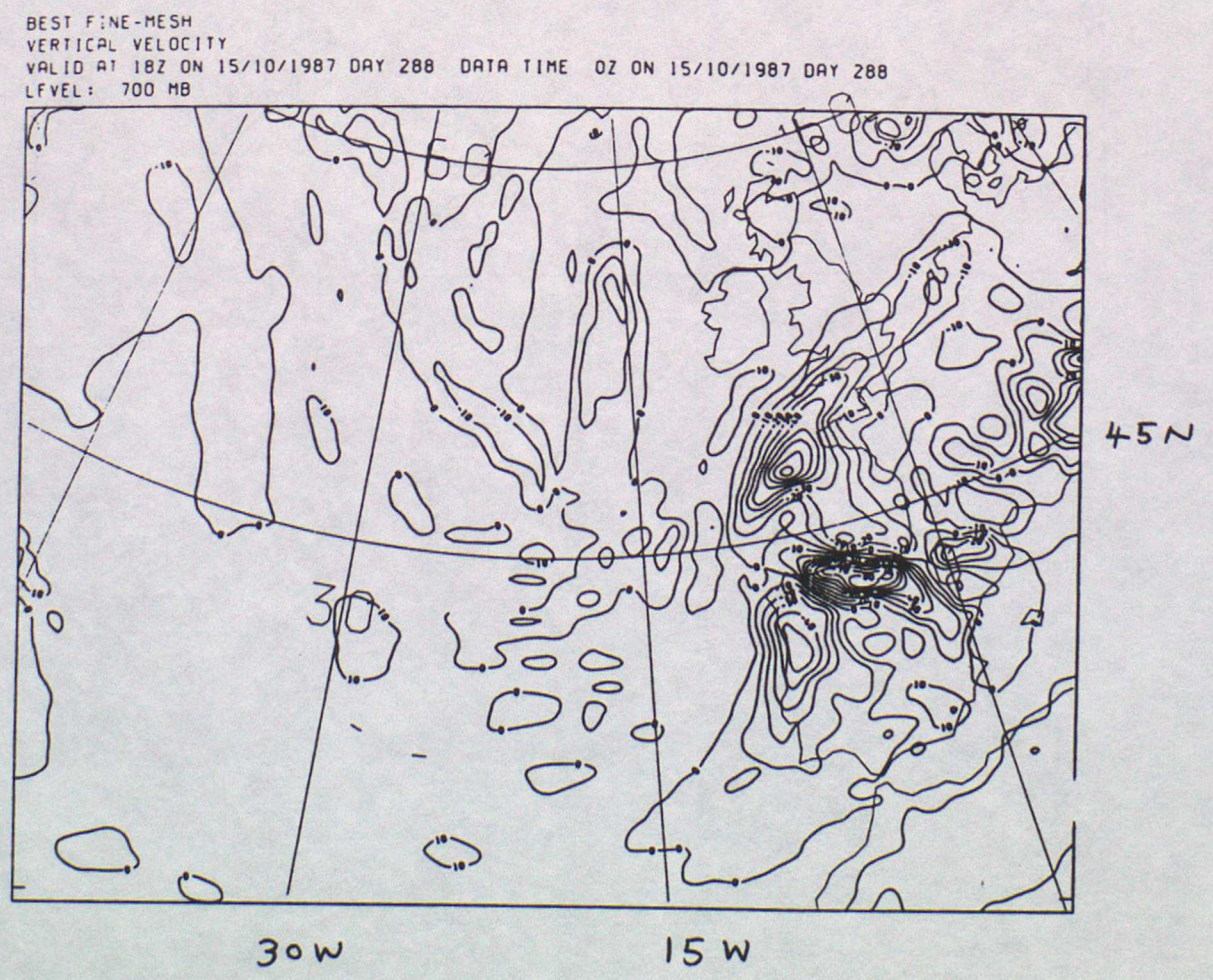
BEST FINE-MESH
VERTICAL VELOCITY
VALID AT 18Z ON 15/10/1987 DAY 288 DATA TIME 0Z ON 15/10/1987 DAY 288
LEVEL: 700 MB
(d)
45N
30
30W
15W

Fig. 5(e)

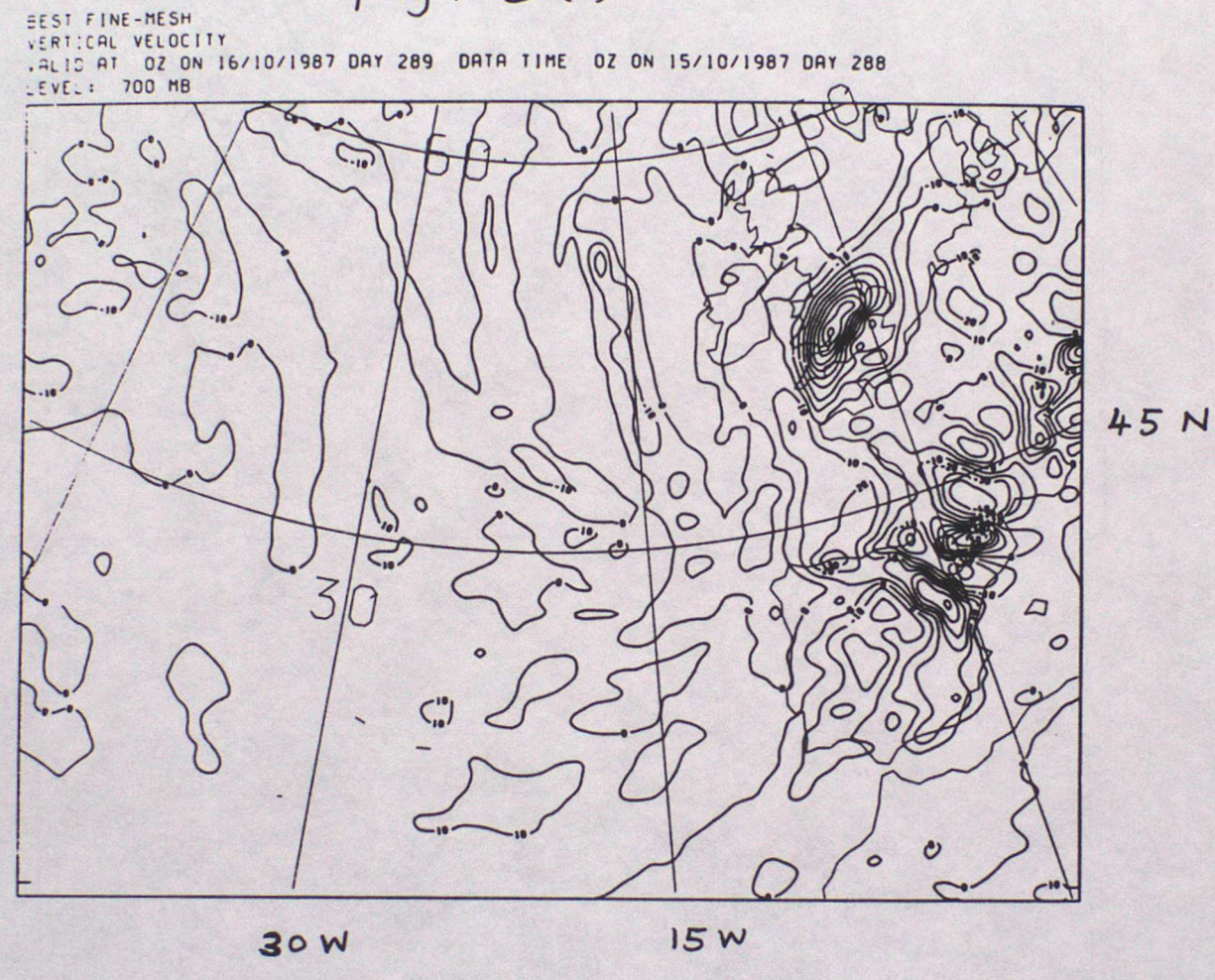
BEST FINE-MESH
VERTICAL VELOCITY
VALID AT 0Z ON 16/10/1987 DAY 289 DATA TIME 0Z ON 15/10/1987 DAY 288
LEVEL: 700 MB
30
45 N
30 W
15 W

Fig. 6

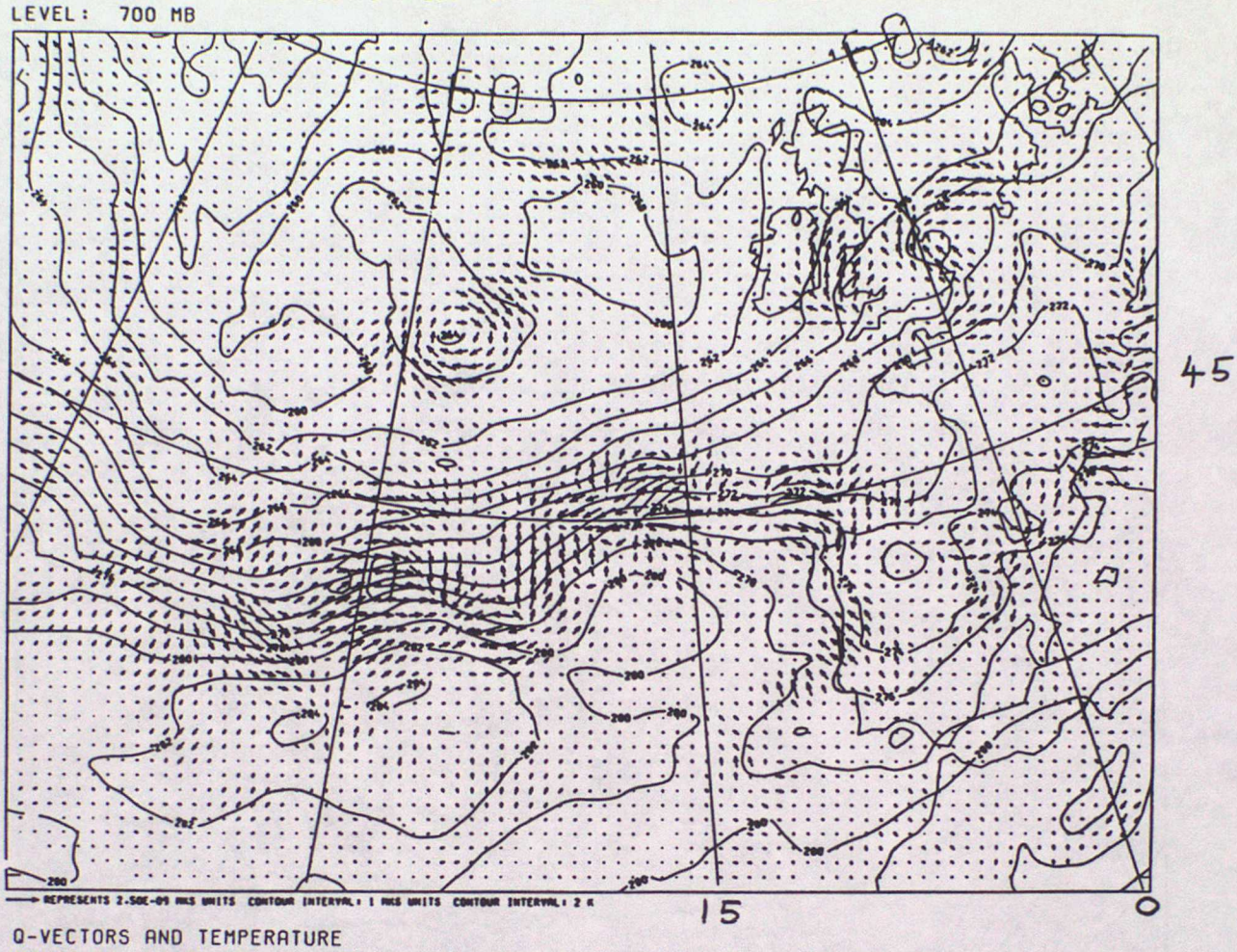
Q-VECTORS AND TEMPERATURE
VALID AT 0Z ON 15/10/1987 DAY 288 DATA TIME 0Z ON 15/10/1987 DAY 288
LEVEL: 700 MB
45
15
0

(a)

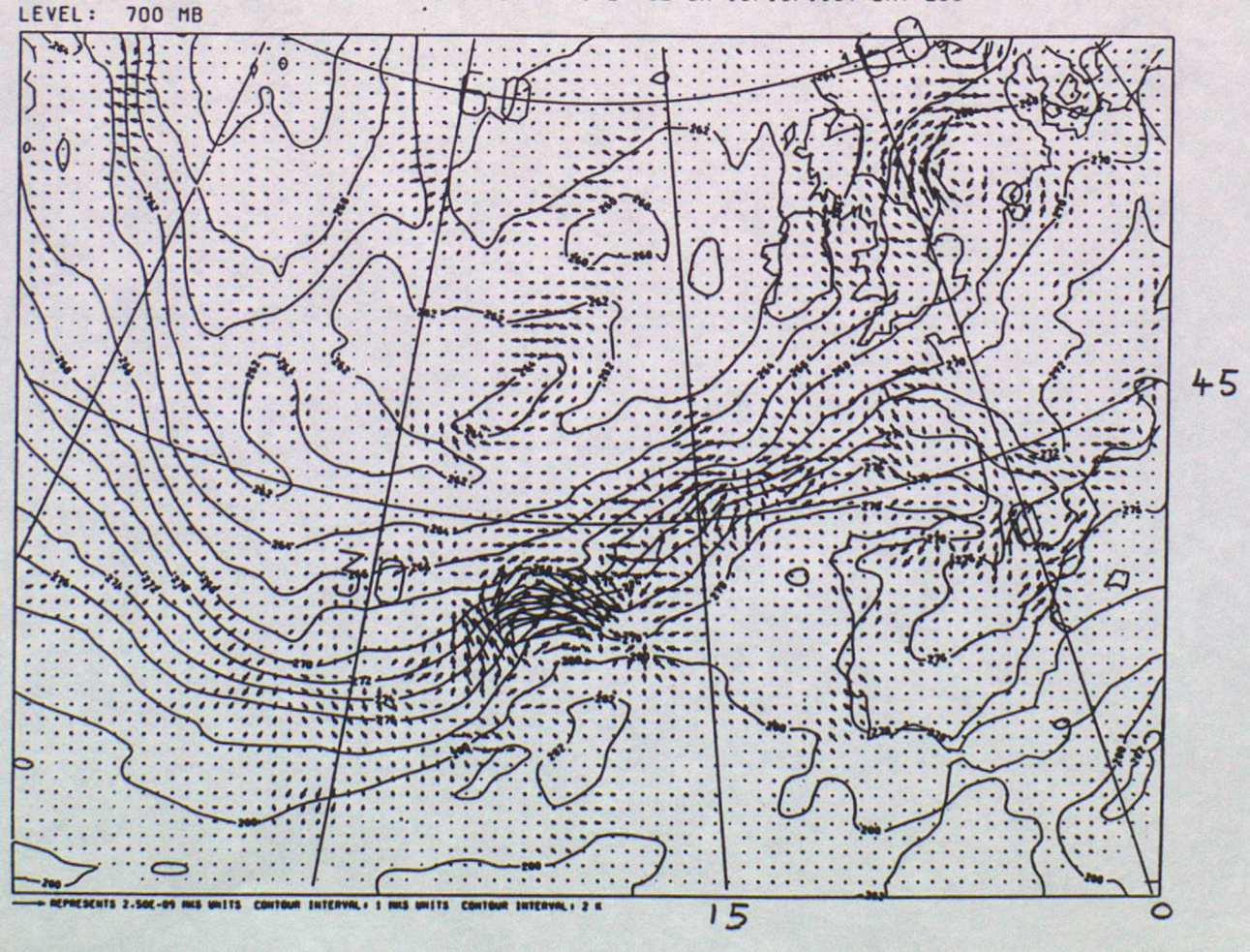
Q-VECTORS AND TEMPERATURE
VALID AT 6Z ON 15/10/1987 DAY 288 DATA TIME 0Z ON 15/10/1987 DAY 288
LEVEL: 700 MB
45
15
0

(b)

Fig. 6 (c)

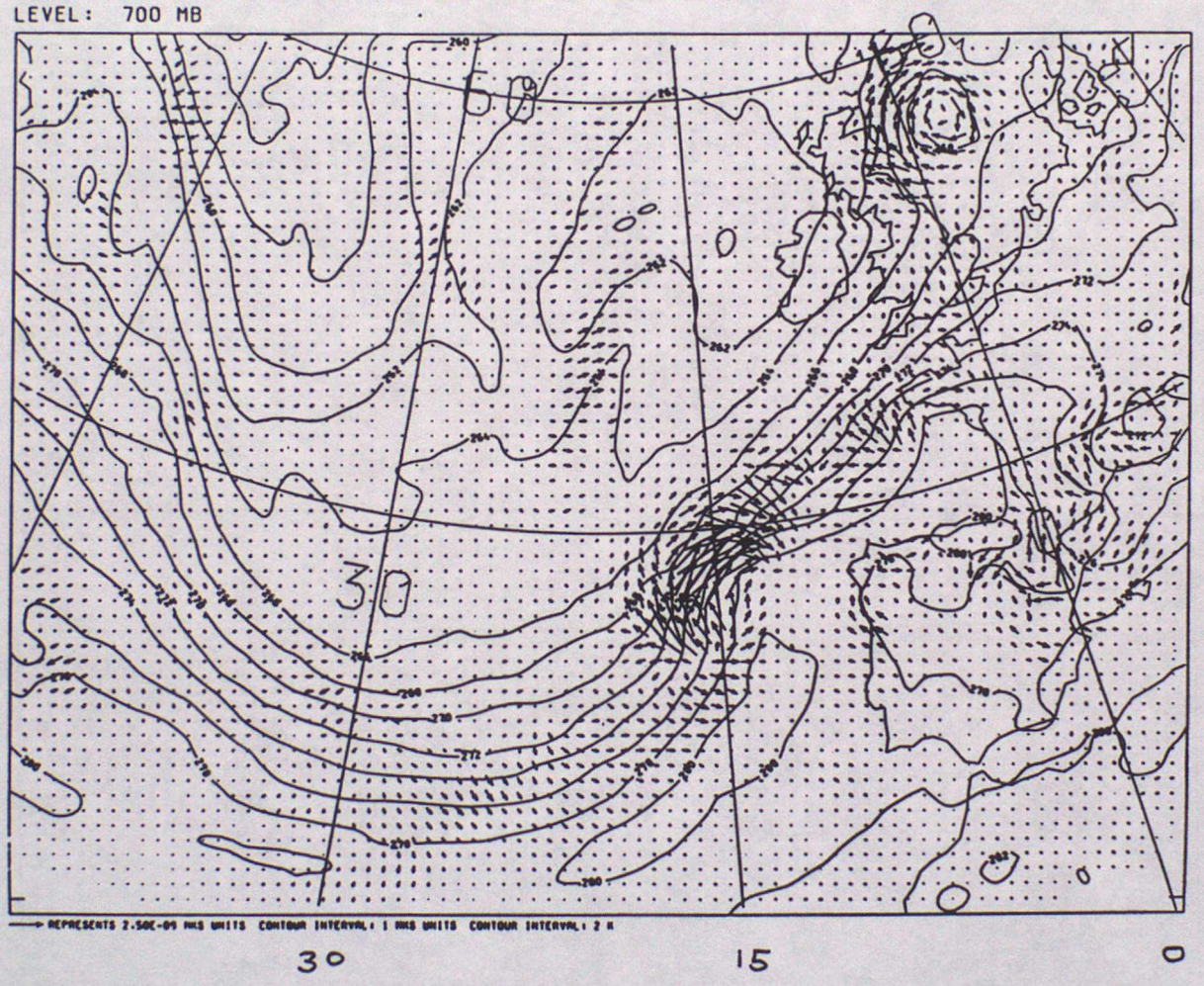
Q-VECTORS AND TEMPERATURE
VALID AT 12Z ON 15/10/1987 DAY 288 DATA TIME 0Z ON 15/10/1987 DAY 288
LEVEL: 700 MB
REPRESENTS 2.50E-09 MKS UNITS CONTOUR INTERVAL: 1 MKS UNITS CONTOUR INTERVAL: 2 K
45
30
15
0

Fig. 7

WET BULB POTENTIAL TEMP
BEST FM ANALYSIS
VALID AT 6Z ON 15/10/1987 DAY 288 DATA TIME 0Z ON 15/10/1987 DAY 288
LEVEL: 850 MB

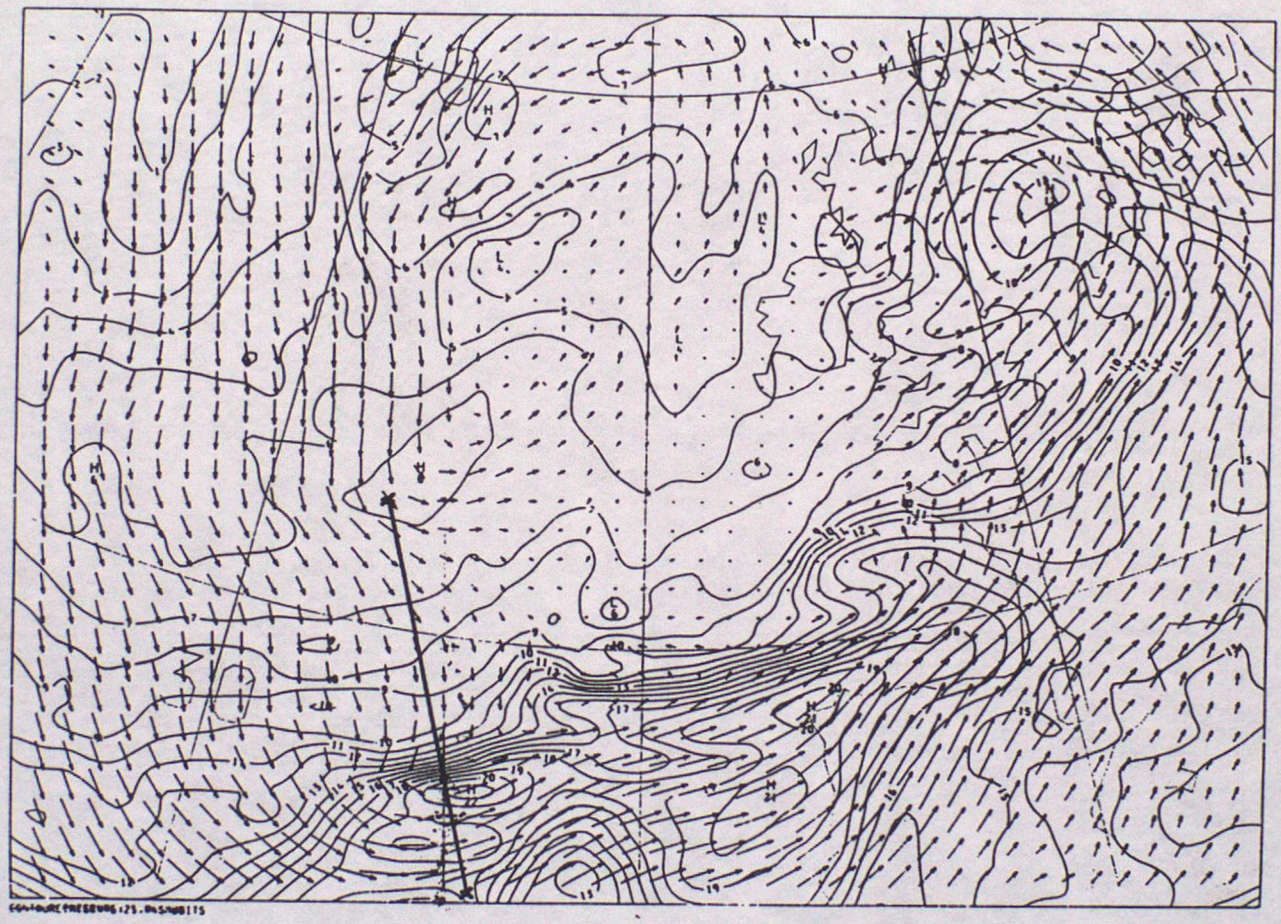

45

30 15 0

Fig. 8

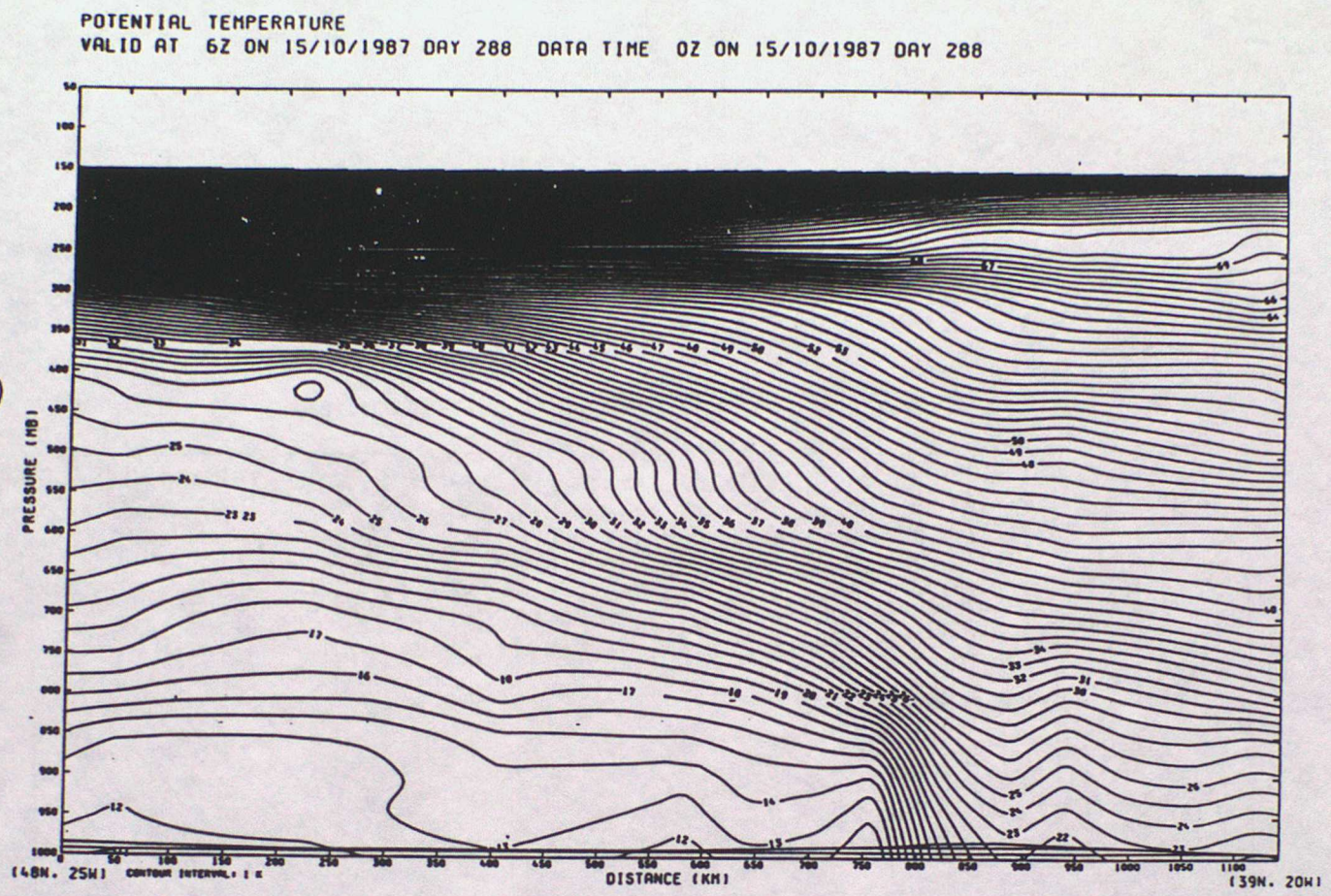
POTENTIAL TEMPERATURE
VALID AT 6Z ON 15/10/1987 DAY 288 DATA TIME 0Z ON 15/10/1987 DAY 288
PRESSURE (MB)
DISTANCE (KM)
(48N. 25W)
(39N. 20W)

(a)

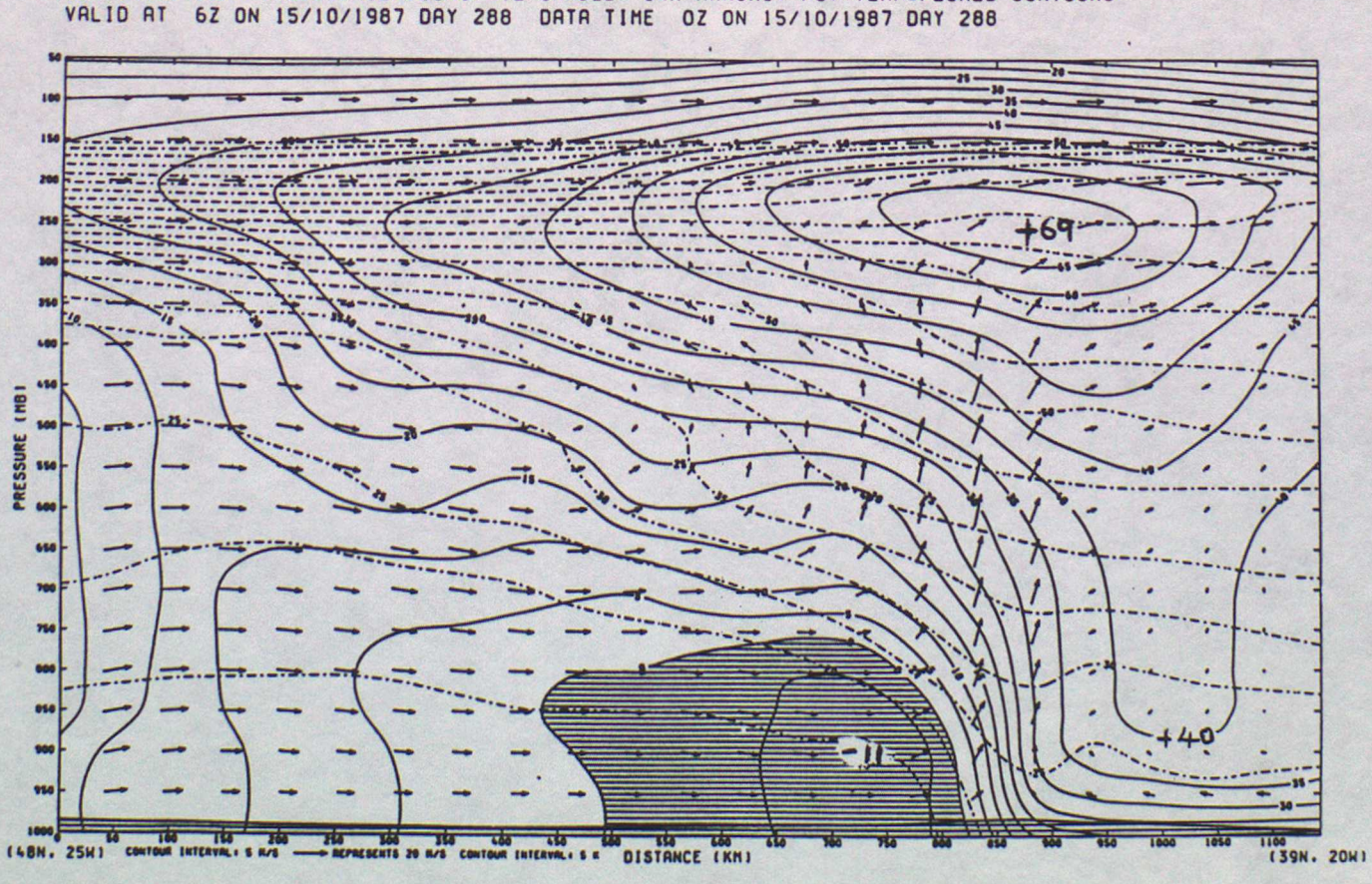
GC. X-SECTION. V=SOLID CONTOURS -VE SHADED. U&W ARROWS. POT.TEMP=PECKED CONTOURS
VALID AT 6Z ON 15/10/1987 DAY 288 DATA TIME 0Z ON 15/10/1987 DAY 288
PRESSURE (MB)
+69
+40
-11
DISTANCE (KM)
(48N. 25W)
(39N. 20W)

(b)

Fig. 8

(c)

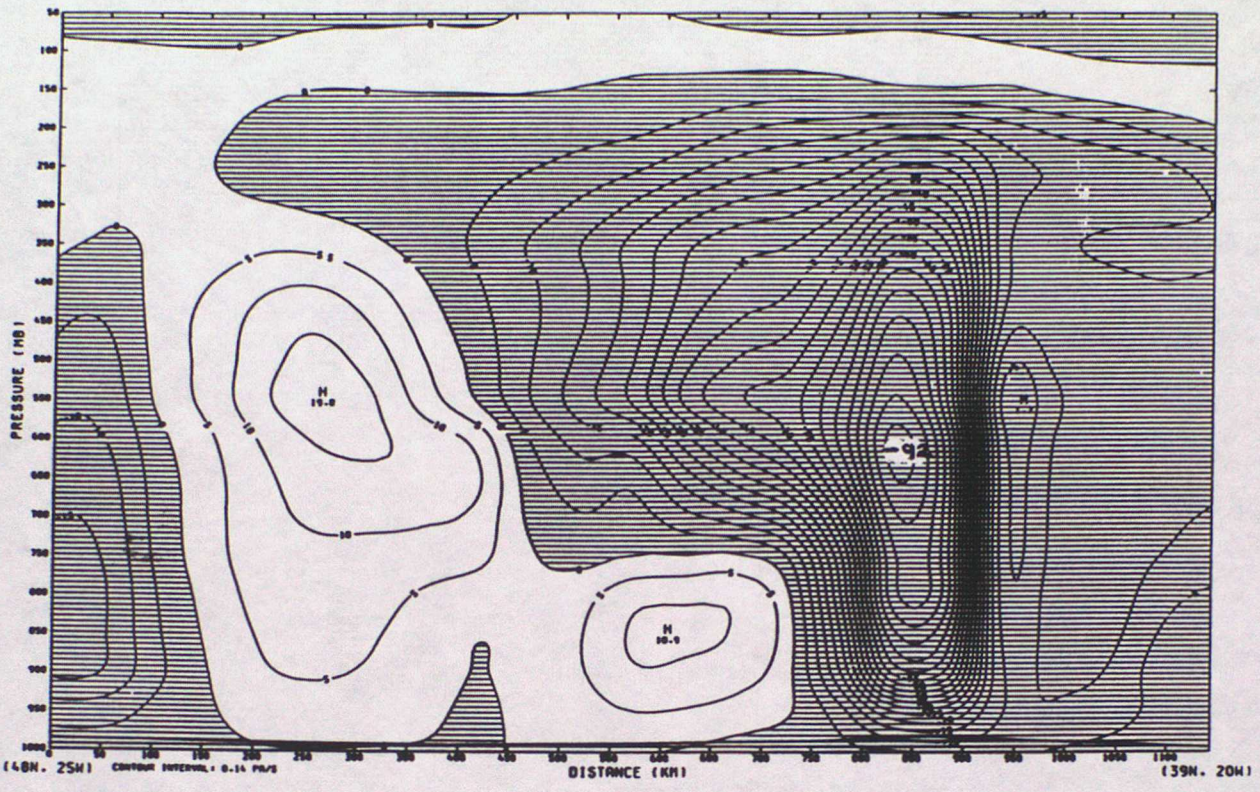
BEST FM
VERT VEL
VALID AT 6Z ON 15/10/1987 DAY 288 DATA TIME 0Z ON 15/10/1987 DAY 288
PRESSURE (MB)
DISTANCE (KM)
(48N. 25W)
(39N. 20W)

(d)

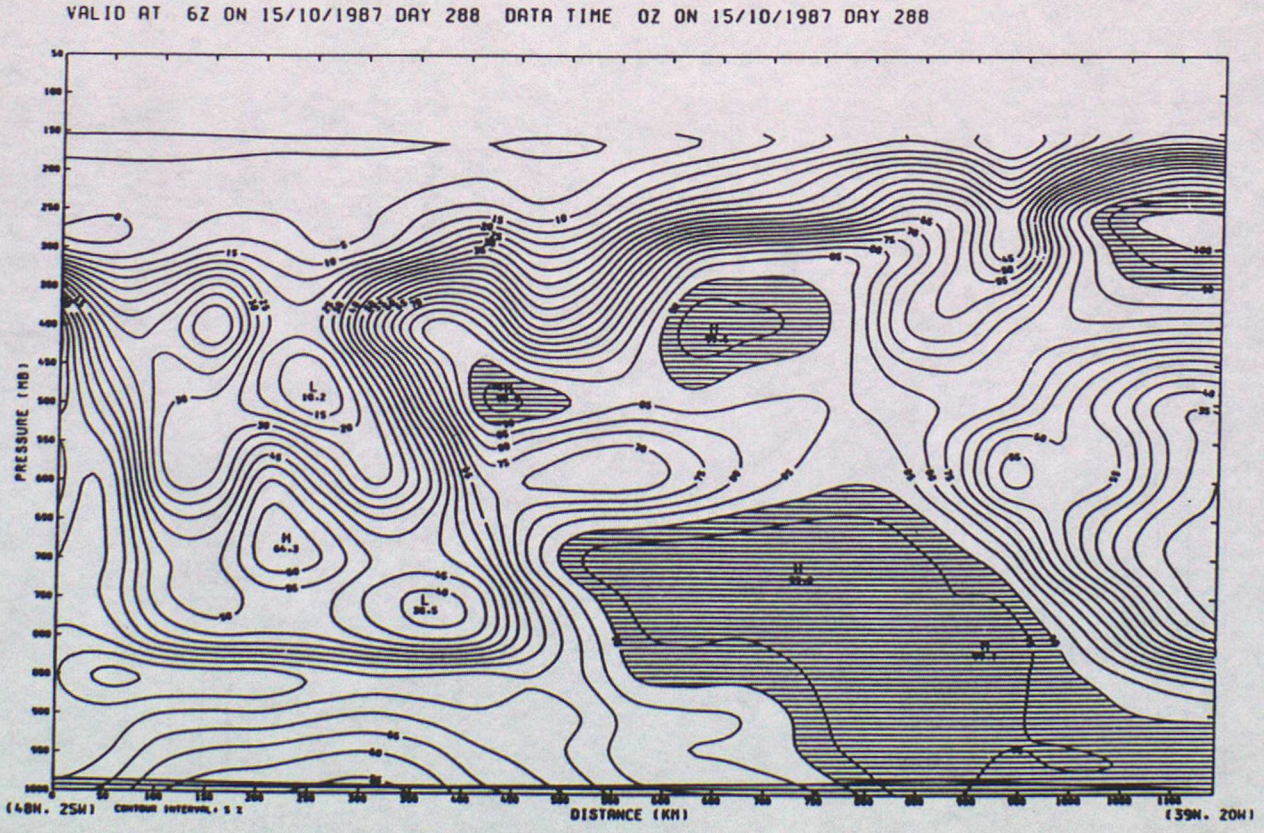
BEST FM
RELH
VALID AT 6Z ON 15/10/1987 DAY 288 DATA TIME 0Z ON 15/10/1987 DAY 288
PRESSURE (MB)
DISTANCE (KM)
(48N. 25W)
(39N. 20W)

Fig. 8

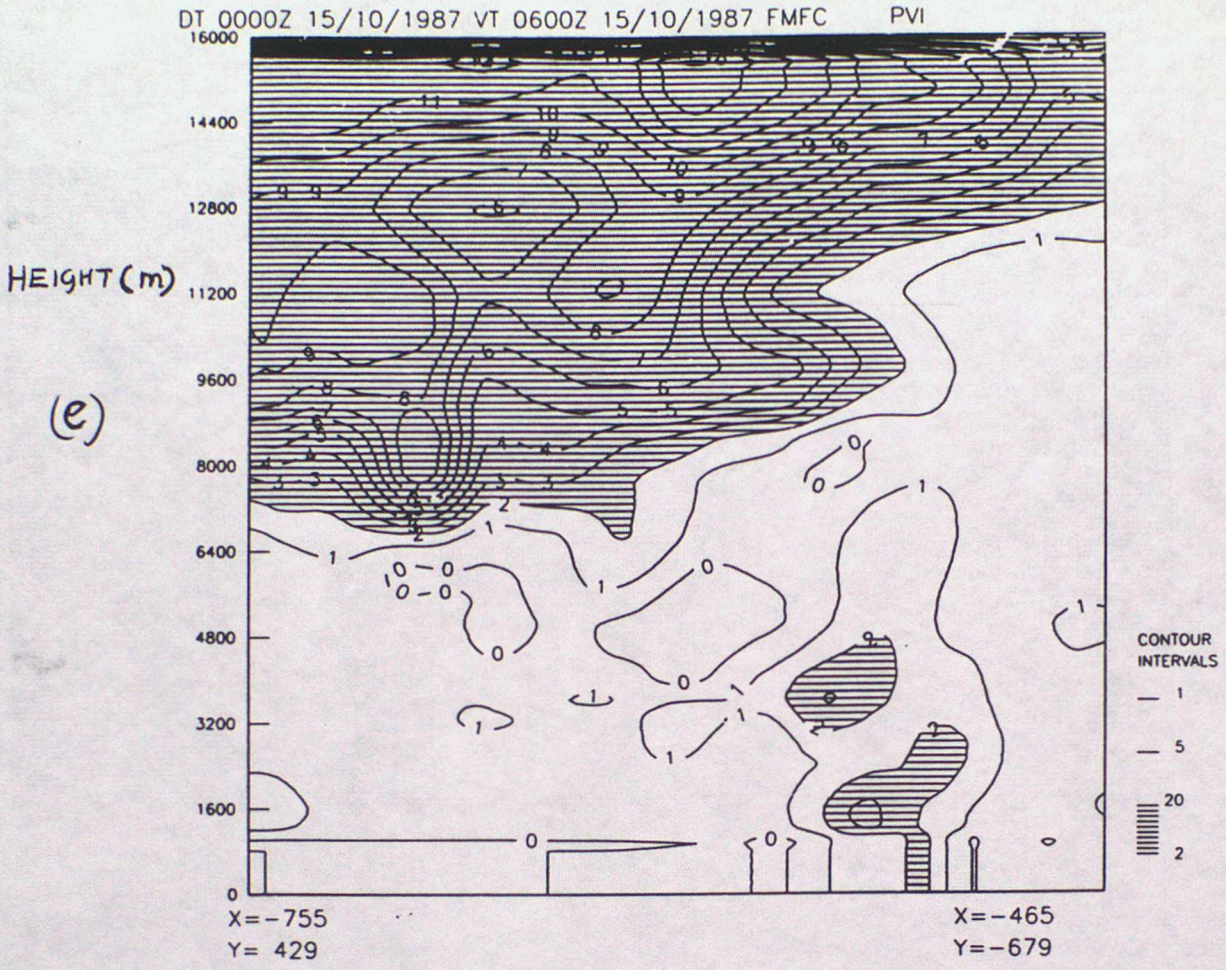
DT 0000Z 15/10/1987 VT 0600Z 15/10/1987 FMFC PVI
HEIGHT (m)
16000
14400
12800
11200
9600
8000
6400
4800
3200
1600
0
X=-755
Y= 429
X=-465
Y=-679
CONTOUR INTERVALS
1
5
20
2

(e)

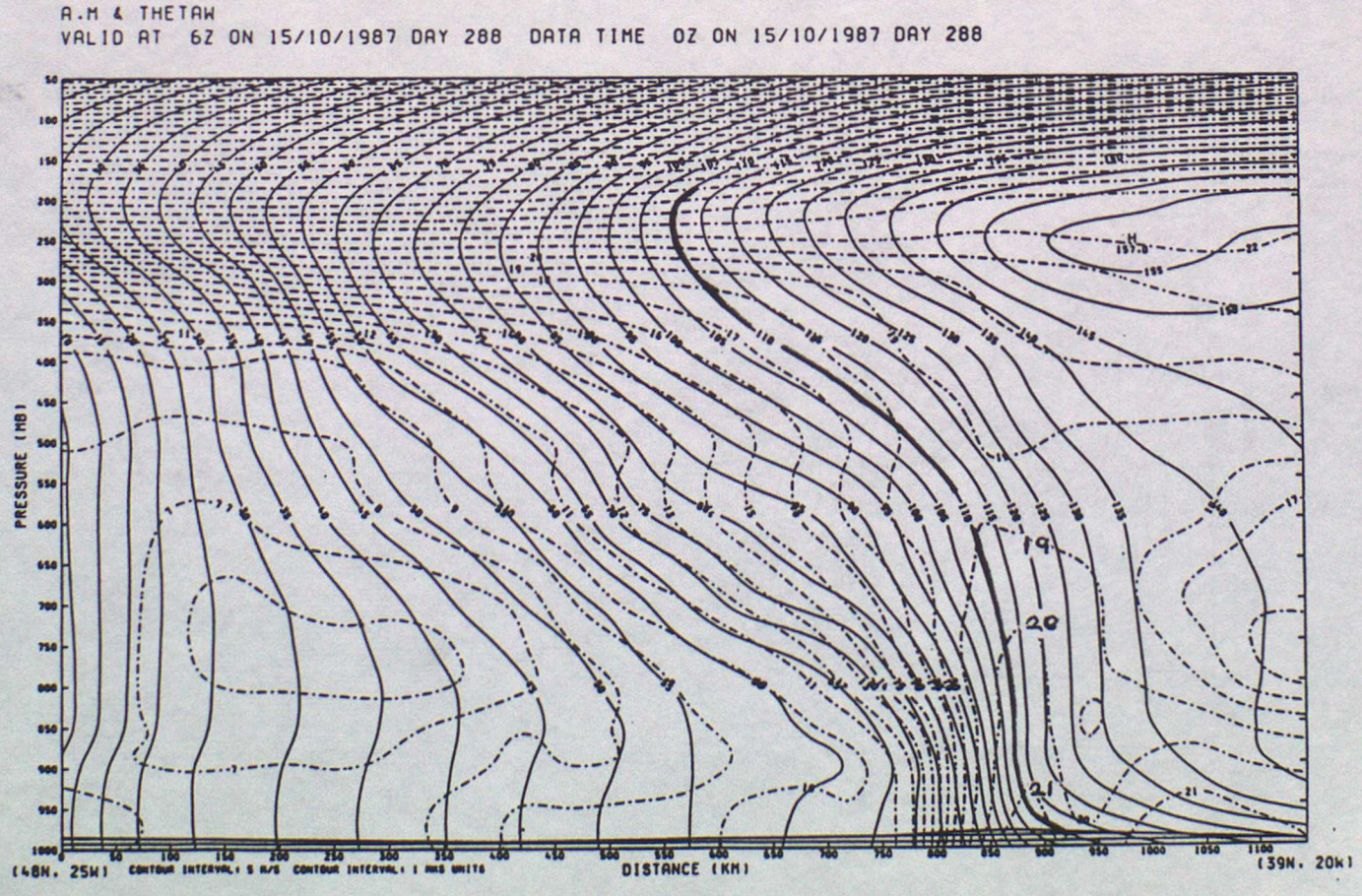
A.M & THETAW
VALID AT 6Z ON 15/10/1987 DAY 288 DATA TIME 0Z ON 15/10/1987 DAY 288
PRESSURE (MB)
DISTANCE (KM)
(48N, 25W)
(39N, 20W)

(f)

Fig. 9

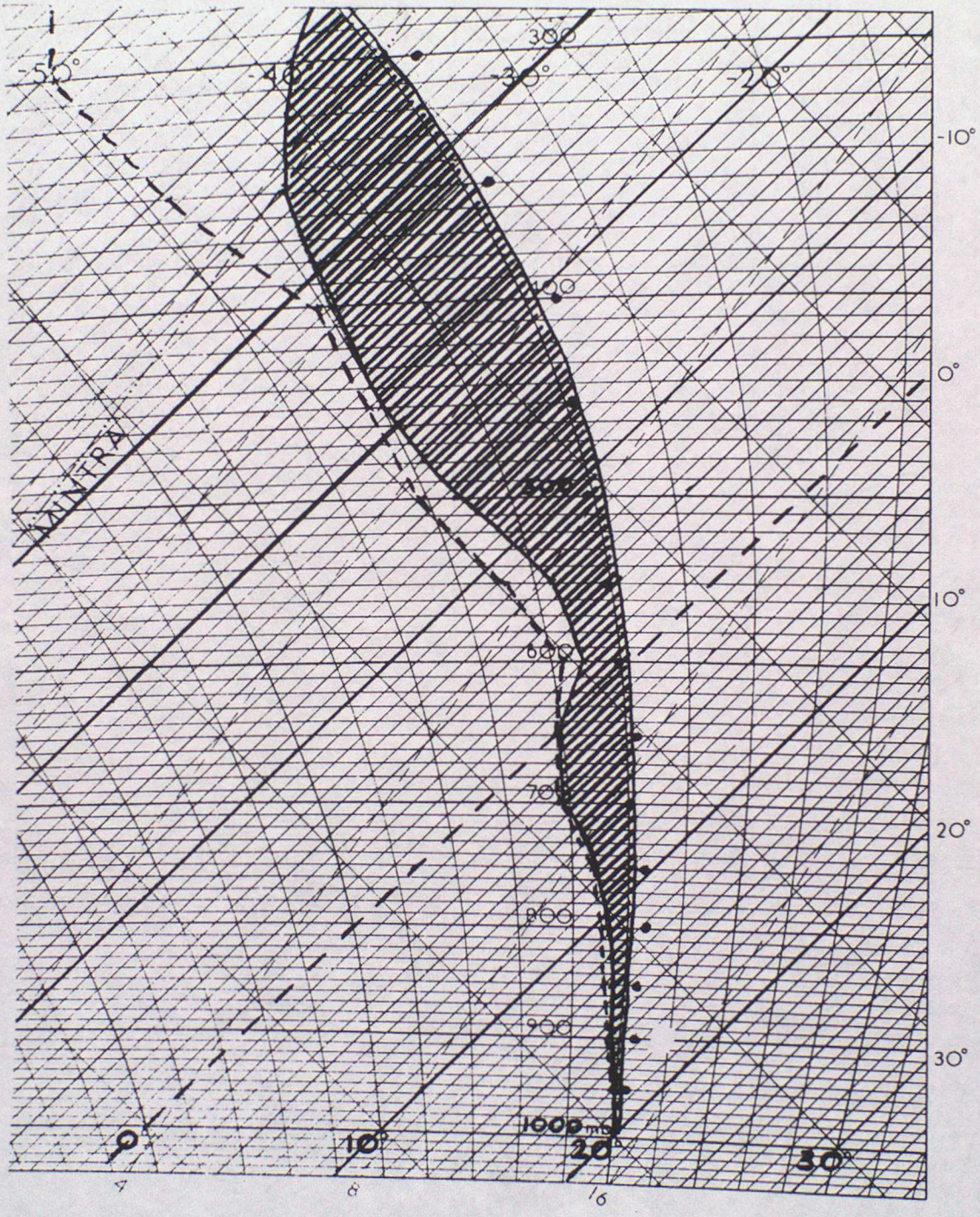
-50°
-40°
-30°
-20°
-10°
0°
10°
20°
30°
300
400
500
600
700
800
900
1000 mb
ADIABATA
0°
10°
20°
30°
4
8
16

Fig. 10

(a)

WET BULB POTENTIAL TEMP
BEST FM ANALYSIS
VALID AT 0Z ON 15/10/1987 DAY 288 DATA TIME 0Z ON 15/10/1987 DAY 288
LEVEL: 850 MB

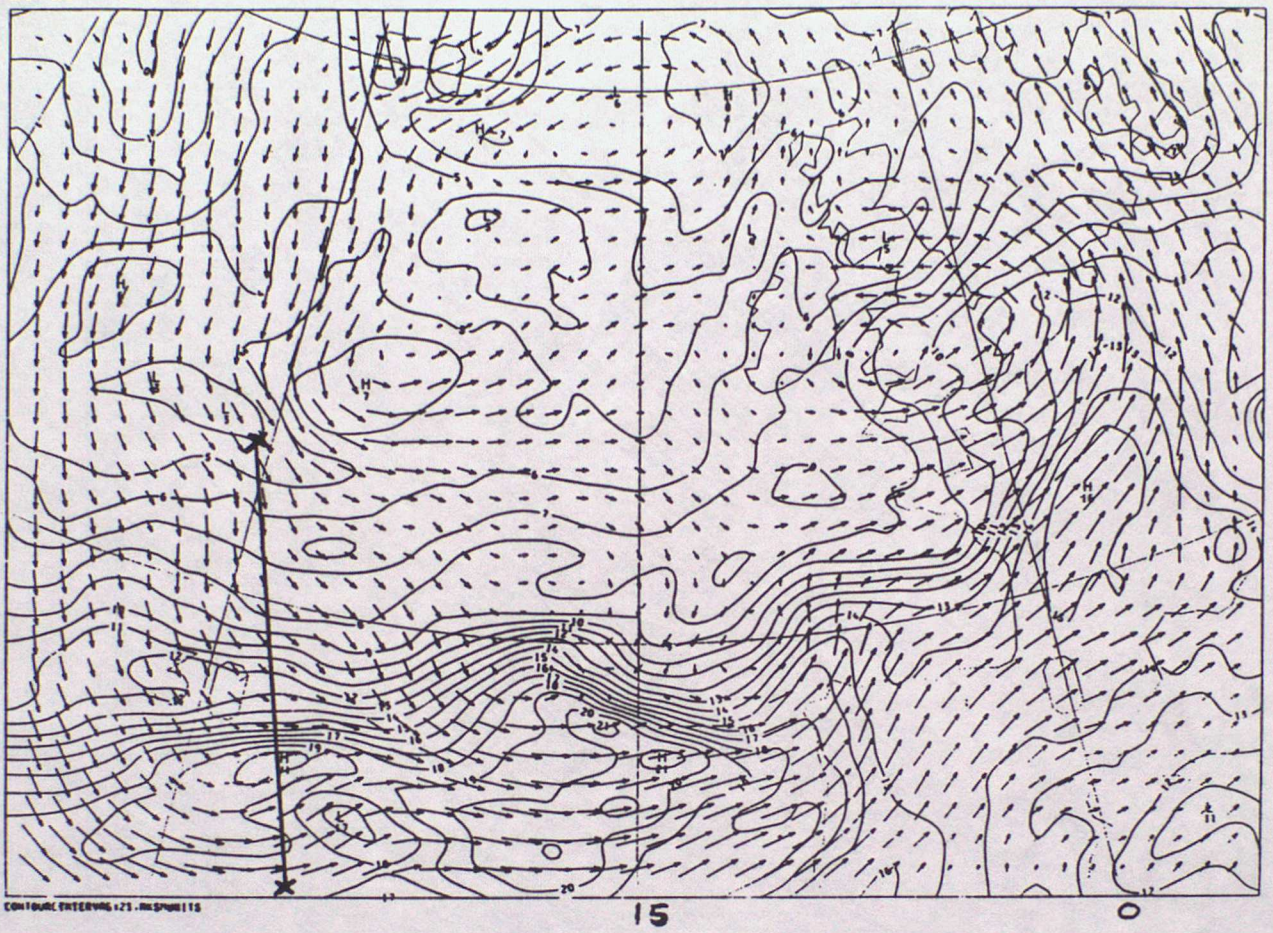

45

15 0

(b)

A.M & THETAW
VALID AT 0Z ON 15/10/1987 DAY 288 DATA TIME 0Z ON 15/10/1987 DAY 288

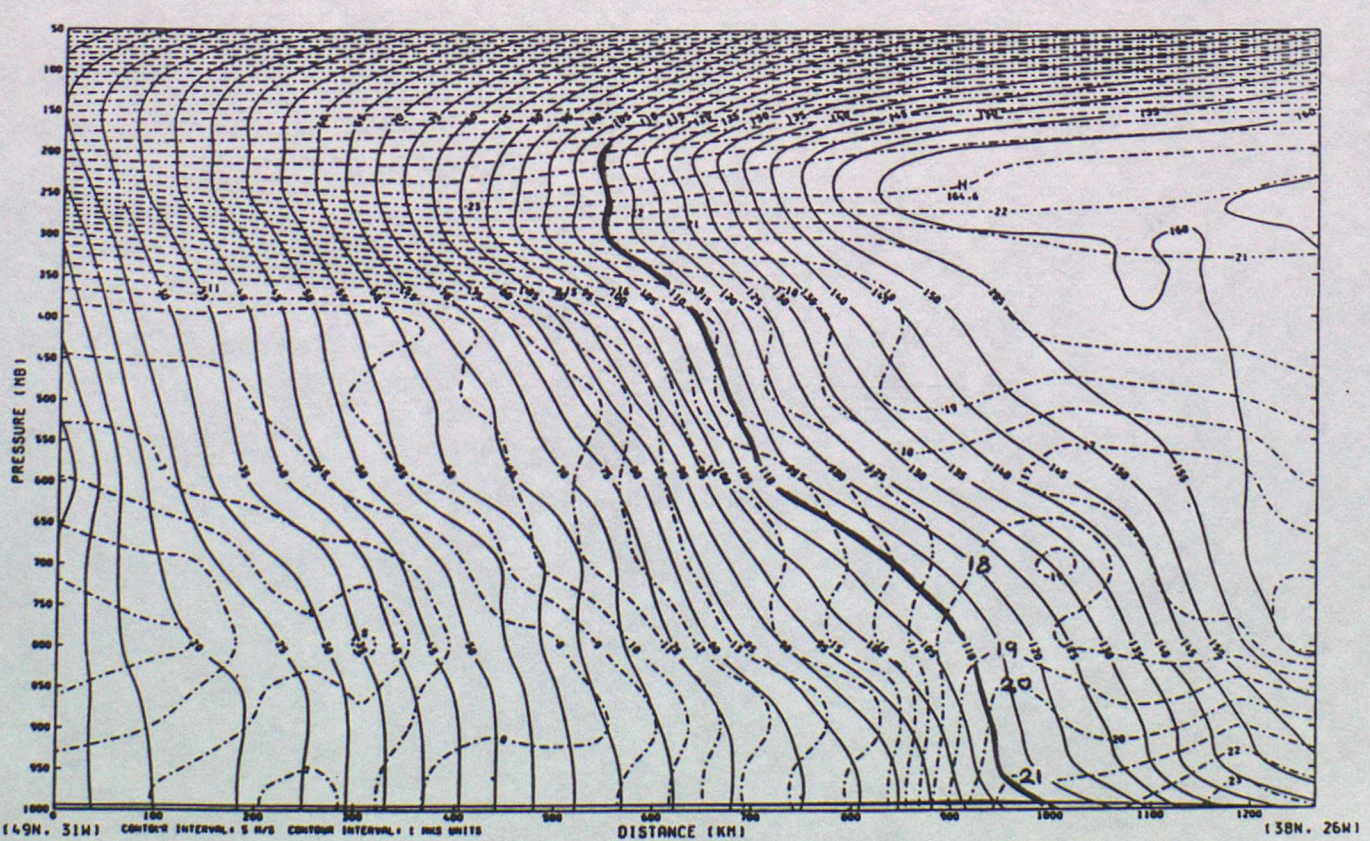

Fig. 10 (c)

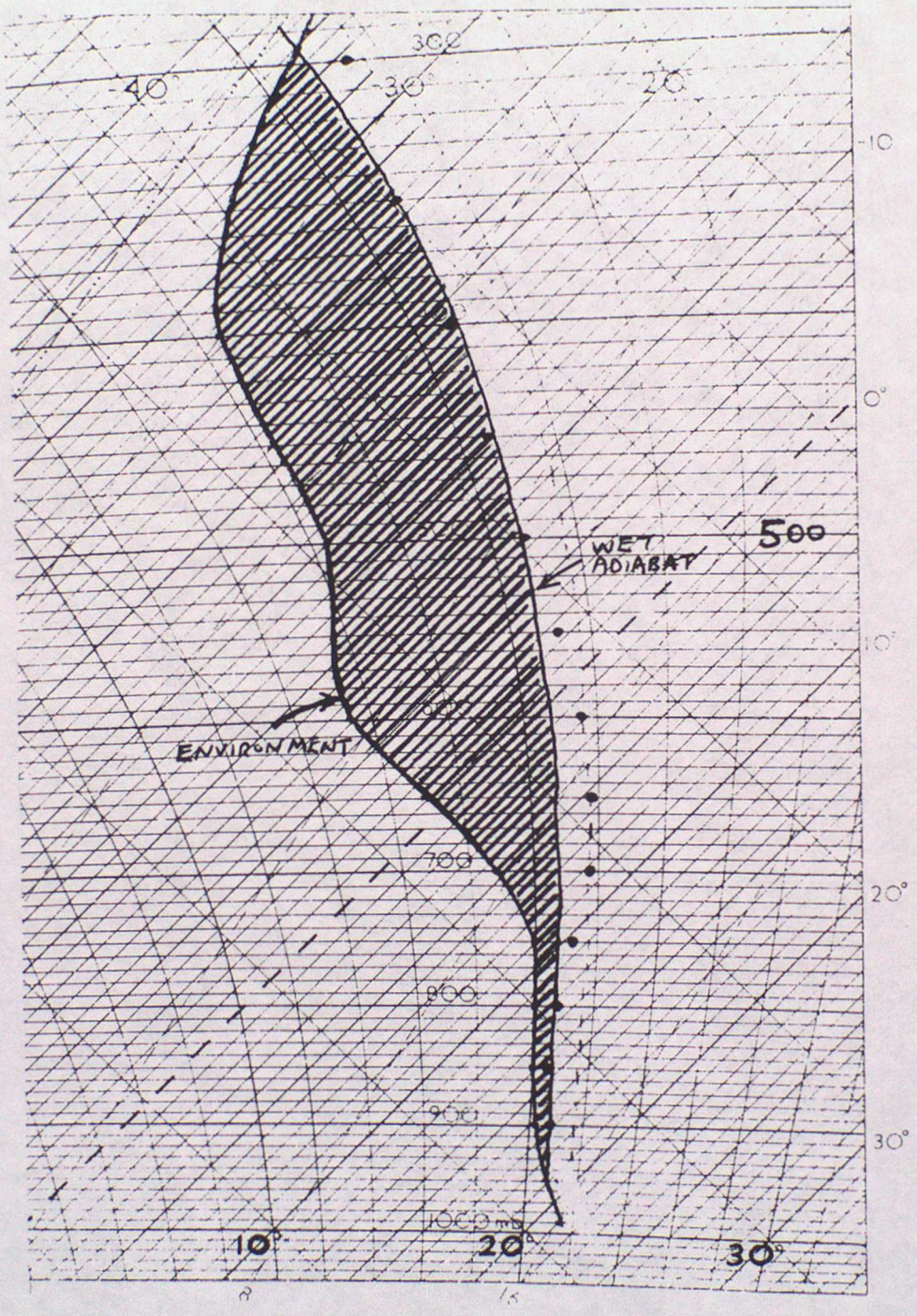
-40°
-30°
-20°
-10°
0°
10°
20°
30°
500
700
800
900
1000 mb
WET ADIABAT
ENVIRONMENT
10°
20°
30°

Fig.11

WET BULB POTENTIAL TEMP
BEST FM ANALYSIS
VALID AT 12Z ON 15/10/1987 DAY 288 DATA TIME 0Z ON 15/10/1987 DAY 288
LEVEL: 850 MB

(a)

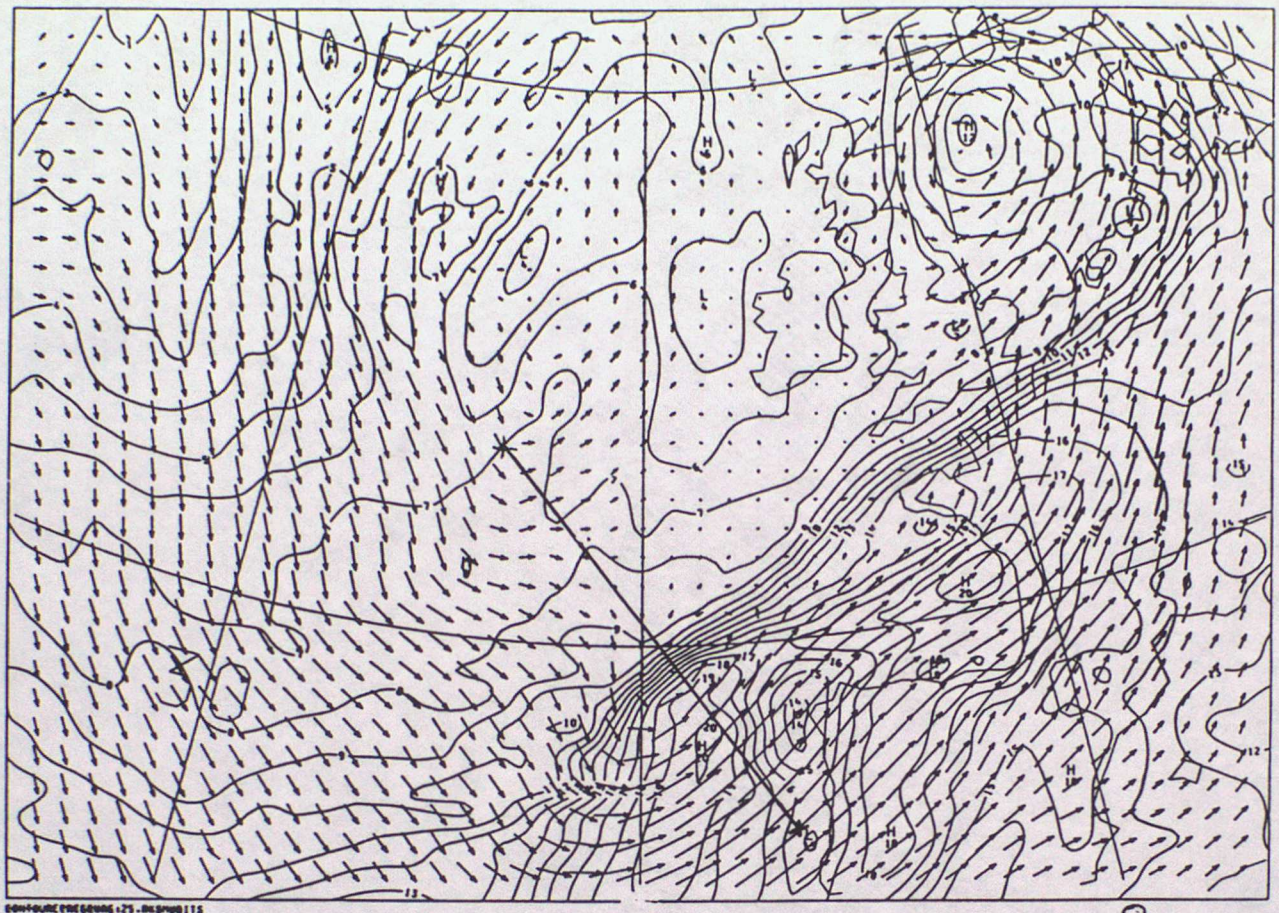

45

30 15 0

A.M & THETAW
VALID AT 12Z ON 15/10/1987 DAY 288 DATA TIME 0Z ON 15/10/1987 DAY 288

(b)

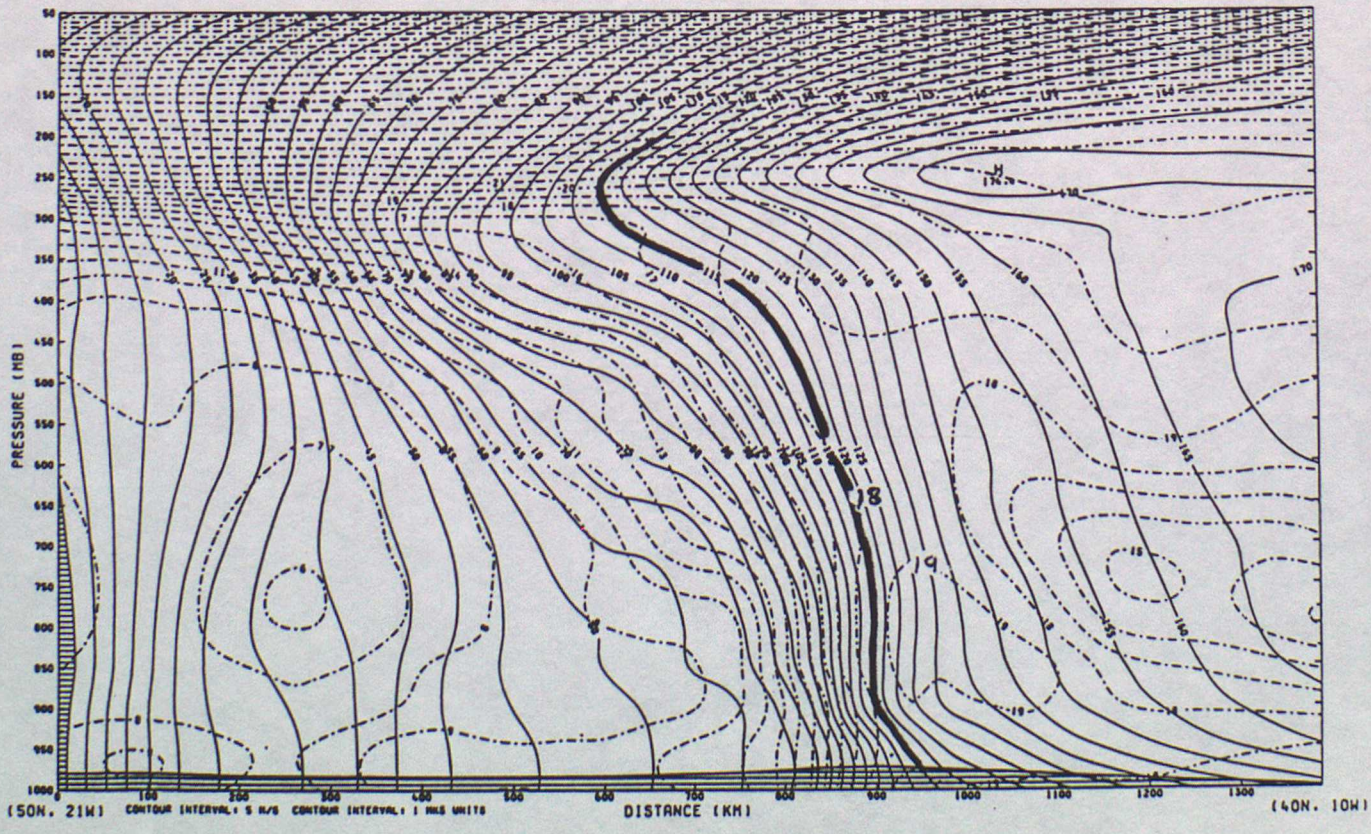

Fig.11

WET BULB POTENTIAL TEMP
BEST FM ANALYSIS
VALID AT 12Z ON 15/10/1987 DAY 288 DATA TIME 0Z ON 15/10/1987 DAY 288
LEVEL: 850 MB

(a)

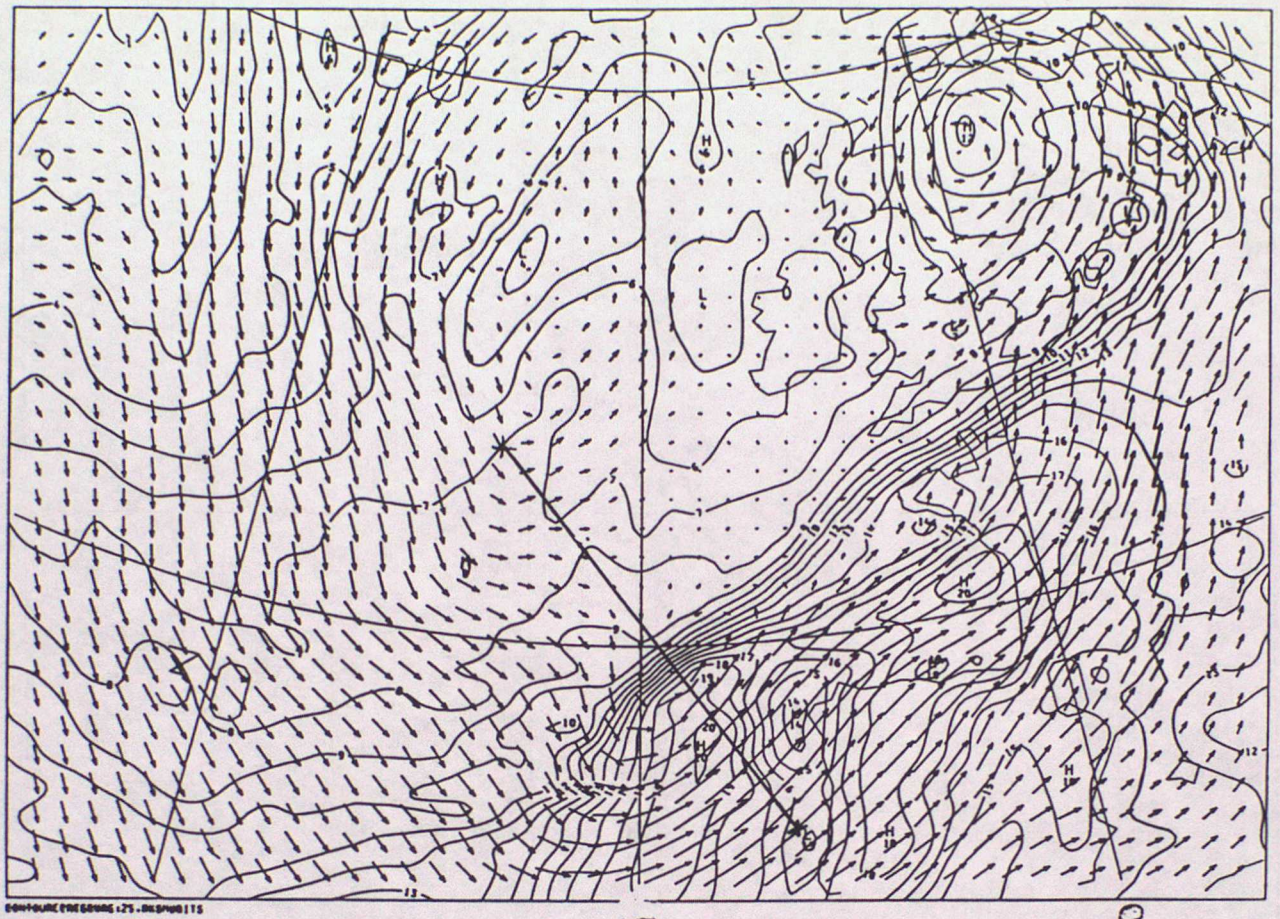

A.M & THETAW
VALID AT 12Z ON 15/10/1987 DAY 288 DATA TIME 0Z ON 15/10/1987 DAY 288

(b)

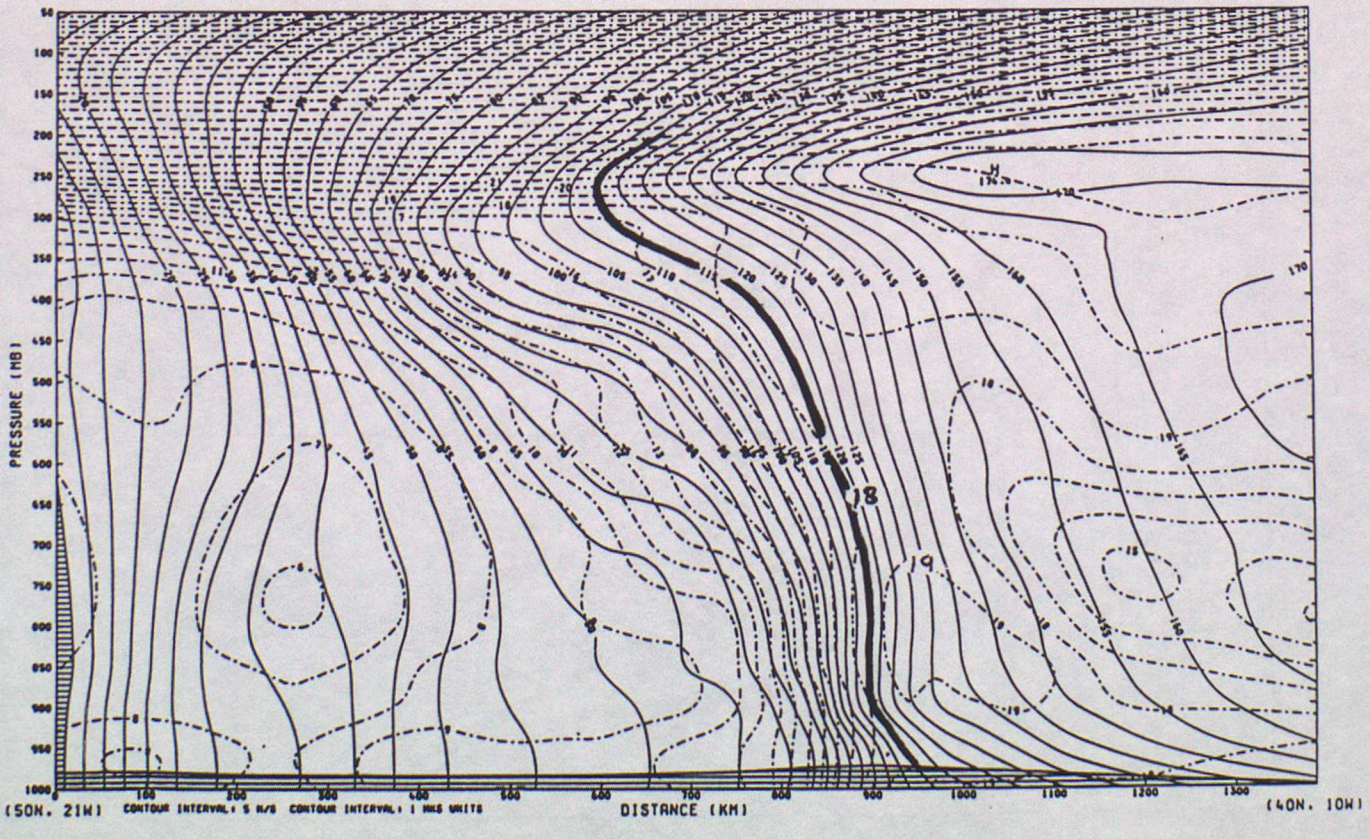

Fig. 12

(a)

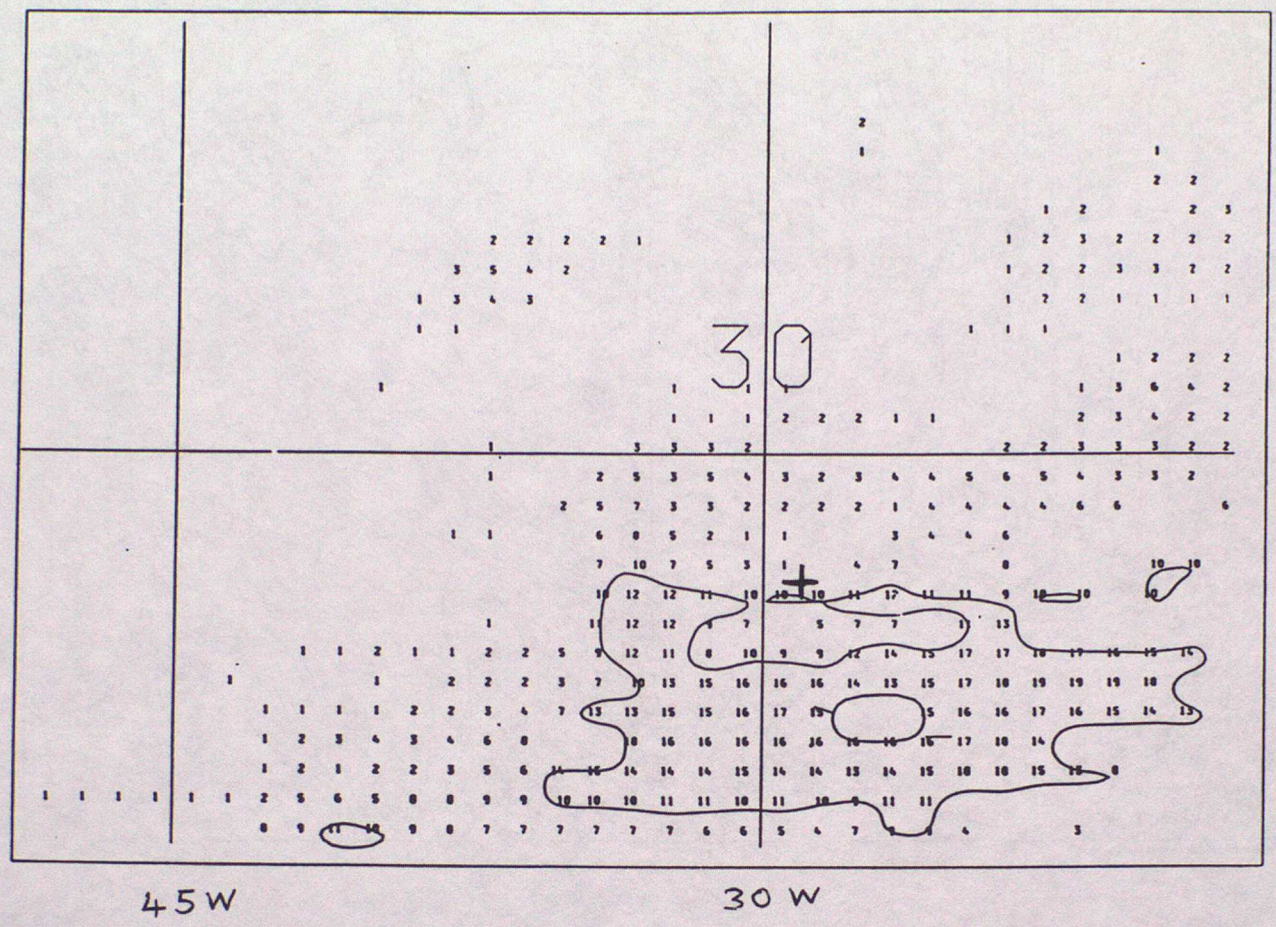
VALID AT : 00Z 15/10/1987 DATA TIME : 00Z 15/10/1987 T + 00
30
45 N
45 W
30 W

(b)

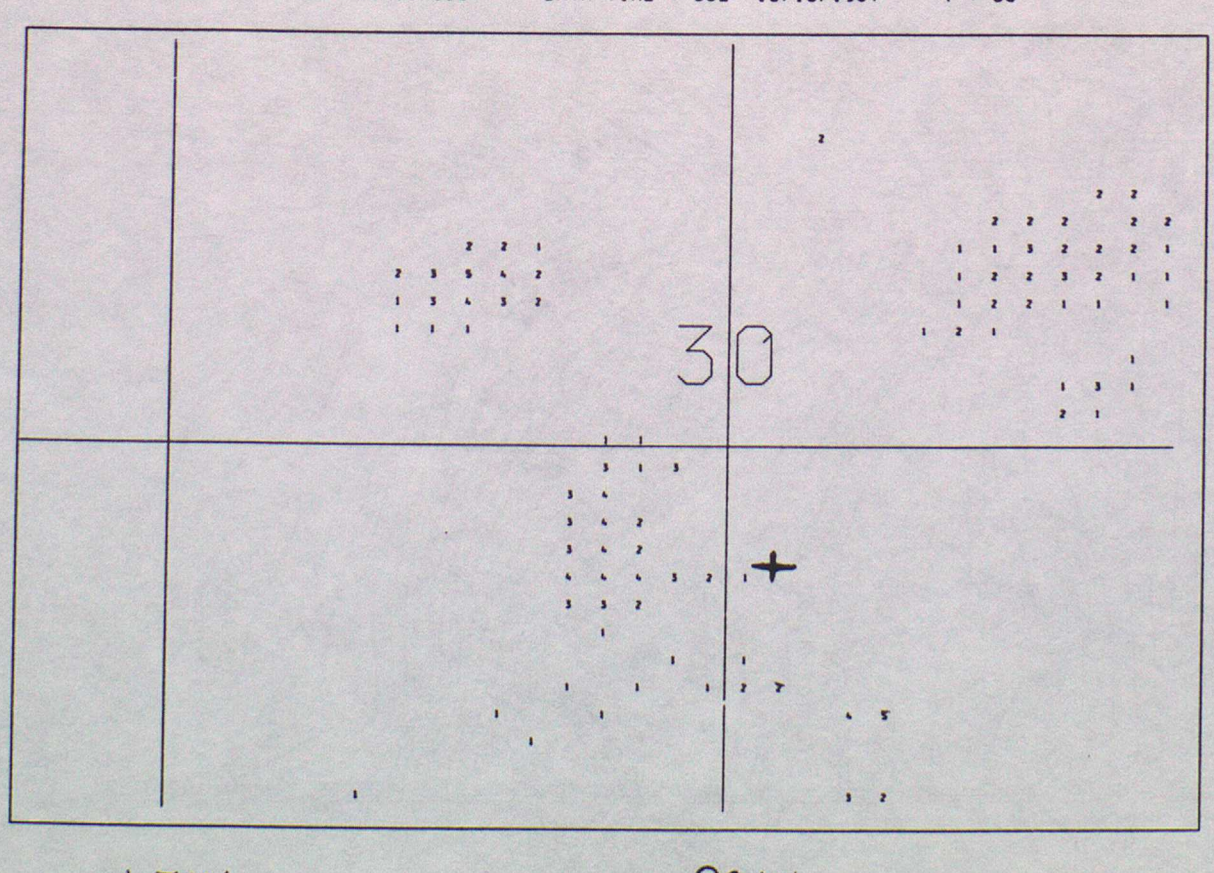
VALID AT : 00Z 15/10/1987 DATA TIME : 00Z 15/10/1987 T + 00
30
45 N
45 W
30 W

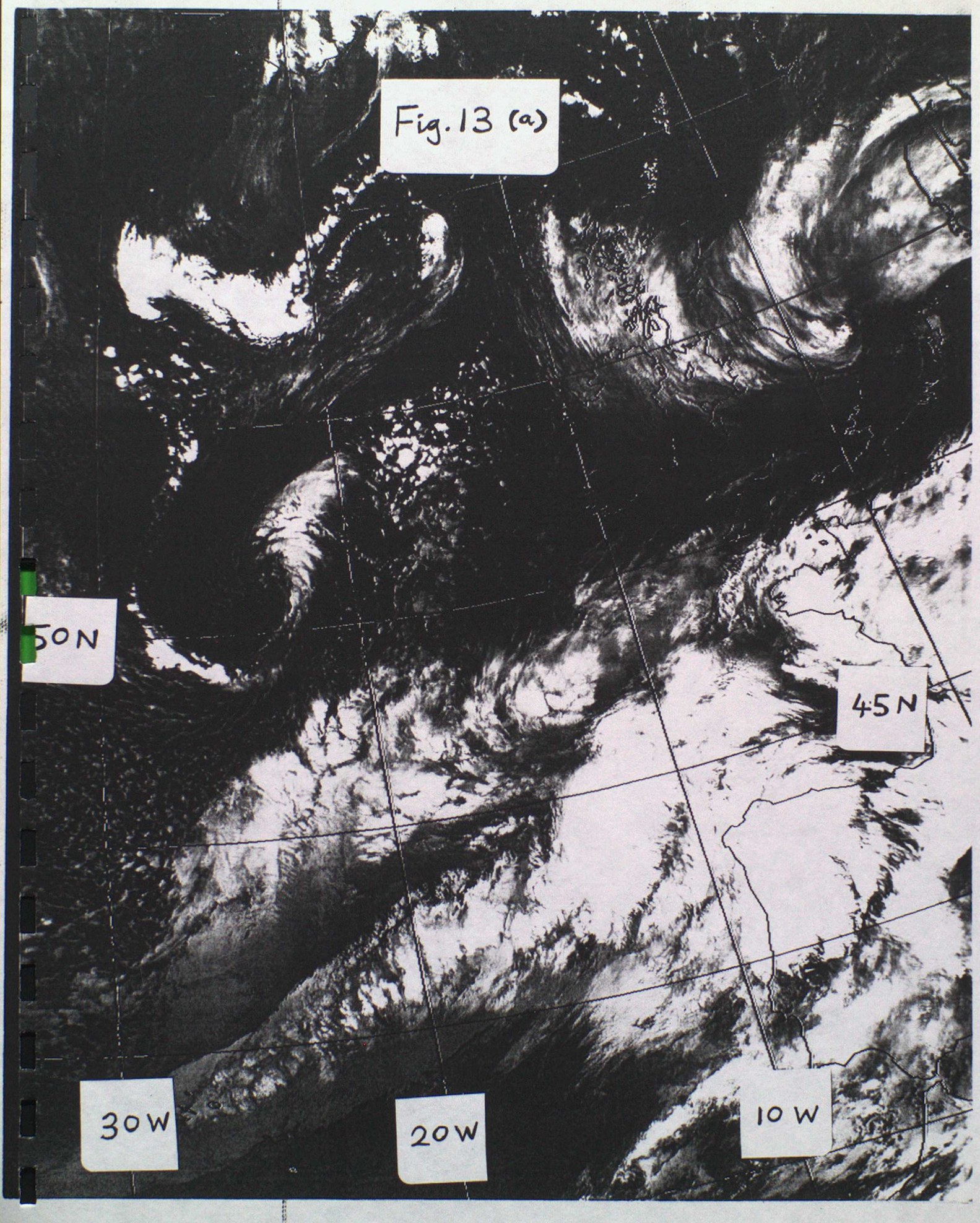
Fig. 13 (a)
50N
45N
30W
20W
10W

Fig. 13 b

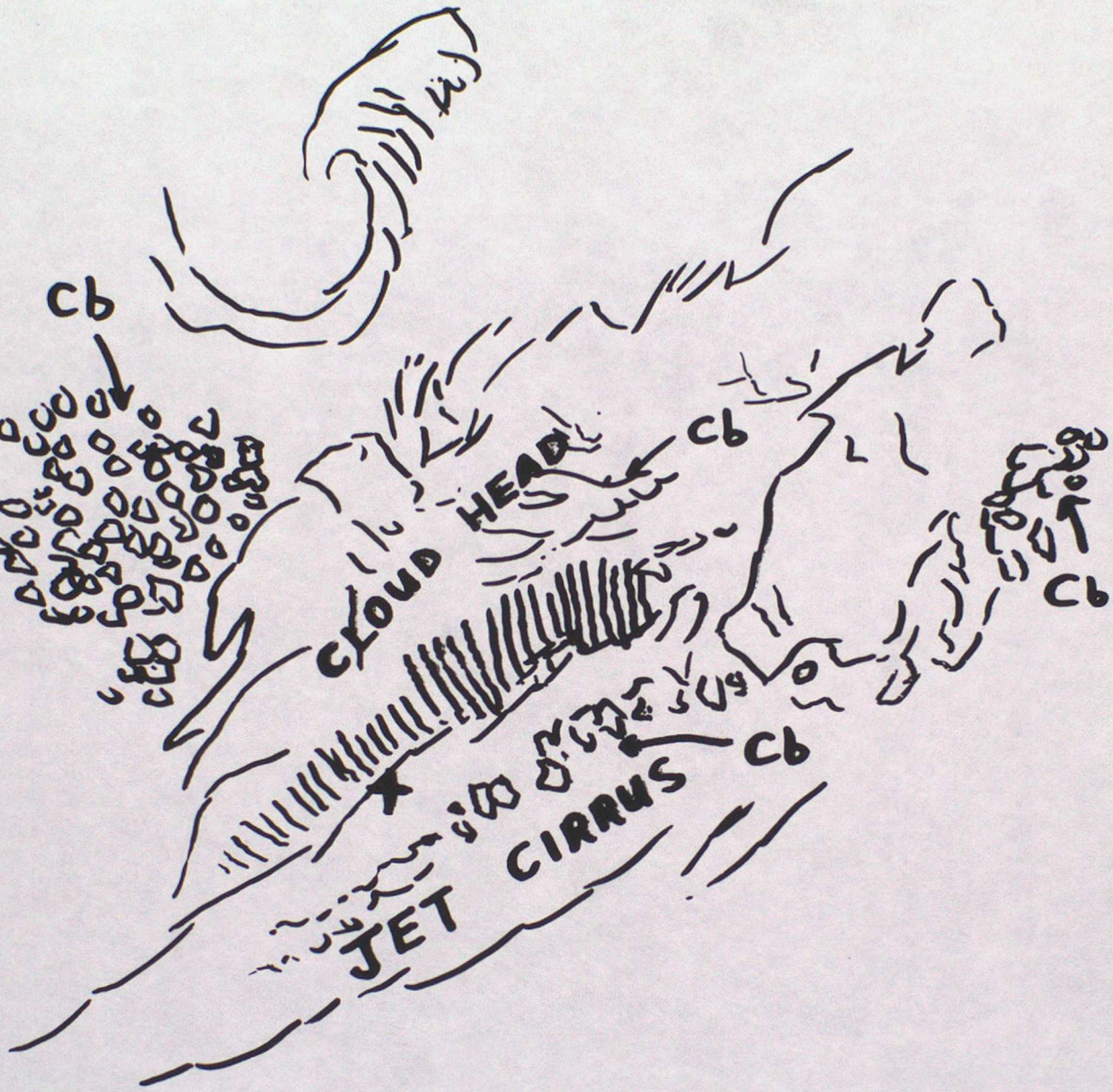

FRONTAL SURFACE STRIATIONS

Fig. 14


BEST FM
RELATIVE HUMIDITY
VALID AT 6Z ON 15/10/1987 DAY 288 DATA TIME 0Z ON 15/10/1987 DAY 288
LEVEL: 400 MB
45
30
15
0


Fig. 15
20W
10W
0°E
50N
45N
40N

Fig. 16

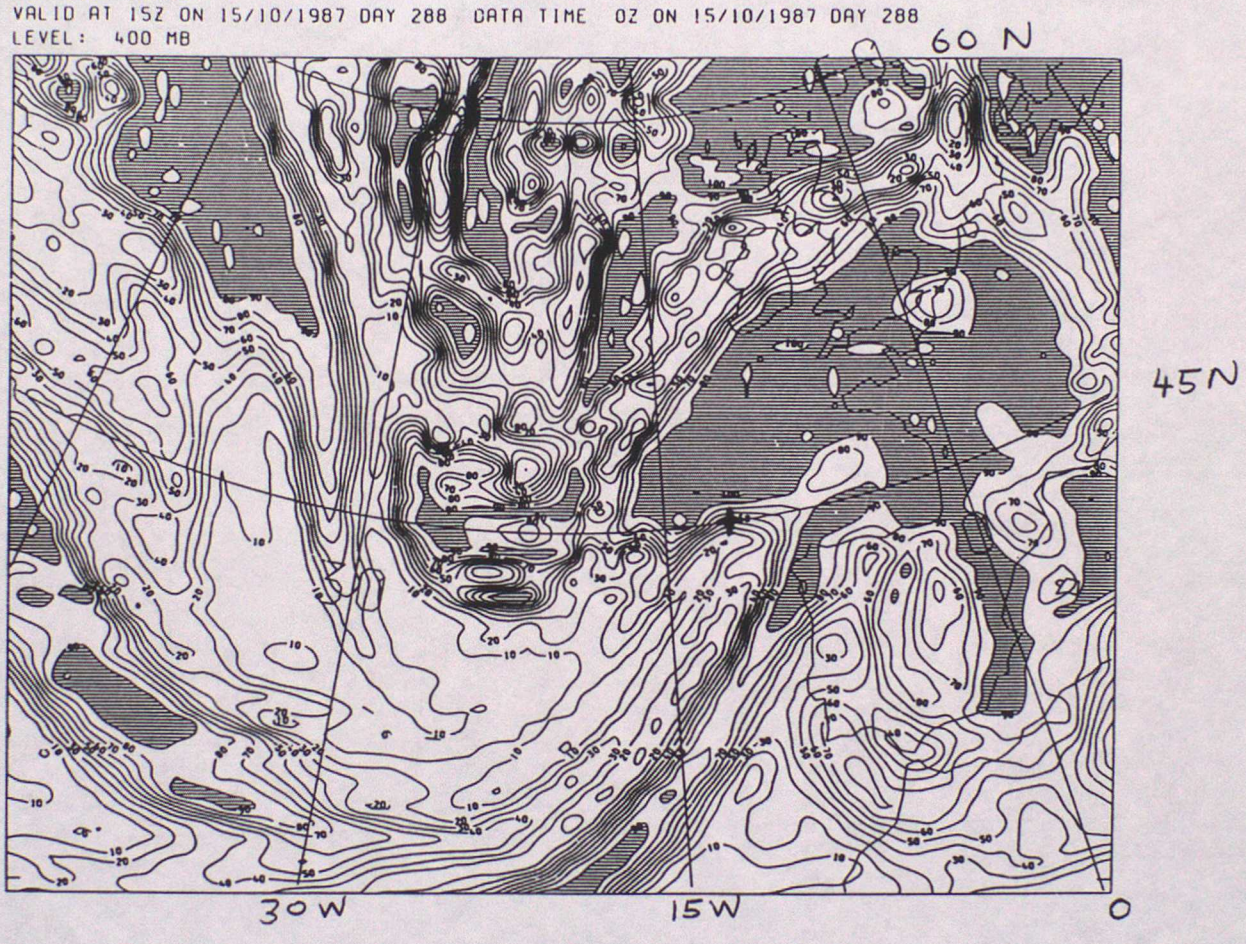
BEST FM
RELATIVE HUMIDITY
VALID AT 15Z ON 15/10/1987 DAY 288 DATA TIME 0Z ON 15/10/1987 DAY 288
LEVEL: 400 MB
60 N
45N
30W
15W
0

Fig. 17

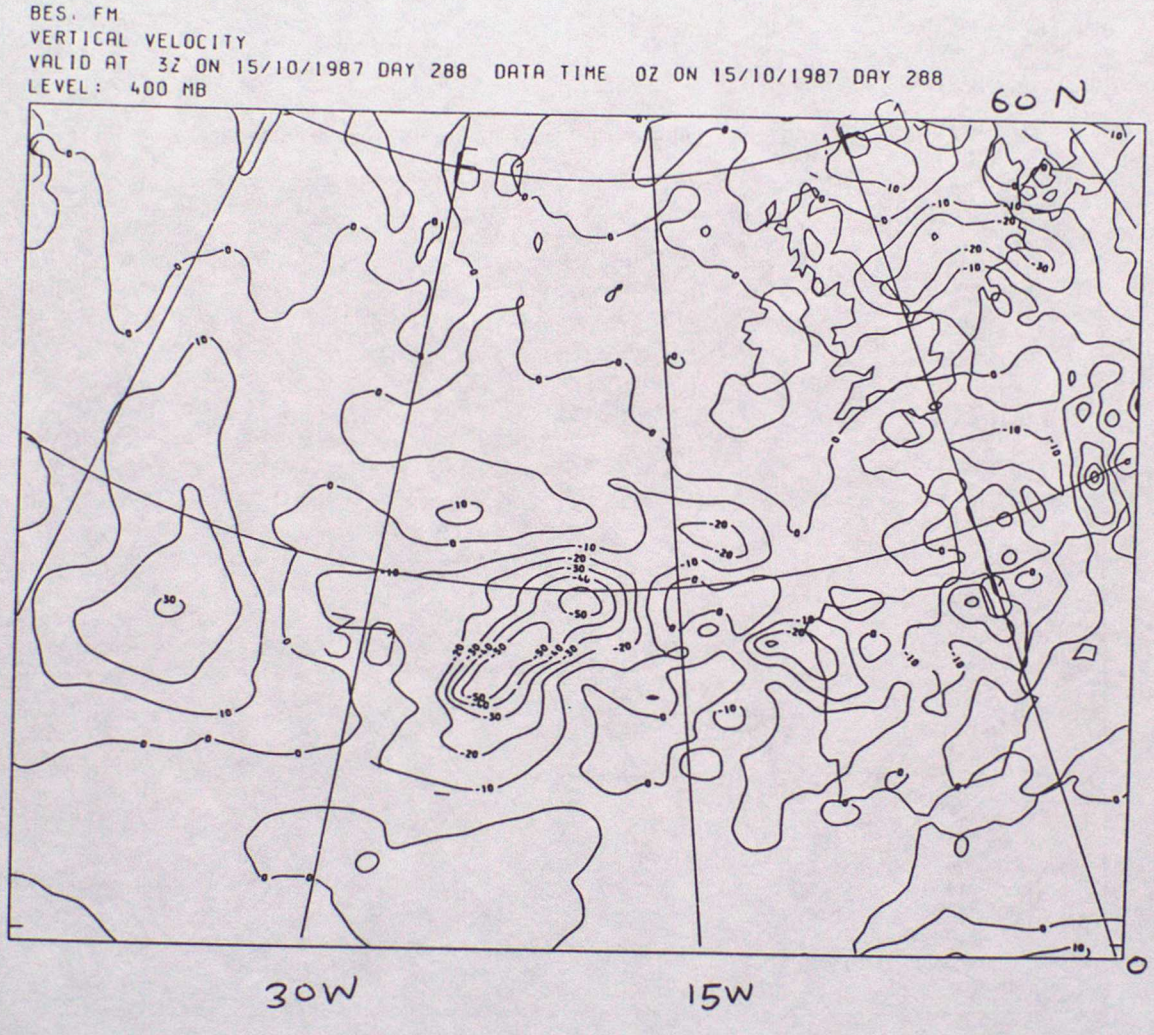
BES. FM
VERTICAL VELOCITY
VALID AT 3Z ON 15/10/1987 DAY 288 DATA TIME 0Z ON 15/10/1987 DAY 288
LEVEL: 400 MB
60 N
45N
30W
15W
0

Fig. 18

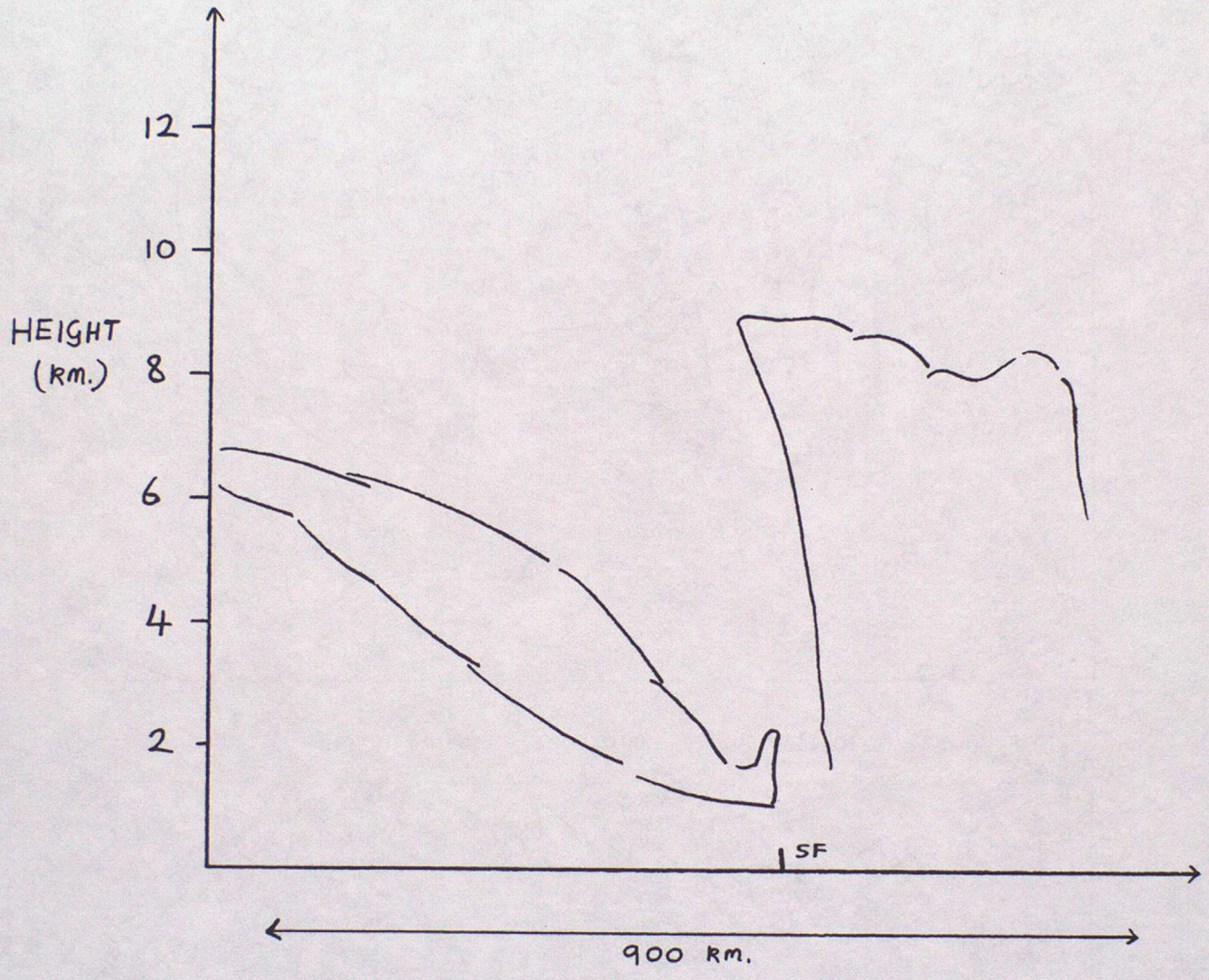

Fig. 19

CM-INT-FM
PMSL
VALID AT 0Z ON 15/10/1987 DAY 288 DATA TIME 0Z ON 15/10/1987 DAY 288
SEA LEVEL

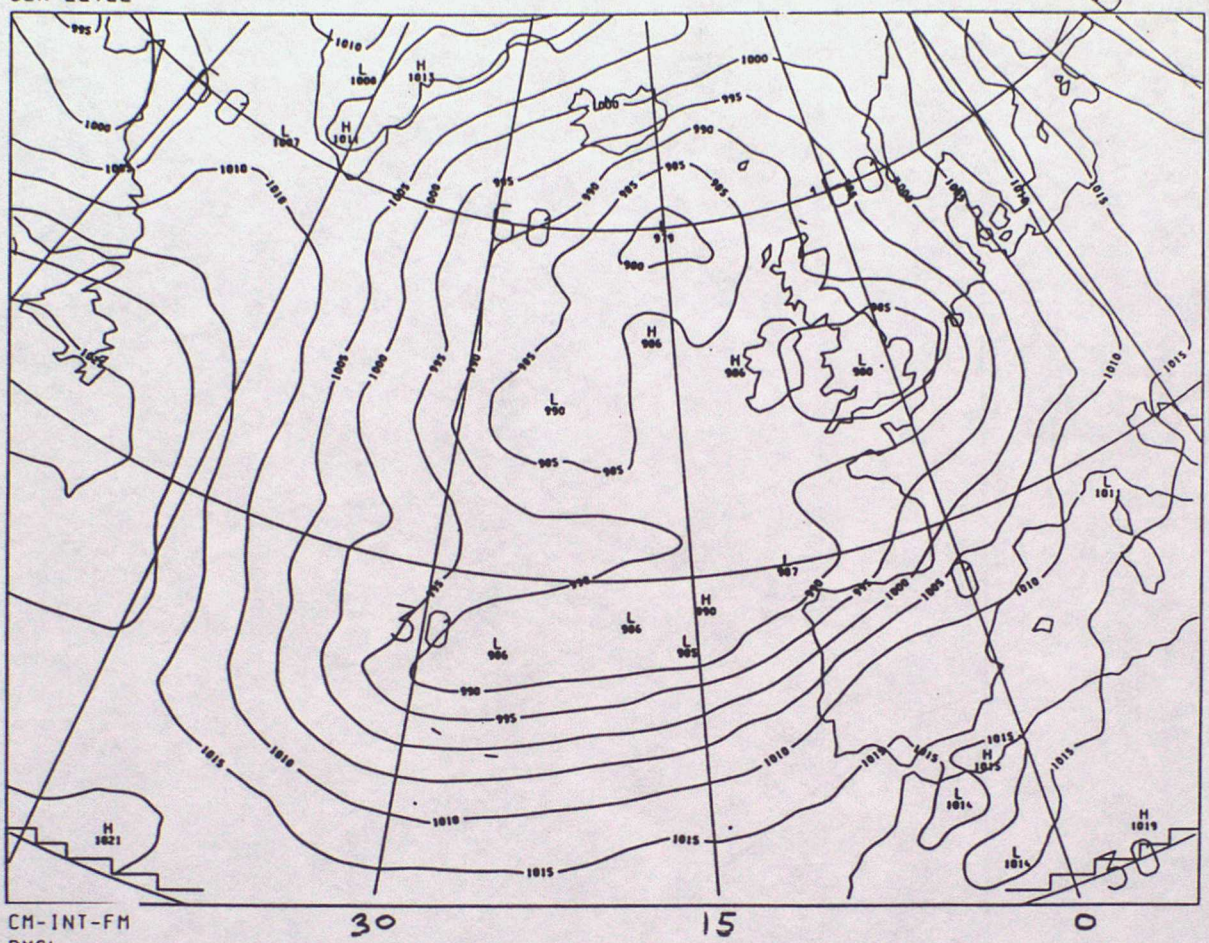

(a)

CM-INT-FM
PMSL
VALID AT 0Z ON 16/10/1987 DAY 289 DATA TIME 0Z ON 15/10/1987 DAY 288
SEA LEVEL

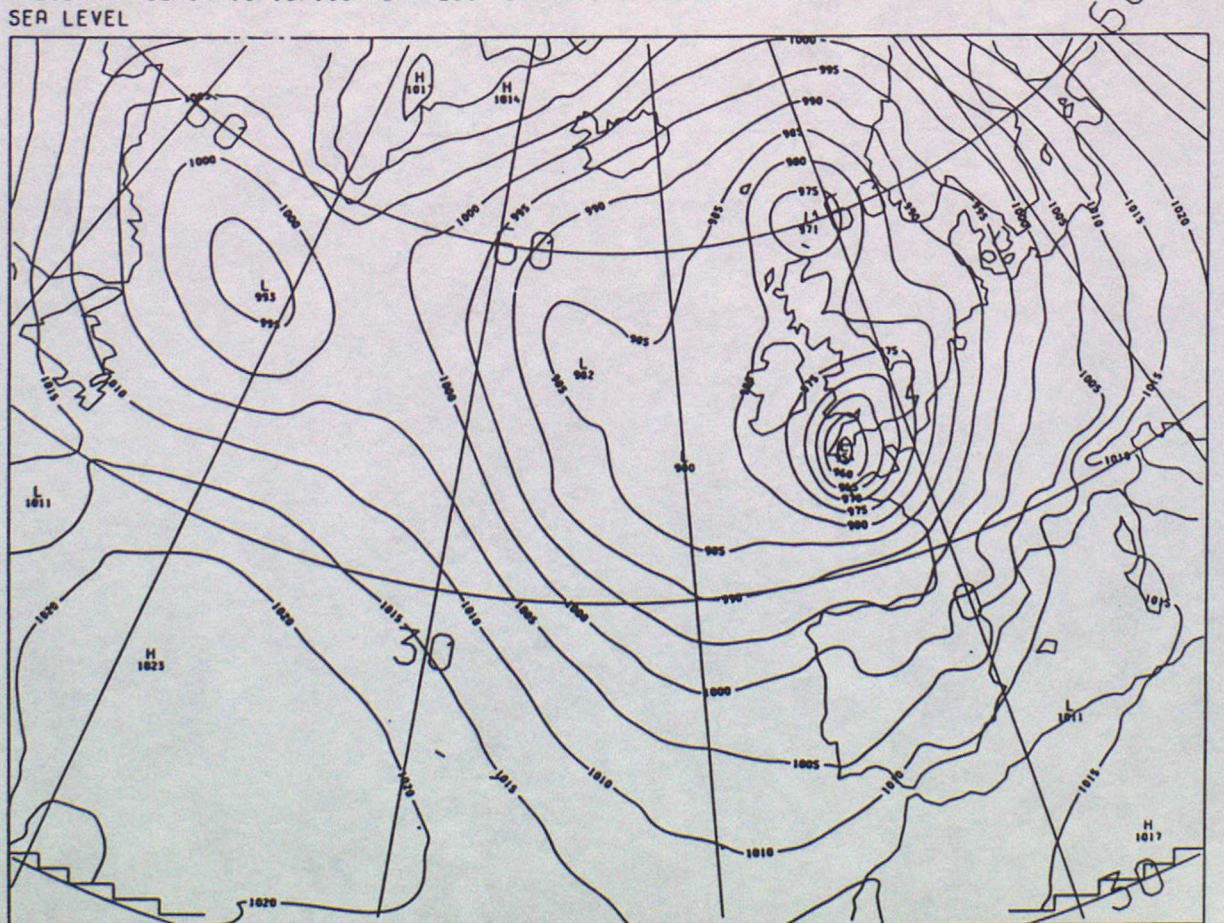

(b)

Fig. 20

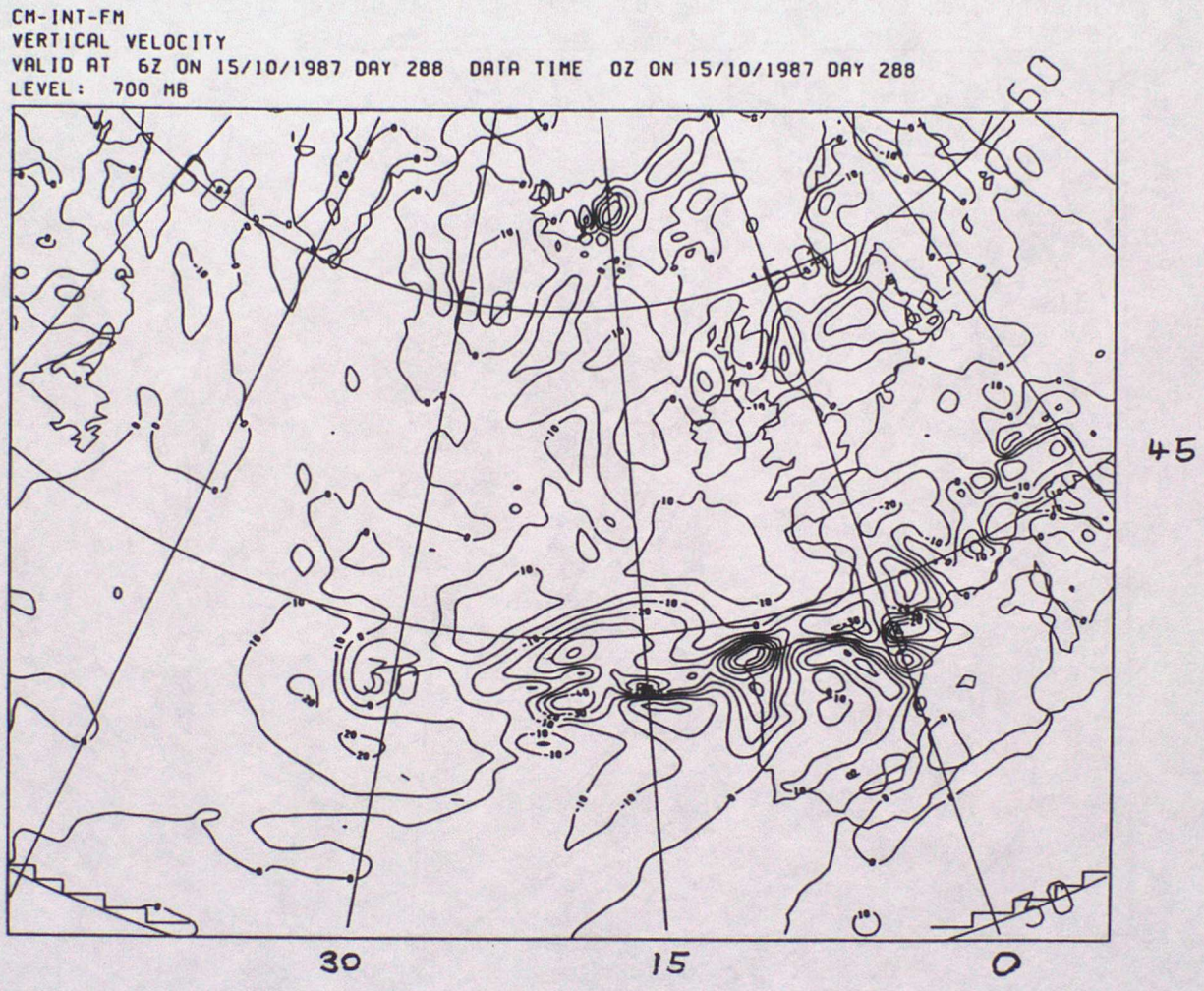
CM-INT-FM
VERTICAL VELOCITY
VALID AT 6Z ON 15/10/1987 DAY 288 DATA TIME 0Z ON 15/10/1987 DAY 288
LEVEL: 700 MB
60
45
30
15
0

Fig. 21

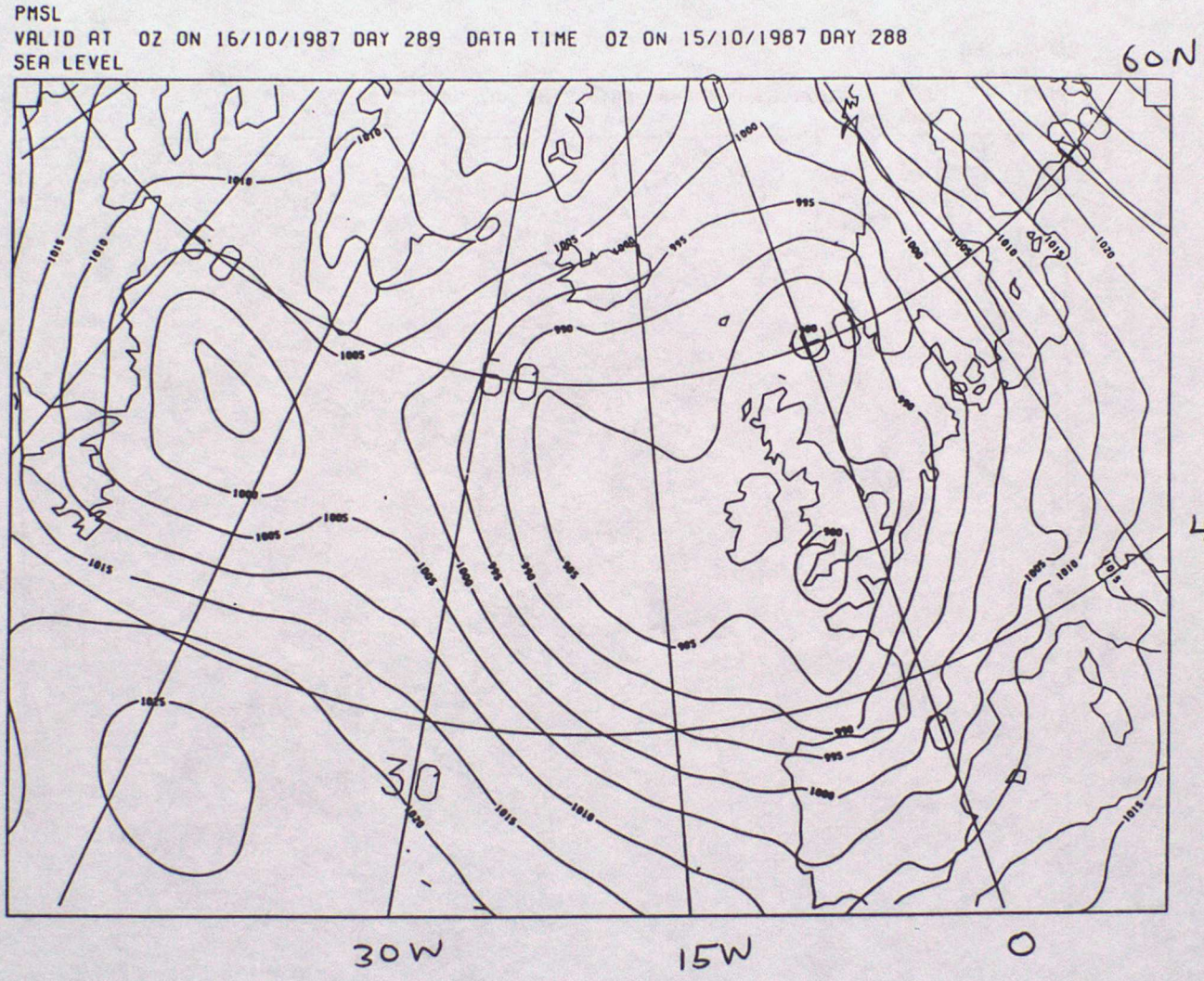
PMSL
VALID AT 0Z ON 16/10/1987 DAY 289 DATA TIME 0Z ON 15/10/1987 DAY 288
SEA LEVEL
60N
45N
30W
15W
0
30

Fig. 22

(a)

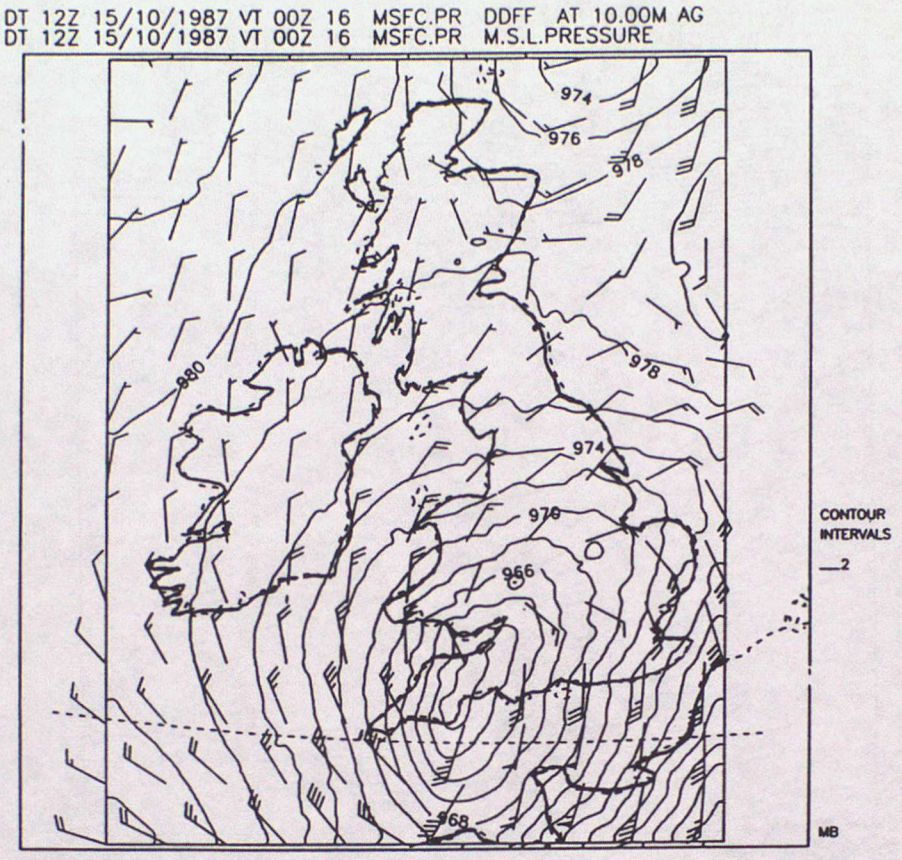
DT 12Z 15/10/1987 VT 00Z 16 MSFC.PR DDFF AT 10.00M AG
DT 12Z 15/10/1987 VT 00Z 16 MSFC.PR M.S.L.PRESSURE
974
976
978
980
978
974
970
966
968
CONTOUR INTERVALS
2
MB

(b)

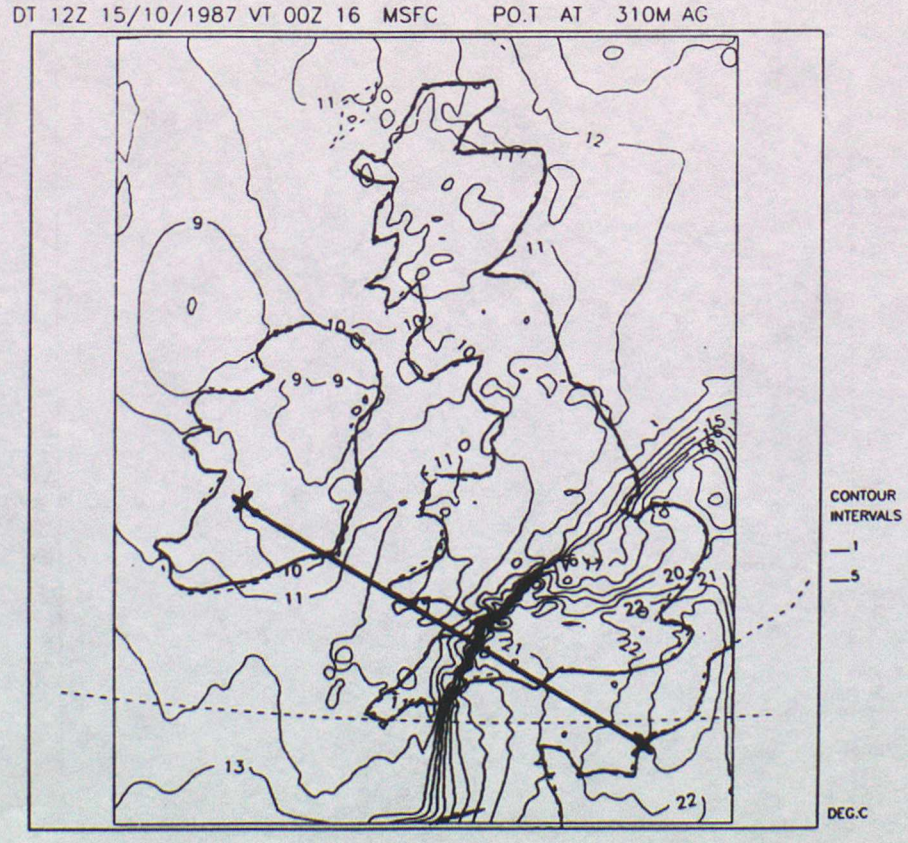
DT 12Z 15/10/1987 VT 00Z 16 MSFC PO.T AT 310M AG
11
12
9
11
10
10
10
9
9
11
10
11
20
21
22
21
13
22
CONTOUR INTERVALS
1
5
DEG.C

Fig. 23

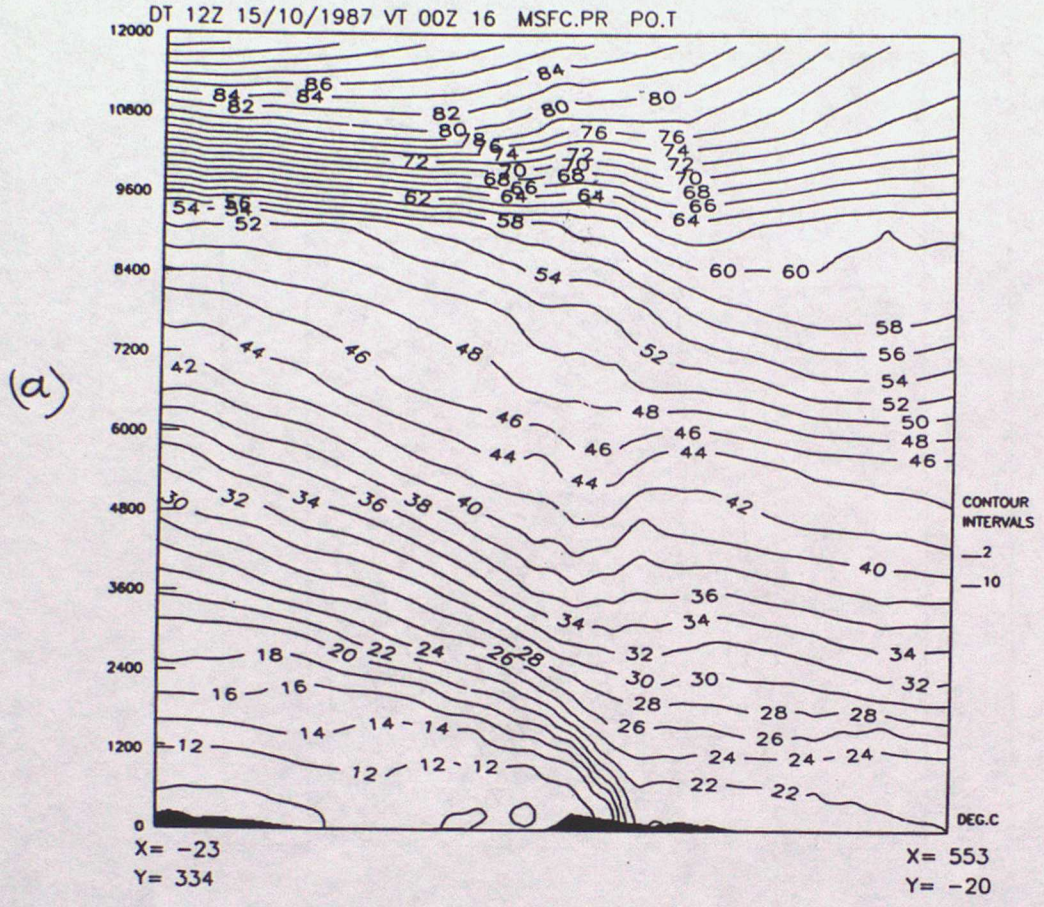
DT 12Z 15/10/1987 VT 00Z 16 MSFC.PR PO.T
12000
10800
9600
8400
7200
6000
4800
3600
2400
1200
0
CONTOUR INTERVALS
2
10
DEG.C
X= -23
Y= 334
X= 553
Y= -20

(a)

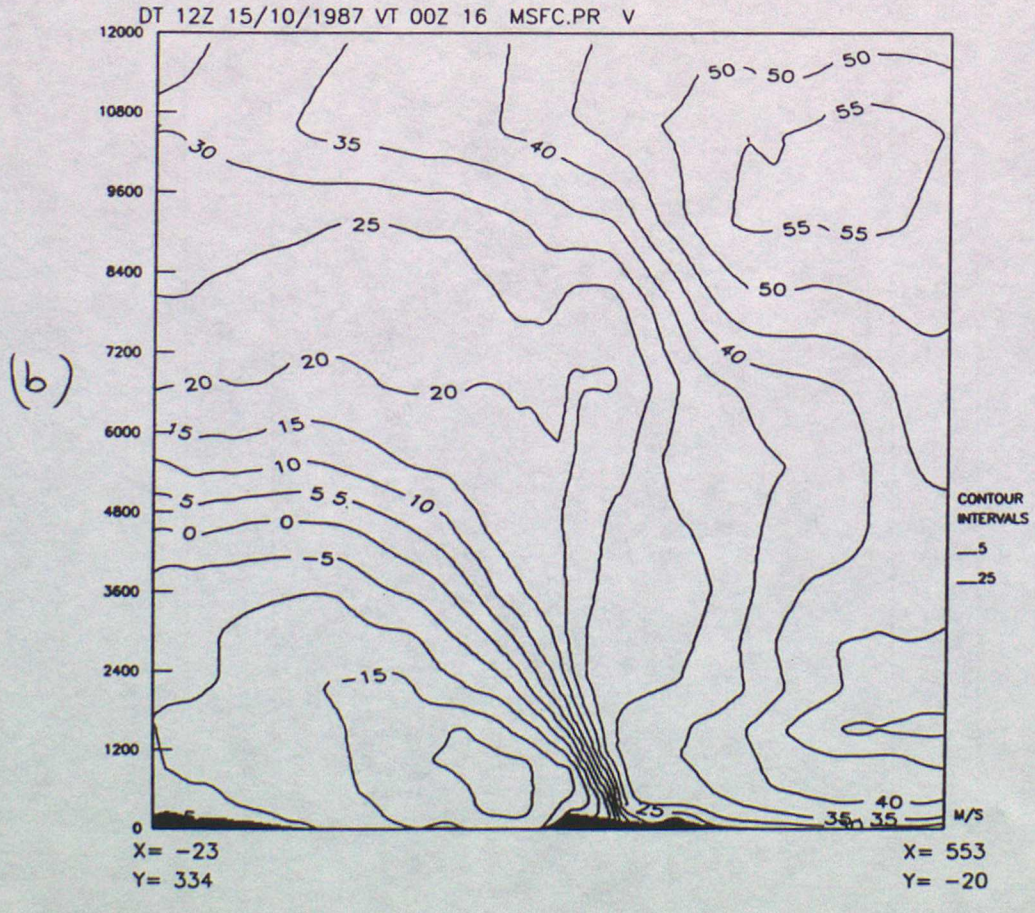
DT 12Z 15/10/1987 VT 00Z 16 MSFC.PR V
12000
10800
9600
8400
7200
6000
4800
3600
2400
1200
0
CONTOUR INTERVALS
5
25
M/S
X= -23
Y= 334
X= 553
Y= -20

(b)

Fig. 23 (c)

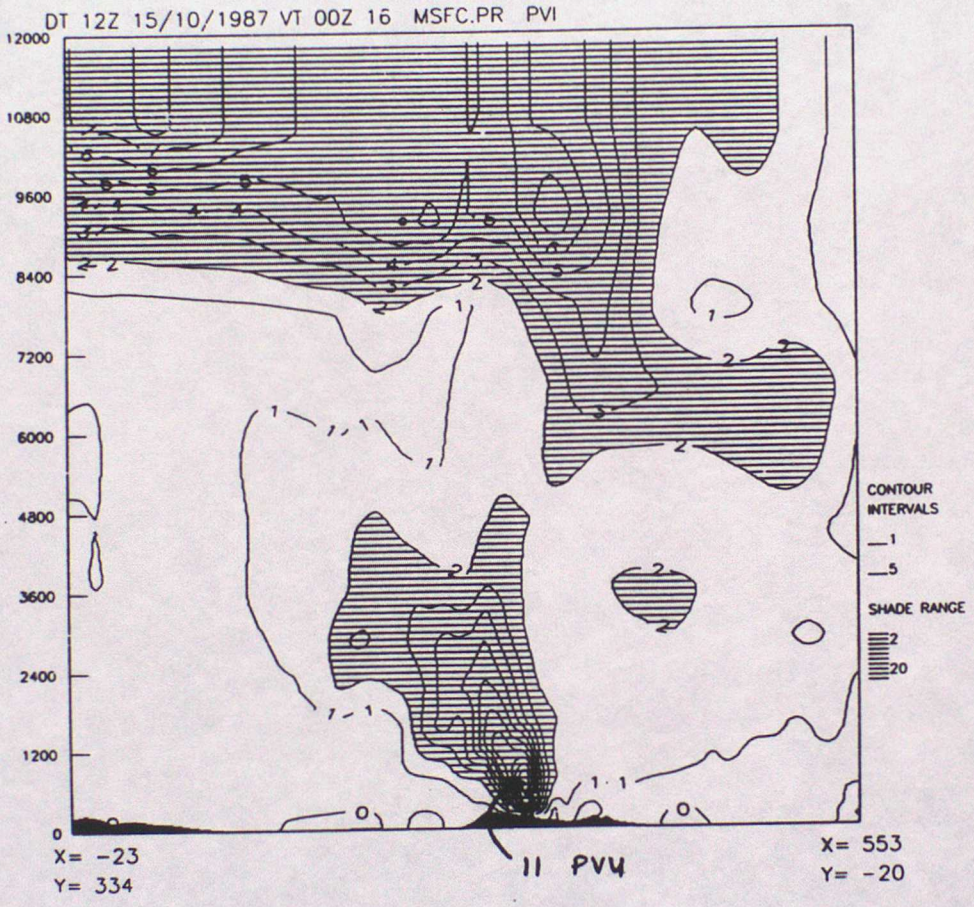
DT 12Z 15/10/1987 VT 00Z 16 MSFC.PR PVI
12000
10800
9600
8400
7200
6000
4800
3600
2400
1200
0
CONTOUR INTERVALS
1
5
SHADE RANGE
2
20
X= -23
Y= 334
11 PVU
X= 553
Y= -20

CURRENT MET O 11 SCIENTIFIC NOTES (SEPTEMBER 1989)

The Met O 11 Scientific Notes which contain information of current use are listed below. The complete set of Scientific Notes is available from the National Meteorological Library on loan, if required.

1. **The theory of periodic solutions of the semi-geostrophic equations.**
   R.J. Purser
   October 1987

2. **Properties of the partial differential equations governing various types of atmospheric motions and implications for numerical methods.**
   M.J.P. Cullen
   December 1987

3. **A geometric model of balanced, axisymmetric flows with embedded penetrative convection.**
   G.J. Shutts, M. Booth and J. Norbury
   February 1988

4. **Implicit finite difference methods for computing discontinuous atmospheric flows.**
   M.J.P. Cullen
   March 1988

5. **Variational aspects of semi-geostrophic theory.**
   R.J. Purser
   August 1988

6. **On the incorporation of atmospheric boundary layer effects into a balanced model.**
   M.J.P. Cullen
   July 1988

7 **Implicit finite difference methods for modelling discontinuous atmospheric flows.**
   M.J.P. Cullen
   June 1988

8. **An analytical model of the growth of a frontal intrusion.**
   M.W. Holt and G.J. Shutts
   November 1988

9. **Planetary semi-geostrophic equations derived from Hamilton's principle.**
   G.J. Shutts
   July 1988

10. **Semi-geostrophic moist frontogenesis in a Lagrangian model.**
    M.W. Holt
    September 1988

11. **Generalised Lagrangian solutions for atmospheric and ocean flows.**
    M.J.P. Cullen, J. Norbury and R.J. Purser
    November 1988

12. **Properties of the Lagrangian semi-geostrophic equations.**
M.J.P. Cullen and R.J. Purser
January 1989

13. **A simple two phase precipitation scheme for use in numerical weather prediction models.**
B.W. Golding
June 1989

14. **A test of a semi-implicit integration technique for a fully compressible non-hydrostatic model.**
M.J.P.Cullen
September 1989

15. **Dynamical aspects of the October storm 1987 : A study of a successful Fine-mesh simulation**
G.J.Shutts
September 1989